Diffraction Analysis and Tactical Applications

of Signal Propagation Over Rough Terrain

THESIS
You-Cheol Jang
Captain, Republic of Korea Army

AFIT/GE/ENG/97J-01

19970805 027

DTIC QUALITY INSPECTED 2

Approved for public release; distribution unlimited

The views expressed in this thesis are those of the author and do not reflect the official policy or position of the Department of Defense or the U. S. Government.

Diffraction Analysis and Tactical Applications
of Signal Propagation Over Rough Terrain

THESIS

Presented to the Faculty of the School of Engineering

of the Air Force Institute of Technology

Air University

In Partial Fulfillment of the

Requirements for the Degree of

Master of Science in Electrical Engineering

You-Cheol Jang, B.S.

Captain, Republic of Korea Army

June, 1997

Table of Contents

List of Figures

AFIT/GE/ENG/97J-01

Abstract

The free space propagation model is inadequate to predict the mean path-loss in ground wireless communication. Also, many existing propagation channel models do not adequately predict path-loss in rough terrain because most of them were based on measurements in urban areas. Hence, a channel model that estimates mean path-loss over many different kinds of terrain conditions is desired.

In this thesis, two new propagation channel models, Real Terrain Diffraction Model (RTDMOD) and Universal Terrain Channel Model (UTCMOD), were developed. Other geometric theory of diffraction (GTD) methods (Epstein-Peterson (EP) and Deygout (DG)) agree within 5 % from 3 MHz to 3GHz with RTDMOD. However, unlike these other methods, RTDMOD can account for an almost unlimited number of obstacles and has the advantage of predicting the significant diffraction point locations as well as the total path-loss for a given set of real terrain data. The computationally efficient stochastic channel model, UTCMOD, was developed from numerous *Monte Carlo* simulations using RTDMOD. UTCMOD agrees within 1 dB/km over a broad carrier frequency range and a large terrain height variance range with the popular Hata model. Furthermore, UTCMOD is applicable to many different kinds of terrain conditions whereas the Hata model is most relevant for terrain conditions characteristic of large cities or medium-small cities. Unlike previous models, UTCMOD considers communication link conditions (i.e the relative heights of transmitter, receiver, and terrain peaks along the path) and provides the correct perspective for analyzing the propagation effects. Also UTCMOD can be used to optimize many tactical communication (TAC COMM) and electronic warfare (EW) scenarios for Low Probability of Interception (LPI) performance.

Since, Low Probability of Interception (LPI) is important in both military and commercial applications, methods of analyzing LPI communication have been developed throughout the past decade. However, the existing LPI formulation is not sufficient because the previous LPI quality factor, Q_{LPI}, definitions are overly simplistic, too sensitive to range, and ignore atmosphere and terrain effects. Fortunately, these problems can

be resolved by using a new terrain quality factor, Q_{TER}, and a tactical quality factor, Q_{TAC}, which incorporates both system and environmental parameters. Finally, Q_{TER} and Q_{TAC} can be used to analyze tactical communication (TAC COMM) and electronic warfare (EW) scenarios in order to exploit terrain to create a communication advantage for friendly forces. Although this work was caste in a military perspective, all of the models, quality factors, and concepts are directly applicable in currently expanding commercial applications involving signal propagation in mountainous rural areas.

Diffraction Analysis and Tactical Applications

of Signal Propagation Over Rough Terrain

I. Introduction

Wireless personal communication is extremely important in modern warfare to enhance the mobility and effectiveness of military forces. The performance of wireless systems is highly predictable in free space where the received signal power(P_r) is a simple function of transmitted power (P_t), transmitter antenna gain (G_t), receiver antenna gain (G_r), wavelength (λ), and propagation distance (d) from the source [*Sklar*, 1988]. Specifically

$$P_r = \frac{P_t G_t G_r \lambda^2}{(4\pi)^2 d^2} \tag{1.1}$$

However, practical systems operate in a non-homogeneous, dispersive, anisotropic, lossy medium with random obstructions along the path. Whereas buildings may be the primary obstacles to radio waves in a flat urban environment, hills and mountains may be a major factor in other situations. In any case, obstacles cause additional propagation loss. In this work the effects of rough terrain are singled out for study and the intervening medium is assumed to be free space.

1.1 Background

In ground communications, the free space channel model is insufficient. There are many obstacles affecting the mean path-loss. Rough terrain such as mountains are an example of obstacles along a ground communication propagation path. Over a period of many years, a number of attempts at predicting the mean path-loss in the ground radio environment have been made. These include the Egli model, the Longley-Rice model, the Okumura method and the Hata model [*Peterson et al.*, 1995]. Of these models, the Hata model has often been used for analyzing ground communication paths to predict the mean

path-loss as a function of distance and antenna height. The model was based on extensive experimental studies that emphasized the height of the receiver point. Hata accounted for terrain conditions between the transmitter (Tx) and the receiver (Rx) with a correction parameter only suitable for "averaged" urban or rural conditions. Thus a different approach is required if one wants to predict path-loss over many different kinds of specific terrain conditions.

In wireless communications, obstacles create multiple propagation paths between the Tx and the Rx which cause constructive and destructive interference or what is commonly called multi-path interference. It is especially a problem in rough terrain and in urban environments [*Woerner et al.*, 1995]. During the past decade, many researchers have discovered communication schemes such as spread spectrum (SS) modulation which mitigate multi-path interference. SS provides resistance to signal interference from multiple transmission paths by exploiting the phase (delay) differences between the multiple signals arriving over paths of variable lengths [*Rappaport*, 1996]. In SS the modulated information is modulated (spread) a second time to expand the bandwidth of the transmitted signal larger than the original information bandwidth [*Feher*, 1995]. Thus single frequency propagation models must be extended to estimate the dispersive effects of wideband signals such as SS.

Secure communications that offer a low probability of interception (LPI) is a current issue in military communications. To achieve secure communications, various technologies such as adaptive antennas, SS modulation, interference suppression filters, and error control coding can be used to reduce the probability of signal interception by hostile forces. LPI quality factors (Q_{LPI}) [*Gutman and Prescott*, 1989][1] can be used to assess the performance of LPI techniques. Since the objective of LPI communications is to reduce, as much as possible, the range at which the signal can be intercepted by unfriendly receivers while at the same time maintaining, or even increasing, the communication range of the intended receiver, the terrain between both friendly and hostile Tx and Rx can be exploited to improve friendly communications while simultaneously degrading enemy interception and jamming. As noted earlier, the terrain between the Tx and the Rx alters path-loss and the received power, P_r. Communication range depends on P_r. Hence, there is a need

---

[1] LPI quality factors are derived in Chapter 6

to incorporated terrain conditions into LPI link analysis and Q_{LPI}. This analysis will result in a better assessment and understanding of the covertness and effectiveness of LPI communications.

1.2 Problem Statement and Objective

Wireless personal communication is one of the fastest growing fields in the engineering world and is an important means of ground communication in the military. This pervasive use of wireless communications in the military necessitates continued propagation research and the development of accurate propagation models. Since the free space propagation model is insufficient for analyzing ground communications, many additional factors such as rough mountainous terrain that can cause additional propagation path-loss and multi-path interference must be considered.

Also since SS is a commonly used technique to reduce signal interference from multiple transmission paths and to improve communication security, an analysis of SS propagation over rough terrain is important. Thus the goal of this thesis is to apply a reasonable propagation model for analyzing the mean path-loss of signals propagating over rough mountainous terrain. The model must be valid over various frequency ranges and provide a valuable tool and insight for analyzing LPI characteristics of ground communication systems.

1.3 Assumption

This research will be based on the following assumptions:

1. Atmospheric attenuation will be neglected because it can be readily accounted for by the Liebe model [*Liebe*, 1989] [*Ghordlo*, 1996].

2. The system losses will be ignored because they are system specific and independent of the propagation path.

3. The terrain conditions are assumed to be static. The time varying case can be handled by repeating the static calculations at each instant in time or by using the terrain statistics as an input to the static model.

4. The propagation path-loss can be estimated with a model that is a function of the terrain statistics. Furthermore, it is assumed that various terrain conditions can be adequately characterized by standard statistical metrics.

5. The ground or surface of the terrain is assumed to be a moderately good conductor to simplify the diffraction analysis. To account for other type materials, only the fundamental knife-edge or wedge diffraction calculations, would have to be changed.

6. Antennas are assumed to be omni-directional to simplify the analysis but antenna gain can be easily incorporated into the link analysis.

1.4 Scope

In this research, the analysis will be limited in the following ways:

1. The deterministic propagation channel model or *Real Terrain Diffraction Model* will be based on the geometric theory of diffraction (GTD) because this is an established method for computing diffracted fields. In this work, a "deterministic model" means that the diffracted fields and hence the path-loss are computed for a specific predetermined terrain profile.

2. Only very rough terrain conditions (relative to wavelength) between transmitter and receiver will be analyzed so that signal reflections from planar surfaces can be ignored. Furthermore, only forward signal diffraction will be considered. Although backward signal diffraction can be considered as a source of multi-path interference, the additional time delay associated with backward diffraction allows one to easily excise it with an appropriate receiver design.

3. The stochastic propagation channel model or *Universal Terrain channel Model* will be developed using *Monte Carlo* computer simulation methods [*Jeruchim et al*, 1992] and path-loss in decibels (dBs) will be computable from the terrain roughness statistics (i.e. mean and variance). In this work, a "stochastic model" means that the

path-loss is estimated from terrain statistics only and ignores the actual terrain profile details.

4. Interception by unfriendly receivers is the only electronic combat situation that will be addressed.

1.5 Approach

This research can be divided into the following steps:

1. Review the literature for effects of rough terrain on wireless communication.

2. Use GTD for estimating fields diffracted from a knife-edge.

3. Derive a method of applying GTD to rough terrain.

4. Show that the knife-edge approximation is reasonable and speeds up computations.

5. Create a computer program to calculate propagation path-loss for a specified terrain profile (i.e. a deterministic model).

6. Use Monte Carlo simulations on the deterministic model to derive a stochastic propagation channel model that predicts path-loss in decibel (dB) as a function of terrain statistics (mean, variance).

7. Modify the stochastic model to analyze dispersive channel effects on SS signals.

8. Develop a Terrain LPI Quality Factor (Q_{TER}) to account for terrain effects LPI performance.

9. Reformulate LPI analysis to account for both system and environmental factors via an overall tactical quality factor (Q_{TAC}).

10. Introduce an approach for simulating tactical communication (TAC COMM) and electronic warfare (EW) scenarios that accounts for the effects of terrain and possibly exploits terrain to create a COMM/EW advantage.

1.6 Materials, Data and Equipment

No special provisions are required for this research. Only the existing Sun SPARC network at the Air Force Institute of Technology (AFIT) will be required. Existing software, such as MATLAB will be adequate for this research.

The stochastic channel model will be applied to synthetic terrain data randomly generated by a MATLAB program. In addition, real terrain data of an area in Texas will be used for computer simulations that introduce a new electronic combat (EC) analysis program specifically designed to incorporate terrain effects for electromagnetic wave propagation.

1.7 Thesis Organization

This thesis consists of seven main chapters and seven appendixes. *Chapter II* of this thesis presents pertinent theory of signal propagation. The inadequacy of the free space propagation model for predicting the mean path-loss in the ground wireless communication are demonstrated with some examples (e.g multi-path interference). Also, problems with existing channel models are highlighted by reviewing the Hata model, one of the most widely used propagation models. It is shown that the Hata model inadequate for many different kinds of terrain conditions and is not valid over various frequency ranges. Finally, the chapter ends with a discussion of the desired characteristics of a good channel model. *Chapter III* covers diffraction theory which is fundamental for analyzing channels over rough terrain. The chapter begins with an introduction to McNamara's knife-edge diffraction equation which uses the geometric theory of diffraction (GTD) to compute the total electric field at the receiving point (E_{total}). The chapter concludes that McNamara's knife-edge equation is a reasonable model (approximation) for a variety of wedge-like obstacles. *Chapter IV* presents a deterministic channel model called the Real Terrain Diffraction Model (RTDMOD) which estimates additional diffraction path-loss from real terrain data. Based on terrain simulations and detailed diffraction calculations with RTDMOD, a stochastic propagation channel model called the Universal Terrain Channel Model is developed. *Chapter V* presents the Universal Terrain Channel Model (UTCMOD) and it's

various applications. UTCMOD is then compared with the Hata model to see how a model based on numerical experiments (UTCMOD) compares to a model based on physical experiments (Hata model). *Chapter VI* presents methods for assessing the LPI performance of tactical communication (TAC COMM) and electronic warfare (EW) scenarios. By using UTCMOD, the terrain LPI quality factor, Q_{TER}, and the tactical LPI quality factor, Q_{TAC}, it is shown than terrain can be exploited to gain a communication advantage for friendly forces. Finally, *Chapter VII* extracts conclusions from the results and proposes recommendations for future research.

The appendixes were written for the convenience of the reader. *Appendix A* lists the abbreviations and symbols used in this thesis. For completeness and to complement McNamara's formulation, Kraus' derivation for the total electric field due to diffractions presented in *Appendix B*. However, throughout the thesis, McNamara's knife-edge diffraction equation is used to compute the total field when a diffraction point is present. To conclude that the McNamara knife-edge equation is a reasonable model (approximation) for a variety of wedge-like obstacles, the Balanis' wedge diffraction equation is used to compare computations. For the reader's convenience, the Balanis' wedge diffraction equation is derived in *Appendix C*. *Appendix D* presents a new method that estimates lit diffraction path-loss (L_{lit}) over multiple subpath obstacles using path clearance and the first Fresnel zone radius as model parameters. The MATLAB codes used in this thesis can be found on the world wide web at *www.afit.af.mil/Schools/EN/ENG/LABS/C3EMRT/jyc.htm*. *Appendix E* contains the code names and details for obtaining the code online on the Internet for those interested in follow-on research. *Appendix F* is a bibliography. Finally, this thesis includes a useful index arranged in alphabetical order for the reader's convenience in *Appendix G*.

Also note that although this work is caste in a military perspective, all of the models, quality factors, and concepts are directly applicable in currently expanding commercial applications involving signal propagation in mountainous rural areas.

II. Pertinent Theory of Wireless Communication

2.1 Overview

A fundamental requirement for wireless communication is to maintain a sufficiently low probability of bit error (P_B) which is a function of the received signal power (P_r). Since, propagation obstacles that cause propagation path-loss and multi-path interference can adversely effect P_B, improvements in wireless communication require a reduction or mitigation of propagation path-loss and the multi-path interference.

In this chapter, pertinent topics in signal propagation, spread spectrum, and channel modeling will be reviewed. A special technique called the SS modulation is widely used in wireless communication because of it's inherent capability to reduce multi-path interference. Furthermore, a number of attempts at predicting the mean path-loss in the ground radio environment have been made. Of these models, the Hata model is often used for analyzing ground communication paths.

2.2 Signal Propagation

If there were no atmosphere nor obstacles in the signal propagation path, the wireless communication propagation problem would be much less complex. However since wireless communication signals are attenuated by the earth's atmosphere and obstacles, their effects must be included to account for the signal loss observed on practical communication links [*O'Brien et al.*, 1985]. In addition to transmitter signal power (P_t), absorption and scattering of signal power by the earth's atmosphere and obstacles along the propagation path are primary factors that determine the communication distance. We call this signal power reduction "path-loss".

In addition, constructive and destructive interference occurs when there are multiple propagation paths between the Tx and the Rx. This is called multi-path interference. Although multi-path interference does not occur in free space, practical ground communication propagation paths require analysis of the multi-path problem. Multi-path interference is especially a problem in rough terrain and in urban environments due to the presence of numerous large scattering objects such as mountains and buildings [*Woerner et al.*,1995].

2.2.1 **Received Power.** In free space, the received signal power(P_r) depends on parameters such as transmitted power, antenna gain, wavelength, and distance [*Sklar*, 1988].

$$P_r = \frac{P_t G_t G_r \lambda^2}{(4\pi d)^2} \tag{2.1}$$

- P_t : Transmitter power

- G_t : Transmitter antenna gain

- G_r : Receiver antenna gain

- λ : Wavelength

- d : Distance between transmitter and receiver

Furthermore, frequency is inversely proportional to wavelength. That is

$$f \;=\; \frac{v_p}{\lambda}$$

where v_p is the velocity of propagation determined by medium. Thus in free space, radio waves propagate with a path-loss characteristic of the form $A(f)d^{-2}$. In ground communications, the free space propagation model is insufficient. There are many factors affecting the mean path-loss. Over a period of many years, a number of attempts at predicting the mean path-loss in the ground radio environment have been made. These include the Egli model, the Longley-Rice model, the Okumura method, and the Hata model [*Peterson et*

al., 1995] which are discussed in section 2.4.

2.2.2 **Multi-Path Interference.** In ground communications, complex propagation paths cause multiple signals to arrive at the Rx as shown in Fig.2.1. Although the signal originates from only one transmitter, the car receiver is subjected to numerous signals that propagate through different paths. Similarly, rough terrain can create many indirect paths in addition to the direct or intended path. The signals over these multiple paths interfere with each others [*Parsons*, 1992]. This phenomena is called "multi-path interference". If the receiver detects the multi-path signals, then the received signal is very different from the transmitted signal and this causes degraded analog signals or decision errors in digital signals.

One way to mitigate multi-path interference is with spread spectrum communication techniques. The next section reviews spread spectrum communication.
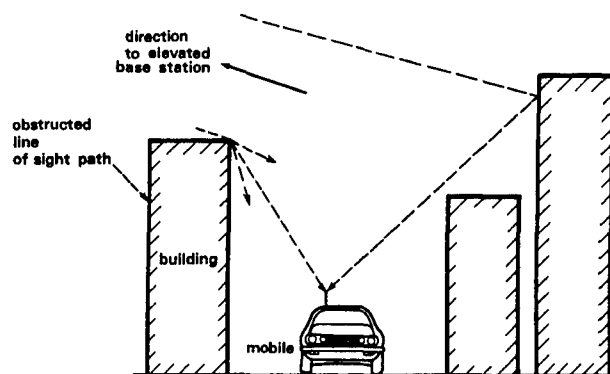
Figure 2.1   Multi-path from the transmitter to the receiver [*Parsons*, 1992]

2.3 Spread Spectrum

In all communications systems, the modulated waveform occupies a frequency bandwidth that is dependent upon the modulation method used and the data being sent. The modulation scheme under consideration for this research is spread spectrum (SS) communications. This field grew out of research efforts during World War II to provide a secure means of communication in hostile environments [*O'Brien et al*, 1985].

In a SS system, the transmitted bandwidth of the signal has been "spread" over a larger bandwidth than the original signal requires. To be classified as a SS system, the communication modem must have the following characteristics [*Rappaport*, 1996]:

1. The transmitted signal energy must occupy a bandwidth which is larger than the information bit rate (usually much larger) and which is approximately independent of the information bit rate.

2. Demodulation must be accomplished, in part, by correlation of the received signal with a replica of the signal used in the transmitter to spread the information signal.

SS has several applications and desirable advantages such as improvement of multi-path interference rejection capabilities, code division multiple access (CDMA) applications, and enhanced low probability of interception (LPI) capabilities[1] [*Feher*, 1995]. As an example, the U.S. Army uses modern tactical communication systems designed with SS technology precisely because these systems allow many users to operate in the same band without excessive interference [*Sass*, 1983]. In this research, only the multi-path interference rejection capabilities of SS is of interest. Also since propagation effects are frequency dependent, one must consider how channel dispersion affects SS performance. Therefore, the multi-path interference rejection capability of SS and the bandwidths of a variety of SS signals are discussed briefly in the next section.

2.3.1 Rejection Capability of Multi-path Interference.

Basically, the SS system is a system in which the transmitted signal is spread over a frequency much wider

---

[1] LPI capabilities will be discussed in chapter 6

than the minimum bandwidth required to send the signal. The baseband signal is spread out with a spreading code sequence. The actual signal spreading may be achieved with one of three basic techniques. These include :

1. Direct Sequence SS (DSSS) in which the information is spread by multiplying the information with a high bit rate pseudo-random digital code sequence.

2. Frequency Hopping SS (FHSS) in which the carrier is pseudo-randomly shifted into a number of different cells of bandwidth equal to that of the information bandwidth. The shifting is controlled by a code sequence.

3. Time Hopping SS (THSS) in which bursts of the modulated information are transmitted at pseudo-random time intervals dictated by a code sequence[2].

As an example of how SS can mitigate multi-path interference, DSSS will now be described in more detail.

DSSS, a popular form of spread spectrum processing is performed by effectively multiplying the original signal by a pseudo-noise (PN) digital signal. The PN signal is a fast code that is many times the data rate. They are called "pseudo-noise" because they are not real random Gaussian noise but are deterministic codes that appear to be random.

First the PN code is modulated onto the information signal using one of several modulation techniques (eg. BPSK, QPSK, etc). Then, a doubly balanced mixer is used to multiply the RF carrier and PN modulated information signal. This process causes the RF signal to be replaced with a very wide bandwidth. The demodulation process then simply consists of the mixing/multiplying of the same PN modulated carrier with the incoming signal. Fig.2.2 shows this basic DSSS technique. The output of the mixer in the receiver is a signal that is a maximum when the two signals are exactly equal to one another or are "correlated." The correlated signal is then filtered and sent to the demodulator. That is the correlation property of SS codes.

In ground communication, rough terrain causes one direct path and any number of indirect paths. If the transmitter and receiver use the same spread code, then the

---

[2]THSS is not addressed in this research because THSS systems have found no commercial application to date. However, the arrival of cheap random access memory (RAM) and fast micro-controller chips make time hopping a viable alternative SS technique for the future.
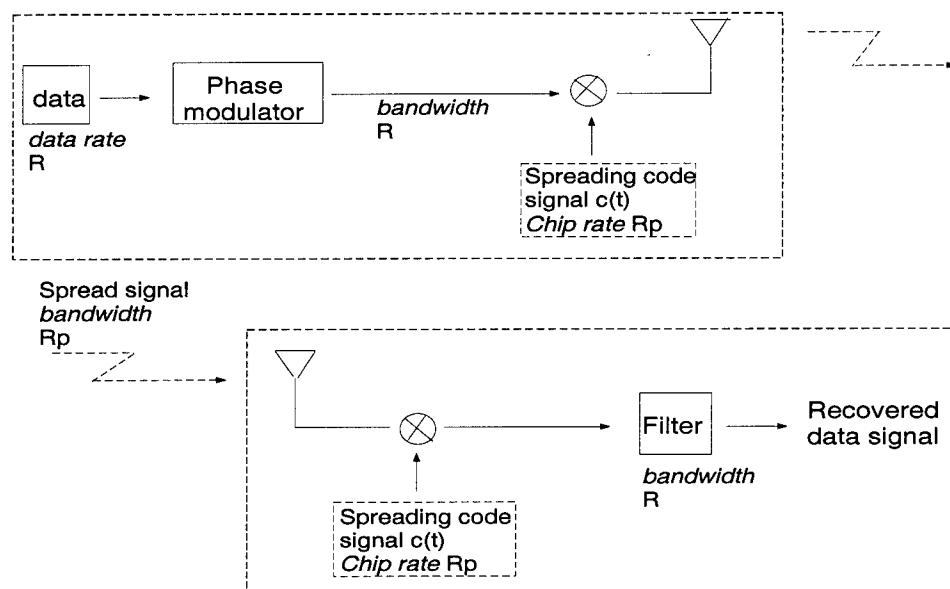
Figure 2.2 Basic SS technique.

receiver is synchronized with the direct path signal spread code and communication is possible. However, the received multi-path signal spread code will be out of phase with the transmitted code because the multi-path received signal has a different time delay. Due to the correlation properties of SS code, the multi-path received signal will be weak and effectively minimizes the multi-path interference problem [*Parsons*, 1992].

Fig.2.3 shows the received power density of the two different cases. In one case, the code is matched; in the other case, the code is unmatched. The direct path signal with the matched code has strong received power in the receiver (Fig.2.3.a). In contrast, the multi-path signal with the unmatched code has much less power (Fig.2.3.b). The receiver ignores the multi-path received signal and detects the direct path signal. In this manner, the multi-path interference problem can be mitigated using SS techniques [*Rappaport*, 1991].

2.3.2 **Spread Spectrum Bandwidth.**   The bandwidth in DSSS systems is often taken as the null-to-null bandwidth of the main lobe of the power spectral density plot. The null-to-null bandwidth of this lobe is 2Rc, where Rc is the chip rate. Therefore, the bandwidth of a DSSS system is a direct function of the chip rate. Fig.2.4 shows a basic

(a) code matched   (b) code unmatched
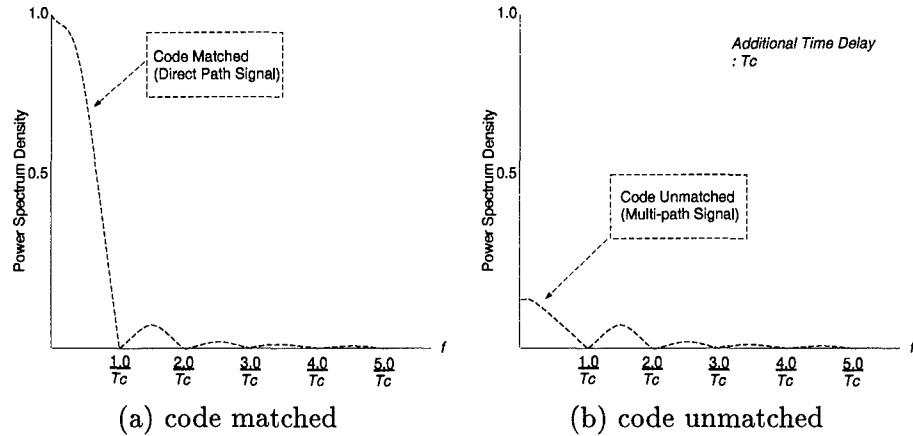
Figure 2.3   Power spectra of the received signal

DSSS signal and power spectrum density.

In contrast to DSSS, the bandwidth of FHSS is determined by the number of hop frequencies because frequency hopping relies on frequency diversity to combat interference. This is accomplished by a multiple frequency, code selected, FSK (frequency shift keying) technique. Basically, the incoming digital stream is shifted in frequency by an amount determined by a code. This effectively spreads the signal power over a wide bandwidth. One can think of the FHSS transmitter as a pseudo-noise PN code controlled frequency synthesizer. Fig.2.5 shows a typical FHSS modem. The instantaneous frequency output of the transmitter jumps from one value to another based on the pseudo-random input from the code generator. Varying the instantaneous frequency results in an output spectrum that is effectively spread over the range of frequencies generated. In this system, the number of discrete frequencies determines the bandwidth of the system. Fig.2.6 shows a pictorial representation of FHSS where W_d is the signal bandwidth before spreading (s_d (t) in Fig.2.5) and W_{ss} is the signal bandwidth after spreading (s_t (t) in Fig.2.5).

Whereas in a DSSS system, bandwidth is a direct function of the chip rate, in a FHSS system, bandwidth is determined by the number of discrete frequencies that in turn is determined by SS the code. Hence, bandwidth can be estimated by an operator who knows the properties of the SS code in use. Also, since the lowest frequency (f_l) and the

2-7
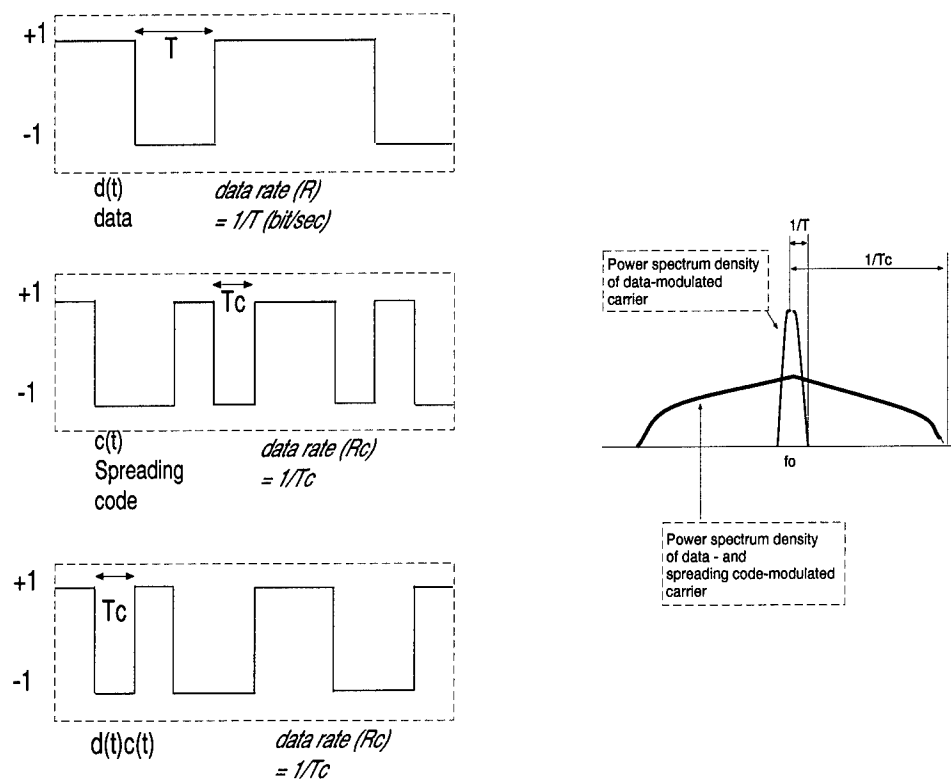
Figure 2.4   Basic DSSS signal and power spectrum density.
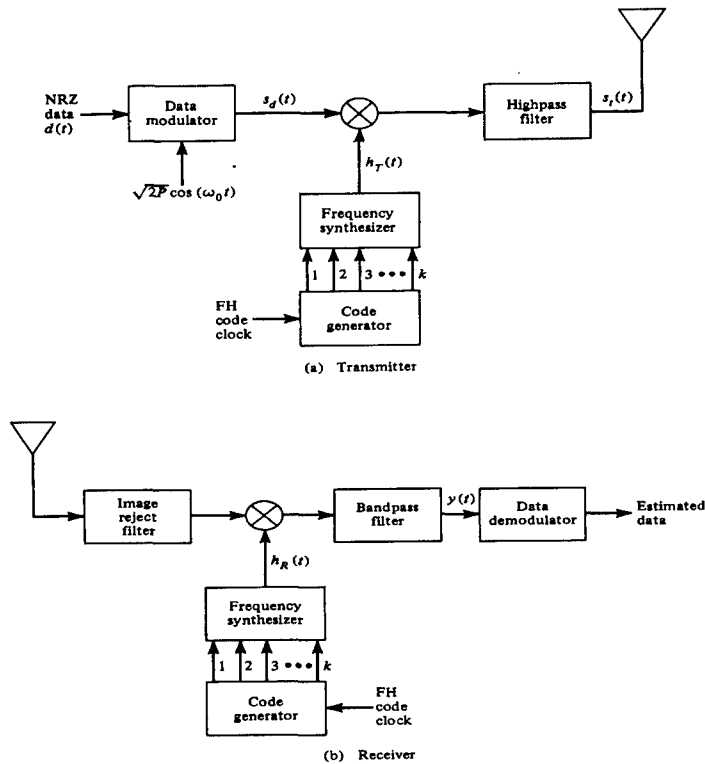
Figure 2.5   Basic FHSS modem [*Peterson et al.*, 1995].

a) Transmitted siganl
4-ary FSK

b) Transmitted signal
4-ary FSK and FHSS
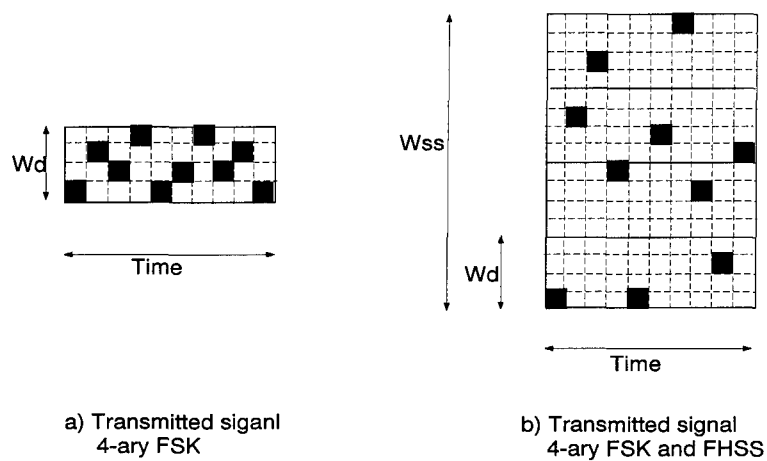
Figure 2.6   Pictorial representation of FHSS [*Peterson et al.*, 1995].

highest frequency (f_h) can be set, the propagation bandwidth is equal to f_h - f_l. For convenience, DSSS and FHSS parameters are summarized below:

1. DSSS.

   - bandwidth: $2R_c$(Hz). where R_c is chip rate.

   - frequency range: $[f_c - R_c] \sim [f_c + R_c]$. where f_c is carrier frequency.

   - f_l: $[f_c - R_c]$

   - f_h: $[f_c + R_c]$

2. FHSS.

   - bandwidth: $k \cdot \Delta f$.where k is the number of discrete frequencies that determined by SS code, Δf is hop frequency spacing.

   - frequency range: $f_c \sim [f_c + k \cdot \Delta f]$. where f_c is carrier frequency.

   - f_l: f_c

   - f_h: $[f_c + k \cdot \Delta f]$

   2.3.3 **Propagation of SS Signals.** Due to the relatively large bandwidth associated with SS, performance can be degraded in dispersive channels. Although SS methods are often effective in reducing multi-path interference problems, the performance of SS in extraordinarily complex propagation paths such as those characterized by extremely rugged terrain is not well understood [*Woener et al*, 1995]. Rough terrain has many different propagation obstacles adding complexity to path-loss predictions for wide bandwidth signals. Analyzing SS propagation over complex terrain is an important step towards improving SS performance in ground communications. Therefore, previous channel models that estimate path-loss are discussed in the next section.

2.4 **Channel Models**

   The prediction of path-loss is a very important step in planning an effective ground wireless radio system. Hence, much research focuses on creating propagation models that

determine the relationship between terrestrial paths and path-loss. There are several propagation models primarily developed for point-to-point mobile communication. These models are based on experimental results and are exemplified by the Egli model [*Egli*, 1957], the Longley-Rice model [*Longley and Rice*, 1968], the Okumura method [*Okumura et al.*, 1968], and the Hata model [*Hata*, 1980], which are all statistical propagation models. For example, the Egli model is a statistical model for predicting propagation loss in an urban or rural environment. However, it does not include diffraction losses caused by propagation over irregular terrain. The Longley-Rice model is applicable to point-to-point communication systems in the frequency range from 40 MHz to 100 GHZ. However, it does not consider correction factors to account for the effects of buildings. The Okumura method is based on an extensive experimental study of propagation path-loss predictions in various terrains for a specific frequency range. Okumura implicitly takes into account the effects of building in urban environments. The Hata model which is based on the Okumura method is a widely used propagation model that predicts path-loss in urban areas as a function of the communication distance and antenna heights in the following way [*Delisle et al.*, 1985] [*Jeruchim et al.*, 1992] [*Peterson et al.*, 1995]:

$$L = 69.55 + 26.16log(f_c) - 13.82log(h_{te}) - \alpha(h_{re}, f_c) + [44.9 - 6.55log(h_{te})] + log(d) \quad (2.2)$$

- L : Path loss (dB)

- f_c : Carrier frequency (MHz)

- h_{te} : Transmitter Antenna Height (m)

- h_{re} : Receiver Antenna Heigh (m)

- $\alpha(h_{re}, f_c)$: Correction factor (dB). Which is an explicit function of receiver antenna height and carrier frequency.

- d : Communication distance between transmitter and receiver (m)

where the correction parameter, α, is used to account for variation in the Rx antenna height. Expressions for the correction parameter for large cities and medium to small cities where developed from measured data and are given below for easy reference.

2-11

$$\alpha(h_{re}, f_c) = [1.1log(f_c) - 0.7]h_{re} - [1.56log(f_c) - 0.8](dB) \qquad \text{for a medium-small city}$$

$$\alpha(h_{re}, f_c) = 8.29[log(1.54h_{re})]^2 - 1.1(dB) \qquad \text{for a large city}, fc < 300MHz$$

$$\alpha(h_{re}, f_c) = 3.2[log(11.75h_{re})]^2 - 4.97(dB) \qquad \text{for a large city}, fc > 300MHz$$

With the Hata model, path-loss can be computed from antenna heights, the communication distance between Tx and Rx, and the carrier frequency. Since these parameters are usually known, the Hata model provides an easy method for predicting path-loss [*Peterson et al.*, 1995]. However the Hata model is not sufficient for predicting path-loss in rough terrain. The model is most relevant for terrain conditions characteristic of large cities or medium-small cities. Hence, the correction parameter is inadequate for many different kinds of terrain conditions not studied by Hata.

2.5 Summary

The prediction of propagation path-loss is a central question in the planning of wireless communication services and a number of approaches and statistical models are available for the prediction and calculation of path-loss for a variety of conditions. However, most propagation models have not been developed specifically for application to a specific communication channel, but rather from a more general perspective [*Delisle et al.*, 1985]. In ground communications, rough terrain presents a variety of propagation obstacles which increase the complexity of the direct path. Since communication channels over rough terrain are highly variable, a channel model that estimates mean path-loss over many different kinds of terrain conditions is desirable.

In addition, analysis of SS signal propagation over rough terrain using channel models that explicitly account for terrain statistics is an important step towards improving SS performance in rough terrain environments.

In the next chapter, the effect of obstacles on the propagation of elctromagnetic fields will be discussed and these results will form the basis for a new propagation model.

III. Diffraction Theory

3.1 Overview

A radio systems engineer may be interested in knowing a communication system's area coverage in areas that are highly mountainous or contain other irregularities that invalidate the standard planar earth approximations typically used for computing path attenuation. With the availability of fast computers, it is now possible to make numerical estimates of path-loss for rough terrain using the *Geometric Theory of Diffraction* (GTD), a technique that evaluates diffraction phenomena. In this thesis, calculations will be limited to diffraction from perfect electronical conducting (PEC) bodies to simplify the diffraction analysis.

Normally signal diffraction occurs when an obstacle exists in between the Tx and the Rx. If the obstacle blocks the direct line of sight (LOS), then the type of diffraction is called "shadow diffraction". On the other hand, if the obstacle is below LOS, then the diffraction is called "lit diffraction". In this chapter, lit diffraction, a common cause of multi-path interference, and shadow diffraction, a typical contribution to path-loss, will be analyzed in different ways.

3.2 History of Diffraction Theory

In 1947, Bullington suggested that a series of obstacles can be replaced by a single equivalent obstacle as a means of obtaining the path-loss in a simple manner [*Bullington*, 1947]. From that idea, numerous methods for computing attenuation due to diffraction were developed [*Pogorzelski*, 1982].

New approaches using the Geometric Theory of Diffraction (GTD) have received considerable attention in the past few years. These methods provide a correct diffraction loss factor and yield results consistent with the predictions of other methods. The GTD, originated by Keller [*Keller*, 1962] and extended by Pathak and Kouyoumjian [*Pathak and Kouyoumjian*, 1974] has been combined with the moment method for analyzing structures

which are small in terms of wavelength [*Burnside et al.*, 1975].

3.3 McNamara Diffraction Equation

3.3.1 **Huygens' Principle.** Huygens' principle states that *each point on a primary wavefront can be considered to be a new source of a secondary spherical wave and that a secondary wavefront can be constructed as the envelope of these secondary spherical waves*, as suggested in Fig.3.1. This fundamental principle of physical optics can be used to explain the apparent bending of radio waves around obstacles, (i.e., the diffraction of waves). A diffracted ray is one that follows a path that cannot be interpreted as either reflection or refraction.
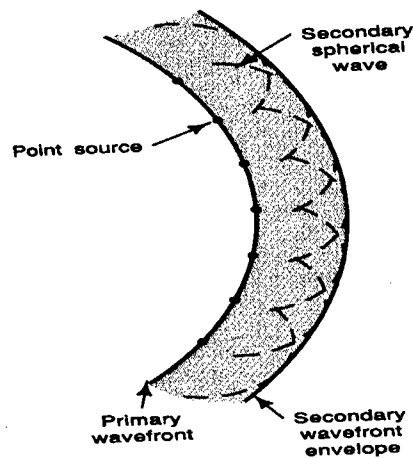
Figure 3.1   Illustrating Huygens' principle of physical optics (point-to wave correspondence) [*Kraus*, 1992].

3.3.2 **Total Received Electric Field (E_{total}) .**   Fig.3.2 illustrates the geometry for analyzing diffraction from a perfectly conducting half plane. By using Huygens' principle, the total field, E_{total}, at an observation point in the region x > 0 can be expressed
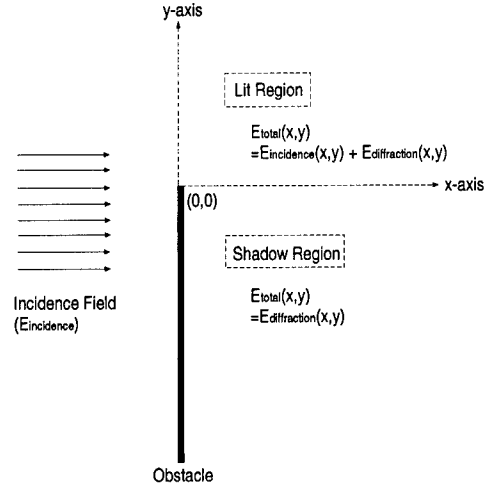
Figure 3.2   Diffraction from a perfectly conducting half-plane illuminated by a plane wave at normal incidence.

in the following manner [*McNamara et al.*, 1990] [1]:

$$E_{total}(x, y) \quad = \quad \frac{E_0 e^{-j(kx-\pi/4)}}{\sqrt{2}} \int_{-\gamma y}^{\infty} e^{-j(\pi/2)u^2} du \tag{3.1}$$

$$= \quad \frac{E_0 e^{-j(kx-\pi/4)}}{\sqrt{2}} \{[\frac{1}{2} - C(-\gamma y)] - j[\frac{1}{2} - S(-\gamma y)]\}. \tag{3.2}$$

for x > 0 where

x = distance from x=0 reference plane containing the obstacle (conducting half-plane),m

y = distance into shadow or lit region,m

λ = wavelength,m

E_0 = free space field strength

k = $2\pi/\lambda$

γ = $2/\sqrt{\lambda x}$.

---

[1]Kraus also derived an equation for total field. See *Appendix B. Kraus Diffraction Method* for more details.

The Fresnel integrals in Eq.3.2 are defined as follows [*Abramowitz and Stegun*, 1964]:

$$C(x) = \int_0^x cos\frac{\pi u^2}{2} du \qquad \text{Fresnel cosine integral}$$

$$S(x) = \int_0^x sin\frac{\pi u^2}{2} du \qquad \text{Fresnel sine integral.}$$

If the obstacle blocks the direct line of sight (LOS) between the Tx and the Rx, only the diffracted signal can be detected because Rx is in the shadow region. In this case, the total field is solely due to *shadow diffraction*.

However, if the obstacle does not block the direct LOS, then the receiver detects both a diffracted field (called *Lit diffraction*) and the original incidence field. Thus these two cases, shadow and lit diffraction, will be distinguished throughout this thesis.

For easy reference, the different diffraction cases are summarized in Table 3.1[2].

Diffraction Boundary	Position of Rx	Direct LOS between Tx and Rx	E_{total}
Shadow Diffraction	Rx in Shadow region	Blocked by Obstacle	$E_{diffraction}$
Lit Diffraction	Rx in Lit region	Not Blocked by Obstacle	$E_{incidence} + E_{diffraction}$

Table 3.1   Diffraction boundary

3.3.3   **X and Y Values.**   In Eq.3.2, total field (E_{total}) at the Rx can be calculated with x (distance from reference plane containing the obstacle) and y (distance into shadow or lit region). If the incidence field ($E_{incidence}$) is not perpendicular to the obstacle, one must redefine the x and y values as shown in Fig.3.5 before using Eq.3.2 to calculate E_{total}. Thus for an arbitrary incidence angle, E_{total} can be computed as follows:

---

[2]The total field in the x < 0 region would be a superposition of the incident and diffracted fields along with a component reflected from the obstacle.

$$E_{total}(x,y) \quad = \quad \frac{E_0 e^{-j(kx-\pi/4)}}{\sqrt{2}} \{[\frac{1}{2} - C(-\gamma y)] - j[\frac{1}{2} - S(-\gamma y)]\} \qquad (3.3)$$

where x and y are now given by

$$x \quad = \quad \rho \cdot cos[\pi - (\phi - \phi')] \qquad \text{in the lit region} \qquad (3.4)$$

$$= \quad \rho \cdot cos[(\phi - \phi') - \pi] \qquad \text{in the shadow region} \qquad (3.5)$$

$$y \quad = \quad \rho \cdot sin[\pi - (\phi - \phi')] \qquad \text{in the lit region} \qquad (3.6)$$

$$= \quad -\rho \cdot sin[(\phi - \phi') - \pi] \qquad \text{in the shadow region.} \qquad (3.7)$$

Note that the lit and shadow regions are now defined in the following manner
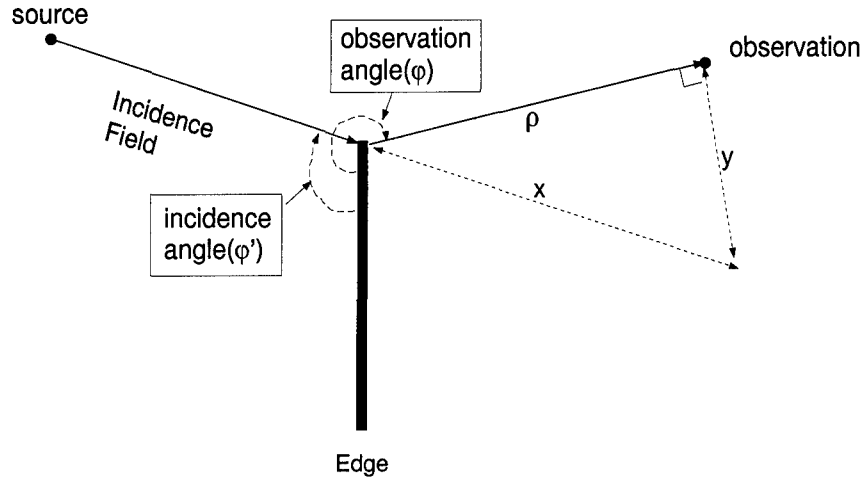
Figure 3.3 Incidence angle(ϕ') and Observation angle(ϕ).

$$\begin{bmatrix} \text{Lit Region} & : & \pi/2 < (\phi - \phi') < \pi \\ \text{Shadow Region} & : & \pi < (\phi - \phi') < 2\pi \end{bmatrix}. \qquad (3.8)$$

3.3.4 **Wedge Obstacles.** Although Eq.3.2 gives E_{total} at an observation point and is easily used as a key concept for estimating signal path-loss, it is based on the assumption that the obstacle is a knife-edge. However, normally the obstacle is not a knife-edge but a wedge which has an angle at it's apex. In the next section, McNamara's

equation (Eq.3.2) for a knife-edge will be compared to the Balanis' equation for a wedge.

3.4 Balanis' Wedge Diffraction Equation

One equation that calculates E_{total} at the Rx by considering the angle of the obstacle is suggested by Balanis [*Balanis*, 1989] [3]. Balanis derived E_{total} has the form of

$$E_{total} = E_0 \cdot \mathcal{D} \cdot \mathcal{A} \cdot e^{-j\beta s} \tag{3.9}$$

where

$$
\begin{aligned}
\mathcal{D} &= \text{Diffraction coefficient} \\
\mathcal{A} &= \text{Spatial attenuation} \\
\beta &= \text{Wave Number}(= 2\pi/\lambda) \\
s &= \text{Distance from the Obstacle}
\end{aligned}
$$

$\mathcal{D}$ and $\mathcal{A}$ are function of the incidence angle (ϕ'), the observation angle (ϕ), and the wedge angle. Also $\mathcal{D}$ and $\mathcal{A}$ are get out of values with different angle of obstacle.

3.5 Knife-Edge and Wedge Diffraction Comparisons

To verify that McNamara's equation is a reasonable approximation for the diffracted field from wedge like obstacles, the following numerical comparisons were performed:

1. Compare E_{total} computed with McNamara's knife-edge equation to E_{total} computed with Balanis' wedge equation with the wedge angle set to zero.

   - Estimate ϕ, ϕ' and ρ for a given obstacle. Calculate x and y.

---

[3]Balanis calculates E_{total} with a diffraction coefficient and spatial attenuation. In *Appendix C. Balanis' Wedge Diffraction Equation*, whole equations are derived.

- Calculate E_{total} with McNamara's knife-edge equation (Eq.3.2).

- Calculate E_{total} with Balanis' wedge equation[4] with the wedge angle of the obstacle set equal to zero.

- Compare the difference in dB between $|E_{total}|^2$ computed using the McNamara and Balanis equations.

2. Compare E_{total} computed with McNamara's knife-edge equation to E_{total} computed with Balanis' wedge equation for a variety of wedge angles.

   - Estimate ϕ, ϕ' and ρ for a given obstacle. Calculate x and y.

   - Calculate E_{total} with McNamara's knife-edge equation (Eq.3.2). In McNamara's equation, the angle of the obstacle is ignored because the actual obstacle is approximated by a knife-edge.

   - Calculate E_{total} with Balanis' wedge equation to account for the wedge angle of the obstacle. Of course E_{total} will be different for obstacles with different wedge angles.

   - Compare the difference in dB between $|E_{total}|^2$ computed using the McNamara and Balanis' equations for wedge angles ranging from $\frac{\pi}{1000}$ to $\frac{\pi}{2}$.

Fig.3.4 shows examples of $|E_{total}|^2$ difference (dB) between the McNamara knife-edge and the Balanis wedge computation (*angle of obstacle is zero*). The results for $|E_{total}|^2$ computed by the two different methods are very close unless $\phi \pm \phi' = n\pi$ where n is an integer[5].

E_{total} varies with the wedge angle of the obstacle(wedge) in Balanis' theory. Fig.3.5 shows examples of the difference (dB) between computating $|E_{total}|^2$ with McNamara's knife-edge calculation and Balanis' equation for a general wedge.[6] The results of the $|E_{total}|^2$ comparison is very close unless the wedge angle is large. Thus obstacles which roughly correspond to wedges (e.g. mountains) can be reasonably replaced by knife-edges and McNamara's equation can be used to calculate E_{total} for many kinds of natural and

---

[4]See *Appendix C. Balanis' Wedge Diffraction Equation.*

[5]Difference of $|E_{total}|^2$ in decibel was calculated with a computer program(MATLAB). The Diffraction coefficient($\mathcal{D}$) is a function of $cot(\phi \pm \phi')$. If $\phi \pm \phi' = n\,\pi$, then $cot(\phi \pm \phi')$ is infinite and the computation is invalid.

[6]See *Appendix C. Balanis Wedge Diffraction Equation.*

man-made obstacles. Therefore, throughout this thesis, McNamara's equation (Eq.3.2) will be used to estimate any additional path-loss due to diffraction from an obstacle.

(a). $\phi = 1.25\,\pi$ (b). $\phi = 1.15\,\pi$
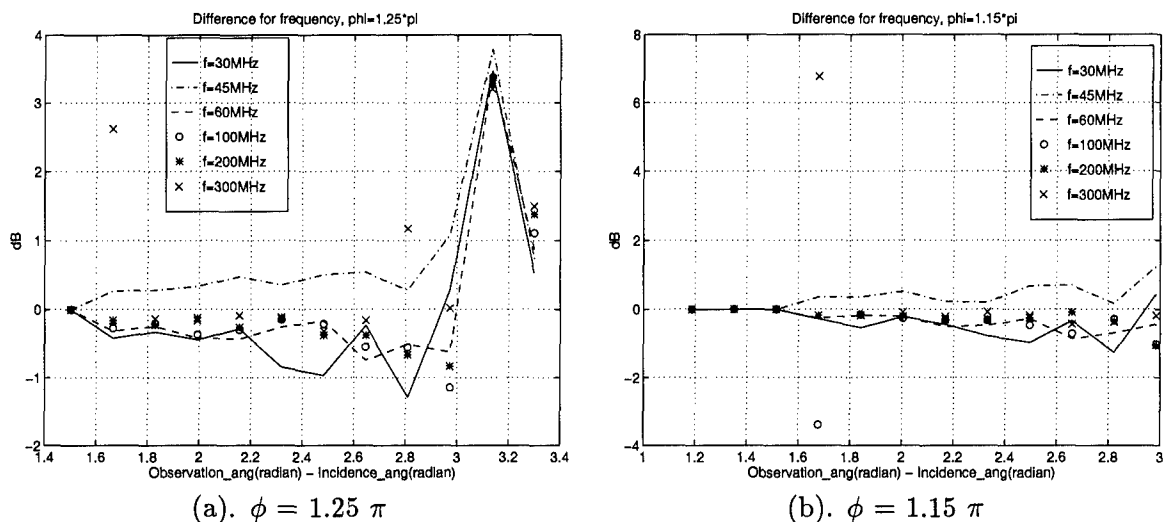
Figure 3.4   The difference between diffraction computations with McNamara's knife equation and Balanis' general wedge equation for the case of a knife-edge (i.e. a wedge with zero angle). *phi* is the observation angle (ϕ).

(a).f = 30MHz   (b). f = 50MHz
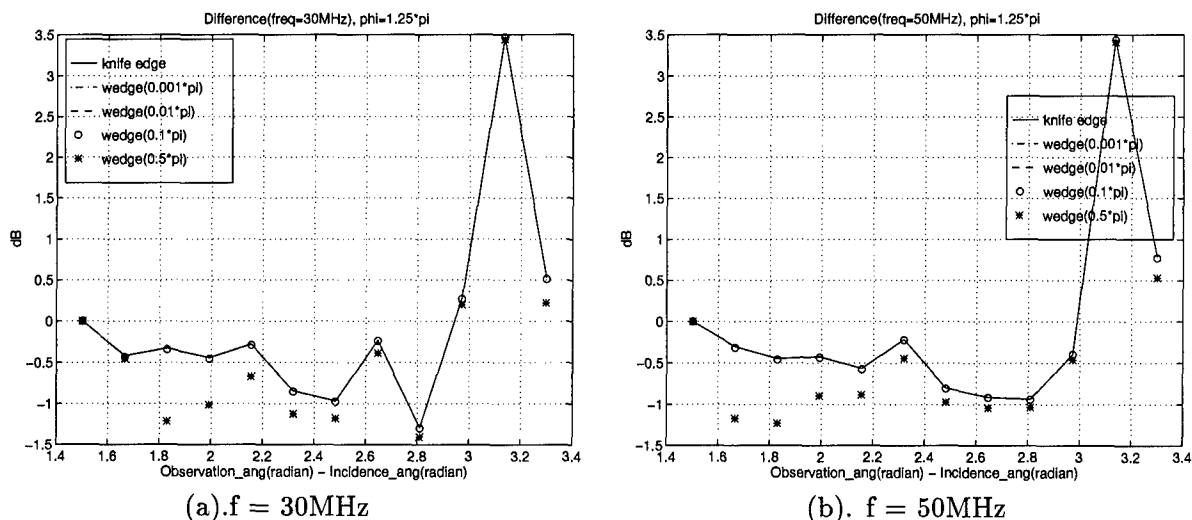
Figure 3.5   The difference between the knife-edge and the wedge diffracted fields for various wedge angles. *phi* is the observation angle (ϕ).

3.6 Summary

In this chapter, expressions for E_{total} based on the geometric theory of diffraction or GTD were given. After comparing computations using Balanis' wedge equation with computations using McNamara's knife-edge equation, one can conclude the McNamara knife-edge equation is a reasonable model (approximation) for a variety of wedge-like obstacles. Thus, additional path-loss due to diffraction can be computed by modeling the obstacle as a knife-edge. The extra precision gained with the Balanis wedge equation is not worth the associated computational burden. Hence, McNamara's equation will be used to estimate additional propagation path-loss due to diffraction throughout this thesis.

Normally, propagation path-loss can be calculated from E_{total}. Received signal power (P_r) has the form of $|E_{total}|^2$. $|E_{total}|$ is the magnitude of the total field at the receiving point. In the next chapter, propagation path-loss prediction theory will be introduced. This theory is the basis for deriving a practical propagation channel model for electromagnetic propagation over rough terrain.

IV. Propagation Path-Loss

4.1 Overview

The actual propagation path-loss often exceeds the free space or plane earth modeled path-loss by several orders of magnitude. Furthermore, it is highly variable and fluctuates randomly as the Rx moves over irregular terrain. Hence, the prediction of path-loss is a very important step in planning mobile radio systems and accurate prediction methods are needed to determine the parameters of a radio system that will provide efficient and reliable service area coverage [*Parsons*, 1992]. In this chapter, a path-loss prediction method, based on the propagation of electromagnetic fields over obstacles, will be introduced. A sample computer application will be presented in section 4.5.

4.2 Path-Loss for One Obstacle

An obstacle between the Tx and the Rx causes additional power loss or *path-loss*. This diffraction path-loss can take several forms. One, *shadow diffraction path-loss* (L_{shadow}), occurs when the Rx is in the geometric shadow region. Another, *lit diffraction path-loss* (L_{lit}), occurs when the Rx is outside of the shadow region and is related to multi-path interference.

4.2.1 **Shadow Diffraction.** Fig.4.1 shows a communication link which has one obstacle between the Tx and the Rx. If the effect of the obstacle is ignored , the received signal power (P_r) will be estimated using the free space formula as following:

$$P_r = \frac{P_t G_t G_r \lambda^2}{(4\pi d)^2}.$$

(4.1)

However, if obstacle blocks the direct LOS between the Tx and the Rx, then a signal will be generated in the shadow region. Normally, in the shadow region, the magnitude of the electromagnetic field at the Rx is less than the free space field. Hence, the power attenuation (L_{shadow}) caused by an obstacle alters P_r from that predicted by Eq.4.1.
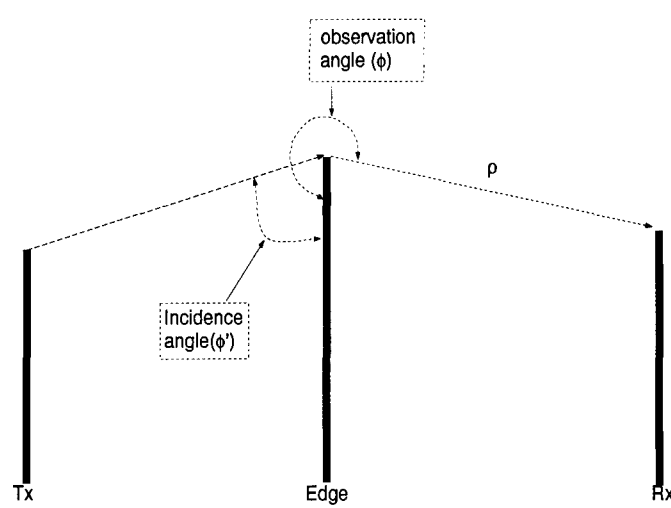
Figure 4.1   One obstacle between Tx and Rx

$$P_r = \frac{P_t G_t G_r \lambda^2}{(4\pi d)^2 L_{shadow}} \qquad (4.2)$$

L_{shadow} in Eq.4.2 is the power loss in addition to free space loss. L_{shadow} can be calculated from the total electric field, E_{total}, at the receiving point for the case of the Rx in the shadow region . The power density at the receiving point is

$$S_{av} = \frac{E_{total} E_{total}^*}{2Z} \qquad (4.3)$$

where Z is the impedance of the medium and E_{total} is given by Eq.3.2 which is repeated here for the reader's convenience.

$$E_{total}(x, y) = \frac{E_0 e^{-j(kx - \pi/4)}}{\sqrt{2}} \{[\frac{1}{2} - C(-\gamma y)] - j[\frac{1}{2} - S(-\gamma y)]\} \quad (4.4)$$

$$x = \rho \cdot cos[(\phi - \phi') - \pi] \quad (4.5)$$

$$y = -\rho \cdot sin[(\phi - \phi') - \pi] \quad (4.6)$$

$$\gamma = 2/\sqrt{\lambda x} \quad (4.7)$$

$$E_0 = \text{Free space electric field} \quad (4.8)$$

Hence,

$$S_{av} = \frac{E_0 E_0^*}{2Z} \frac{1}{2}([\frac{1}{2} - C(-\gamma y)]^2 + [\frac{1}{2} - S(-\gamma y)]^2)(W m^{-2}) \quad (4.9)$$

or

$$S_{av} = S_0 \frac{1}{2}([\frac{1}{2} - C(-\gamma y)]^2 + [\frac{1}{2} - S(-\gamma y)]^2)(W m^{-2}) \quad (4.10)$$

where

$$S_0 = \frac{E_0 E_0^*}{2Z}. \quad (4.11)$$

where S_0 is free space power density. The unit-less relative value (S_{rel}) is defined as the actual average received power density normalized by the free space power density.

$$S_{rel} = \frac{S_{av}}{S_0} = \frac{1}{2}([\frac{1}{2} - C(-\gamma y)]^2 + [\frac{1}{2} - S(-\gamma y)]^2) \quad (4.12)$$

$$S_{av} = S_0 \cdot S_{rel} \quad (4.13)$$

Therefore

$$P_r = S_{av} A_r \quad (4.14)$$

where A_r is Rx antenna effective area (m^2) and

$$A_r = \frac{G_r \lambda^2}{4\pi} \quad (4.15)$$

$$S_0 = \frac{P_t G_t}{4\pi d^2} \tag{4.16}$$

Thus

$$P_r = \frac{P_t G_t G_r \lambda^2}{(4\pi d)^2} \frac{1}{2}([\tfrac{1}{2} - C(-\gamma y)]^2 + [\tfrac{1}{2} - S(-\gamma y)]^2). \tag{4.17}$$

Or written another way

$$P_r = \frac{P_t G_t G_r \lambda^2}{(4\pi d)^2 L_{shadow}} \tag{4.18}$$

and

$$L_{shadow} = \frac{1}{\frac{1}{2}([\tfrac{1}{2} - C(-\gamma y)]^2 + [\tfrac{1}{2} - S(-\gamma y)]^2)}. \tag{4.19}$$

4.2.2 Lit Diffraction.

L_{shadow} occurs when an obstacle blocks the direct LOS between the Tx and the Rx. However, even if the obstacle did not block the direct LOS, the path-loss may still exceed the free space case. This path-loss is called *lit diffraction path-loss* (L_{lit}). The term lit means being excited by the incidence wave (field).

For this case, the total field at the Rx is composed of two terms. One is the incidence field, the other is the diffraction field. Thus the total electric field at the Rx is given by Eq.3.2 which are repeated here.

$$E_{total} = E_{incidence} + E_{diffraction} \tag{4.20}$$

$$= \frac{E_0 e^{-j(kx-\pi/4)}}{\sqrt{2}} \{[\tfrac{1}{2} - C(-\gamma y)] - j[\tfrac{1}{2} - S(-\gamma y)]\} \tag{4.21}$$

where

$$\gamma = 2/\sqrt{\lambda x} \tag{4.22}$$

The x and y values are given by Eq.3.3 and Eq.3.5 which are also repeated here for convenience.

$$x = \rho \cdot cos[\pi - (\phi - \phi')]$$

$$y = \rho \cdot sin[\pi - (\phi - \phi')].$$

It is often convenient to express L_{lit} in terms of the first Fresnel zone radius, F_1, and the path clearance, h_c. Referring to Fig.4.2, the radius of first Fresnel zone (F_1) is [*Flock*, 1987],

$$F_1 = \sqrt{\frac{\lambda d_T d_R}{d_T + d_R}} (m).$$ (4.23)

To avoid significant additional path-loss, a clearance of about $(0.6)F_1$ or more is required.
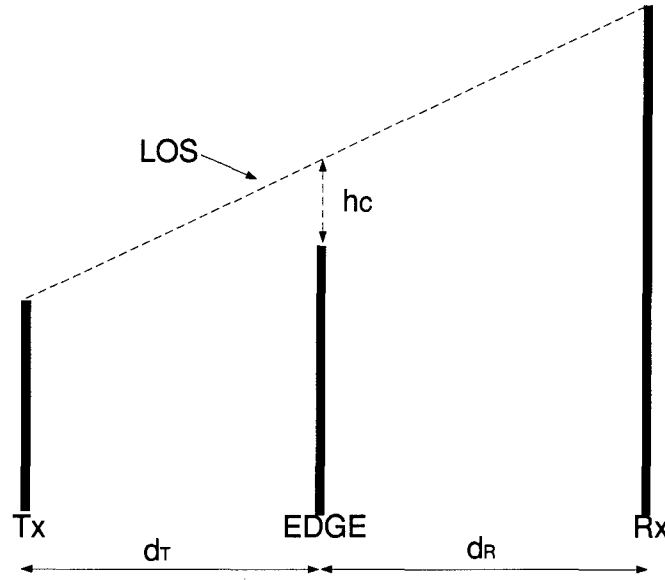
Figure 4.2   Subpath Diffraction

Defining the diffraction parameter (v) equal to $\sqrt{2} \frac{h_c}{F_1}$, the total electric field will be [*Flock*. 1987];

$$E_{total} = \frac{E_0 e^{-j(kx - \pi/4)}}{\sqrt{2}} \{ [\frac{1}{2} + C(v)] - j[\frac{1}{2} + S(v)] \}$$ (4.24)

Thus

$$S_{av} = \frac{E_{total} E_{total}^*}{2Z}$$ (4.25)

Hence,

$$S_{av} = \frac{E_0 E_0^*}{2Z} \frac{1}{2} ([\frac{1}{2} + C(v)]^2 + [\frac{1}{2} + S(v)]^2)(Wm^{-2})$$ (4.26)

or

$$S_{av} = S_0 \frac{1}{2}([\frac{1}{2} + C(v)]^2 + [\frac{1}{2} + S(v)]^2)(Wm^{-2}) \qquad (4.27)$$

where

$$S_0 = \frac{E_0 E_0^*}{2Z}. \qquad (4.28)$$

Hence, the unit-less relative value (S_{rel}) is

$$S_{rel} = \frac{S_{av}}{S_0} = \frac{1}{2}([\frac{1}{2} + C(v)]^2 + [\frac{1}{2} + S(v)]^2) \qquad (4.29)$$

and

$$S_{av} = S_0 \cdot S_{rel} \qquad (4.30)$$

Therefore

$$P_r = S_{av} A_r \qquad (4.31)$$

where A_r is Rx antenna effective area (m^2) and

$$A_r = \frac{G_r \lambda^2}{4\pi} \qquad (4.32)$$

$$S_0 = \frac{P_t G_t}{4\pi d^2} \qquad (4.33)$$

After substitution of the above quantities, the received power can be written as

$$P_r = \frac{P_t G_t G_r \lambda^2}{(4\pi d)^2} \frac{1}{2}([\frac{1}{2} + C(v)]^2 + [\frac{1}{2} + S(v)]^2) \qquad (4.34)$$

or

$$P_r = \frac{P_t G_t G_r \lambda^2}{(4\pi d)^2 L_{lit}} \qquad (4.35)$$

where

$$L_{lit} = \frac{1}{\frac{1}{2}([\frac{1}{2} + C(v)]^2 + [\frac{1}{2} + S(v)]^2)}. \qquad (4.36)$$

4.2.3 **Multiple Obstacle Considerations.** The analysis as described above applies to the case of only one obstacle between the Tx and the Rx. However, in general ground communication, there are many obstacles that cause signal diffraction and path-loss. Hence, a channel model or method that calculates propagation path-loss over rough terrain must be able to:

1. Analyze terrain data to determine the Lit and Shadow diffraction points.

2. Replace the diffraction points with a multiple knife-edge sequence.

3. Calculate L_{shadow} and L_{lit} for propagation over multiple knife-edges.

In the next section, a method for calculating path-loss over rough terrain that has multiple diffraction points (knife-edges) will be introduced.

4.3 **Path-Loss for Multiple Diffraction Points**

The diffraction path-loss for multiple diffraction points is divided into two terms. One is L_{shadow}, the other is L_{lit}. L_{shadow} may be estimated by using a sequence of shadow diffraction knife-edges (shadow edge). However, L_{lit} is not easily derived from a sequence of knife-edges. In this section, a method for computing L_{shadow} for multiple diffraction points will be introduced and a new method that calculates L_{lit} for rough terrain will be suggested.

4.3.1 **Shadow Diffraction.** It was suggested that a series of obstacles can be approximated by a sequence of knife-edges as a means of obtaining the path-loss in a simple manner. If we find the shadow diffraction points that satisfy the following conditions, each point can then be approximated by a shadow edge.

1. Each diffraction point must lie on or above a direct LOS line between the Tx and the Rx.

2. Each diffraction point lies along the shortest propagation path between the previous diffraction point and the next diffraction point.

3. The LOS between each adjacent diffraction point must be free of obstruction.

Fig.4.3 shows how a sequence of shadow edges are used to model real terrain. Note that the two diffraction points meet all three of the conditions stated above. From the sequence of shadow edges, the total L_{shadow} between the Tx and the Rx can be estimated. Each shadow edge results in a loss that be estimated with Eq.4.19.
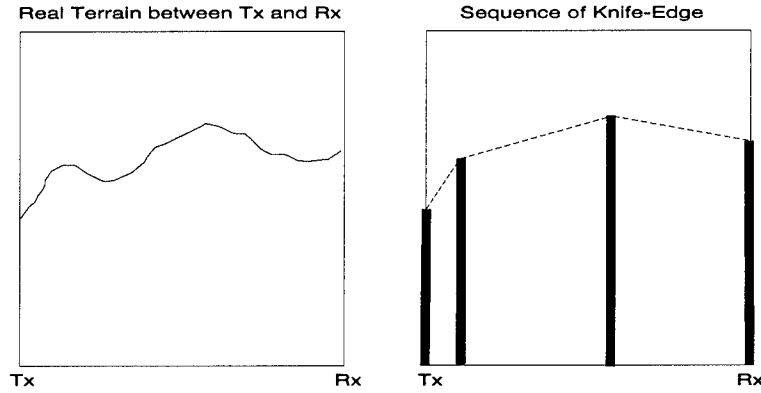
Figure 4.3   Real terrain and sequence of shadow knife-edge

$$L_{shadow} = \frac{1}{\frac{1}{2}([\frac{1}{2} - C(-\gamma y)]^2 + [\frac{1}{2} - S(-\gamma y)]^2)} \qquad (4.37)$$

$$x = \rho \cdot cos[(\phi - \phi') - \pi] \qquad (4.38)$$

$$y = -\rho \cdot sin[(\phi - \phi') - \pi] \qquad (4.39)$$

$$\gamma = 2/\sqrt{\lambda x} \qquad (4.40)$$

where

ϕ' :   Incidence angle from the front edge   See Fig.4.1

ϕ :   Observation angle to the next edge   See Fig.4.1

The total shadow diffraction loss, L_{shadow} (in dB), between the Tx and the Rx can be calculated by simply summing each of the individual L_{shadow} (in dB) due to each knife-edge along the path.

$$L_{shadow} = \sum_{i=1}^{N} L_i \qquad\qquad \text{N : Number of shadow diffraction edges} \qquad (4.41)$$

4.3.2 **Lit Diffraction.** Eq.3.2 gives the total field at the receiving point. In the lit region, the total field is composed of an incidence field and a diffraction field. The diffraction field due to one subpath obstacle can be obtained by subtracting the incidence field from the total field.

$$E_{diffraction} = E_{total} - E_{incidence} \qquad (4.42)$$

The total field in the lit region due to multiple subpath obstacles is

$$E_{total} = \sum_{i=1}^{N} E_i + E_{incidence} \qquad (4.43)$$

where N is the number of lit edges (subpath obstacles) and E_i is the diffraction field, $E_{diffraction}$, due to the i-th lit edge (subpath obstacle). However, Eq.4.43 is not practical for calculating L_{lit} over rough terrain because of the many possible path one could consider. Hence, a new method that represents lit diffraction path-loss over multiple subpath obstacles using path clearance(h_c) and the first Fresnel zone radius(F_1) is simple to use. For a single subpath obstacle, the lit diffraction loss is given by[1]

$$L_{lit}(dB) \;=\; 6 - \frac{h_c}{F_1} \cdot 10 \qquad \text{for } 0 < h_c < (0.6)F_1 \qquad (4.44)$$

$$L_{lit}(dB) \;=\; 0 \qquad\qquad\qquad \text{otherwise} \qquad (4.45)$$

For multiple subpath obstacles, only the obstacle point that is closest to the LOS (line of sight) between Tx and Rx is used to evaluated h_c and F_1 in Eq.4.44. The effects of all other obstacles are ignored. Fig. 4.4 shows how real terrain can be modeled for lit diffraction calculations. The parameters in Fig. 4.4 are defined as follows:

- h_c: Height difference between LOS(line of sight) and terrain point that is closest to the LOS.

---

[1]See *Appendix D. L_{lit} for multiple subpath edges*
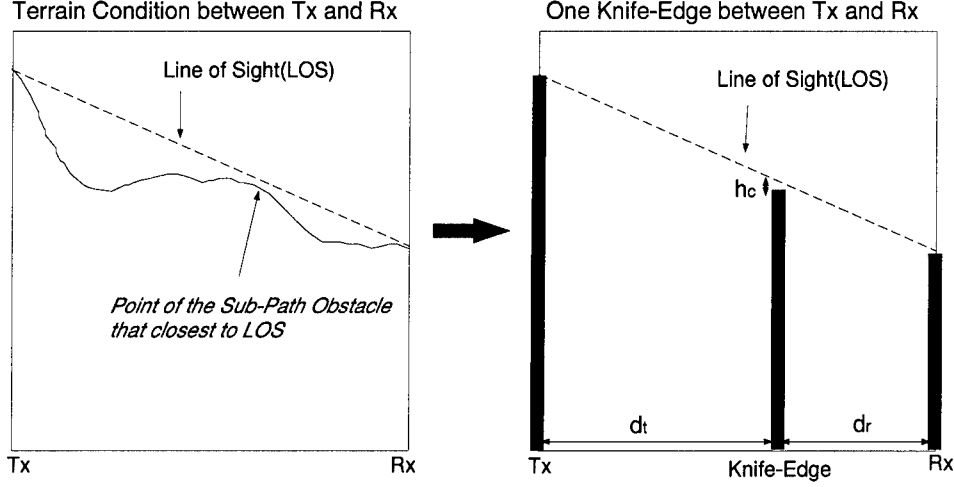
Figure 4.4 Modeling real terrain with knife-edges for computing L_{lit}

- d_t: Distance between the Tx and the point that is closest to the LOS.

- d_r: Distance between the diffraction point and the Rx.

- F_1: Radius of First Fresnel Zone($=\sqrt{\frac{\lambda \cdot d_t \cdot d_r}{d_t + d_r}}$)

In the next section, a method for calculating path-loss from real terrain data will be introduced. With this method, we can create a real terrain channel model that calculates overall path-loss.

4.4 Real Terrain Diffraction Model (RTDMOD)

In the previous section, L_{shadow}, and L_{lit} were derived. With these additional path-losses, the received signal power, P_r, arriving over a rough terrain channel can be estimated by

$$P_r = \frac{P_t G_t G_r \lambda^2}{(4\pi d)^2 L_{shadow} L_{lit} L_{atmosphere}} \tag{4.46}$$

where $L_{atmosphere}$ is the additional path-loss due to the atmosphere between the Tx and the Rx. However, throughout this thesis, atmospheric effects are neglected. Hence, the received signal power (P_r) is given by

$$P_r = \frac{P_t G_t G_r \lambda^2}{(4\pi d)^2 L_{shadow} L_{lit}}. \tag{4.47}$$

In Eq.4.47, P_r is clearly dependent on wavelength (λ) and communication distance (d) which determine the free space path-loss (L_{free}). Thus we can express P_r in the following compact form:

$$P_r = \frac{P_t G_t G_r}{L_{total}} \qquad (4.48)$$

where

$$L_{total} \;=\; L_{shadow} L_{lit} L_{free} \qquad (4.49)$$

$$L_{free} \;=\; \frac{(4\pi d)^2}{\lambda^2}. \qquad (4.50)$$

The total path-loss (L_{total}) between the Tx and the Rx can be calculated from real terrain data with the following steps:

1. Calculate L_{shadow}.

   (a) Model the terrain as a sequence of shadow diffraction edges using the procedures described in section 4.3.1.

   (b) Calculate L_{shadow} for each shadow diffraction edge using Eq.4.37.

   (c) Calculate total L_{shadow} by summing the individual diffraction losses.

2. Calculate L_{lit}.

   (a) Find the lit diffraction edge location as described in section 4.3.2.

   - Consider only the terrain data between the last shadow diffraction knife-edge and the receiver[2].

   - Find the point that is closest to the LOS(line of sight) between the last shadow diffraction knife-edge and the Rx. The other points will be ignored.

   (b) Calculate L_{lit} using Eq.4.44.

3. Calculate L_{free} using Eq.4.50.

---

[2]The lit diffraction resulting from a knife-edge that is in front of the last shadow diffraction knife-edge can be ignored because additional shadow diffraction will prevent the lit diffracted field from making a significant contribution to the total field at the Rx.

4. Compute L_{total} (in dB) by summing the different losses. L_{total} (dB) $= L_{shadow}$ (dB) $+ L_{lit}$ (dB) $+ L_{free}$ (dB)

Fig.4.5 shows how real terrain data can be replaced by an appropriate sequence of knife-edges. To simplify subsequent discussion, this method of computing diffraction loss will be called the Real Terrain Diffraction Model (RTDMOD).
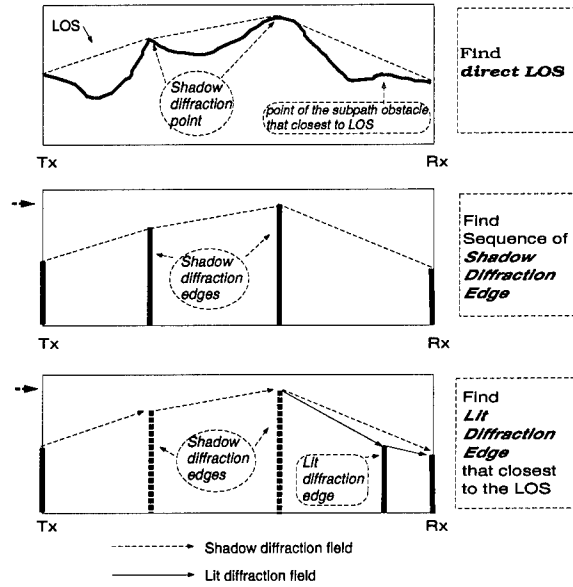
Figure 4.5   Sequence of knife-edges from real terrain

4.5   RTDMOD Computer Simulation

The method for calculating L_{total} from real terrain data discussed in the previous section was implemented in a MATLAB simulation (see Fig.4.6). In this section, some of the simulation results will be discussed.

The simulation depicted in Fig.4.6 computes propagation path-loss between a specific Tx point and each Rx point. Only the shortest communication path between the Tx and each Rx point was considered for this simulation.

A 1km × 1km section of the state of Texas as shown in Fig.4.7 was used as the real terrain data input. For this example simulation, 30MHz frequency was used for the carrier

(a)JANG1.m (MATLAB Function)   (b)PL-total.m (MATLAB Function)
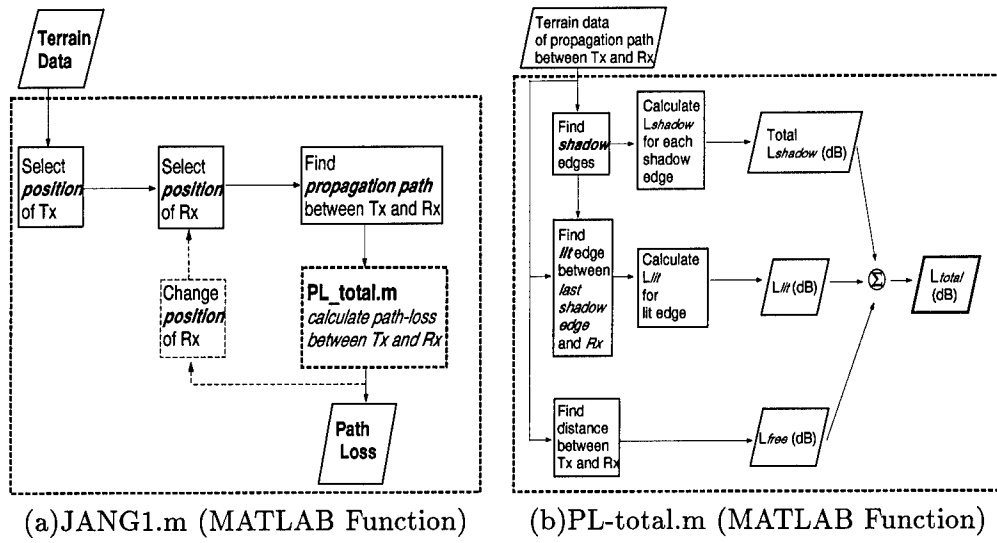
Figure 4.6   Outline of simulation

frequency.

L_{total} (dB), the total propagation path-loss, is shown in Fig.4.8. L_{shadow}, L_{lit}, and

(a)Terrain Mesh Plot   (b)Terrain Image Plot
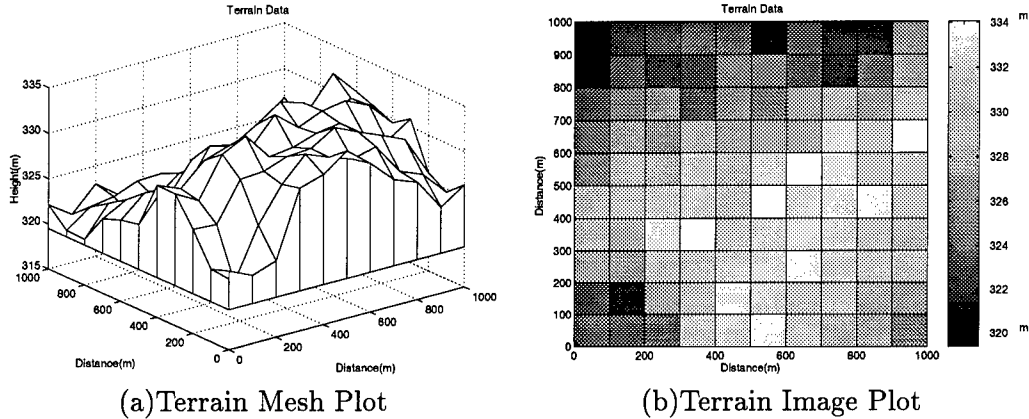
Figure 4.7   Input Terrain data

L_{free} for each receiving point are individually shown in Fig.4.9. Then with L_{total} available for each receiving point and knowledge of the transmit power, P_t, and the antenna gain, G_t and G_r, we can easily compute the received power, P_r, for each point with the following dB version of Eq.4.51:

$$P_r(dB) = P_t(dB) + G_t(dB) + G_r(dB) - L_{total}(dB). \tag{4.51}$$
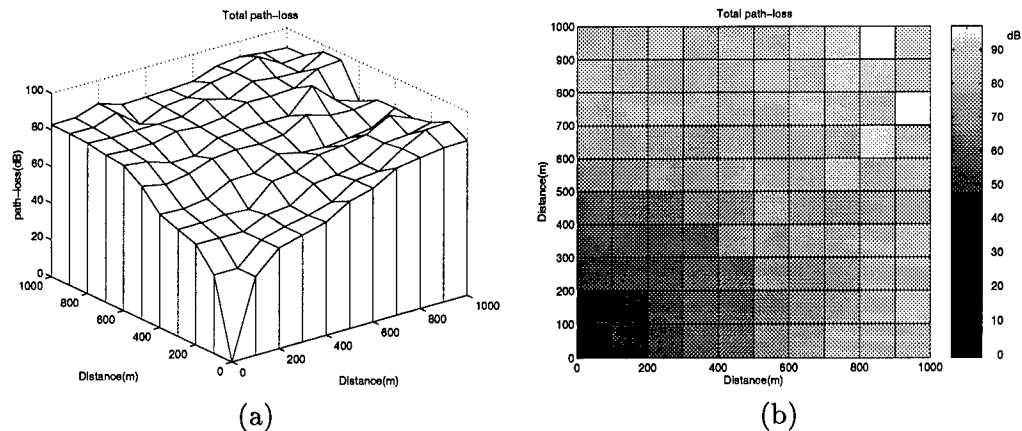
Figure 4.8   Total path-loss (L_{total}) profile

(a)L_{shadow} (b)L_{lit} (c)L_{free}
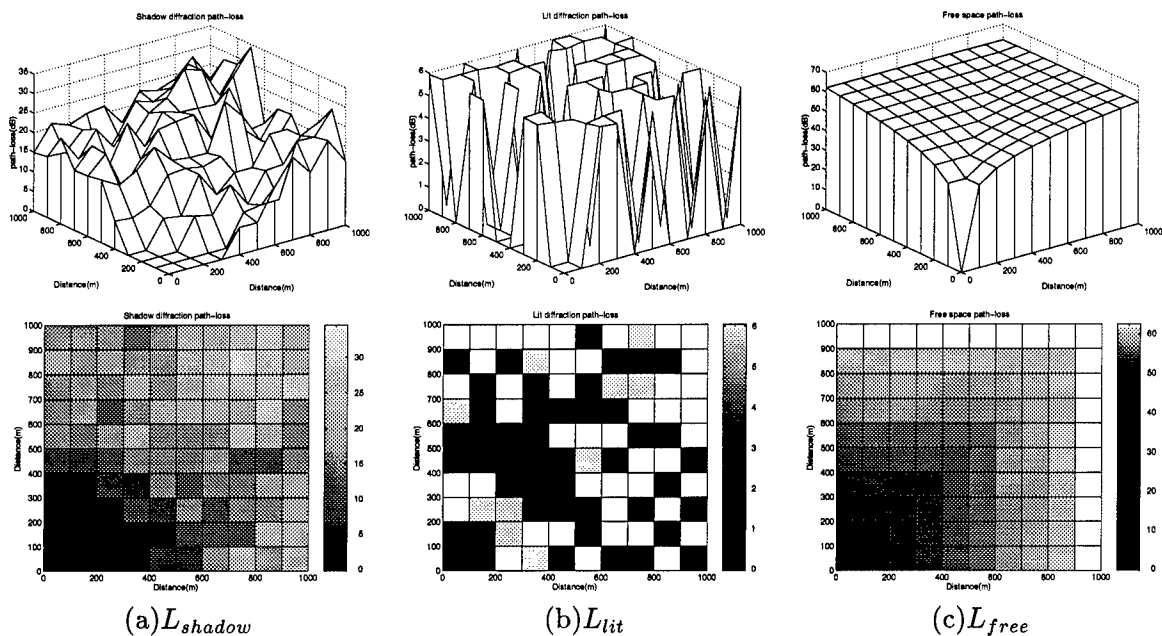
Figure 4.9   Path-Loss profile

4.6 RTDMOD Validation

Based on Bullington's ideas [*Bullington*, 1947], some techniques which predict the power attenuation due to signal diffraction were developed. Of these techniques, the Epstein-Peterson (EP) and the Deygout (DG) methods lead to the familiar GTD results [*Pogorzelski*, 1982]. Furthermore, the path-loss calculation model introduced in the previ-

ous section is also based on the GTD. In this section, the validity of this new model, the Real Terrain Diffraction Model (RTDMOD), will be confirmed by comparison with both the EP and the DG methods.

4.6.1 **Multiple Edge Construction of EP and DG Method.**   In both the EP and DG methods, the diffraction loss is dependent on the distance parameters (the sets $\{s_n\}$ and $\{d_n\}$). These distance parameters are calculated using the constructions shown in Fig.4.10. Notice that the set $\{s_n\}$ is the same for both the EP and DG constructions but the set $\{d_n\}$ is defined differently in each case.

Using these distance parameters, the propagation path-loss can be predicted by the EP
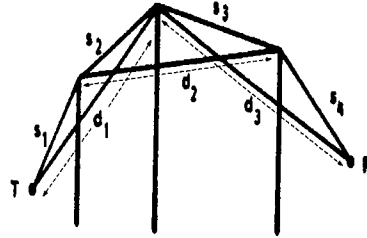
(a). Epstein-Peterson construction
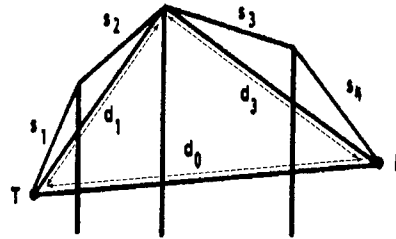
(b). Deygout construction

Figure 4.10   Multiple Edge Construction

and DG methods in the following manner [*Pogorzelski*, 1982]:

$$L_{total} = (\frac{kd_1}{ks_1 ks_2})(\frac{kd_2}{ks_2 ks_3})(\frac{kd_3}{ks_3 ks_4}) \cdot [2\sqrt{2\pi}]^{-6} \quad \text{EP construction} \qquad (4.52)$$

$$= (\frac{kd_1}{ks_1 ks_2})(\frac{kd_0}{ks_1 ks_3})(\frac{kd_3}{ks_3 ks_4}) \cdot [2\sqrt{2\pi}]^{-6} \quad \text{DG construction} \qquad (4.53)$$

where

$$k = 2\pi/\lambda \qquad\qquad (4.54)$$

4.6.2 **Comparison Results.** Fig.4.11 compares EP, DG, and RTDMOD predictions for a variety of sample multiple edge geometries over a wide frequency range. The predictions of the three GTD based methods differ by less then 5 %.

However, both the EP and the DG methods have significant limitations as the number of obstacles increases. Even though, both methods show good agreement with the rigorous theory for a small number of edges, the accuracy of both methods decrease as the number of obstructions increase whereas the accuracy of RTDMOD is not limited by the number of obstructions.
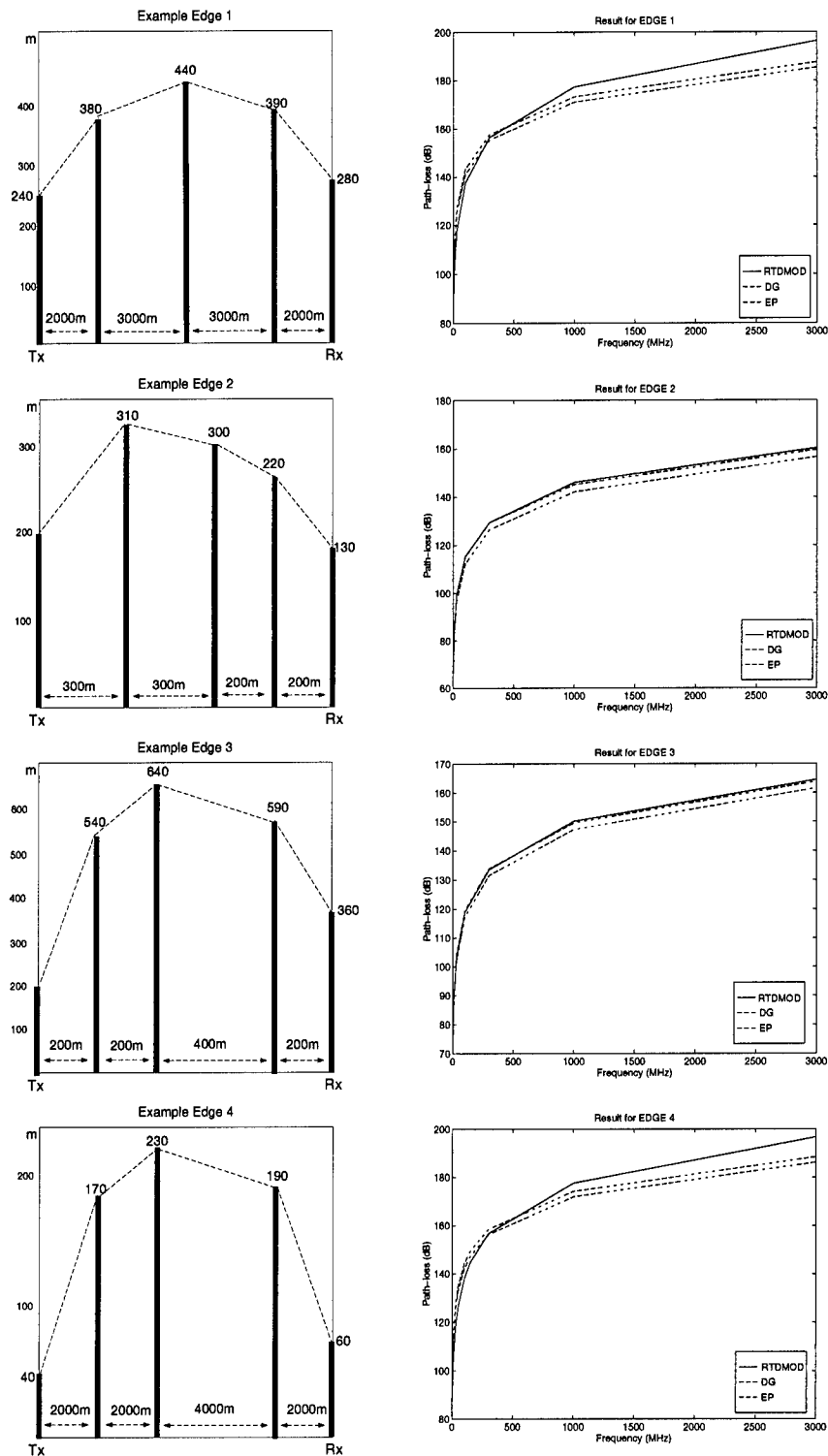
Figure 4.11   Multiple Edge Construction and Path-loss Comparison

4-17

4.7 Summary

Path-loss was derived using the definition for the electric field and power density. Starting with E_{total} at the receiving point, a path-loss calculation method was derived. RTDMOD has the advantage of predicting the significant diffraction point locations as well as the total path-loss for a given set of real terrain data. Unlike previous methods, this new method can account for an almost unlimited number of obstructions. Although RTDMOD involves complicated calculations, with the speed of modern computers, it is now possible to rigorously estimate propagation path-loss from terrain data. Nonetheless, the method described in section 4.5 is computationally intensive. Hence, a computationally efficient stochastic channel model that predicts propagation path-loss as a function of terrain statistics (mean, variance) would be very useful. This is the topic of the next chapter.

V. Universal Terrain Channel Model (UTCMOD) and Applications

5.1 Overview

Once the path-loss calculation method (RTDMOD) introduced in the previous chapter is implemented in a computer program, one can readily use this method to predict the effect of obstacles. In this chapter, a stochastic propagation channel model (Universal Terrain Channel Model) which predicts path-loss in decibel as a function of terrain statistics (mean, variance), signal wavelength and propagation distance is introduced. In contrast to RTDMOD path-loss predictions, the Universal Terrain Channel Model (UTCMOD) can be easily done on a hand-held calculator. UTCMOD will be compared with the Hata model in section 5.6 to see how a model based on numerical experiments (UTCMOD) compares to a model based on physical experiments (Hata model). An extended UTCMOD for spread spectrum (SS) signals will be derived in section 5.7.

5.2 Propagation Parameters and Assumptions

In wireless ground communication, the propagation path between the Tx and the Rx is not trivial. Unlike free space, rough terrain channels are random and are not easily analyzed. Hence, a broadly applicable rough terrain channel model which predicts path-loss effects of terrain between the Tx and the Rx is urgently needed for improving wireless communication systems. A perfect channel model is impossible. However, if sufficient propagation path-loss parameters can be determined, then a broadly applicable channel model can be created with these parameters. In this thesis, two terrain statistics (height mean and variance), signal wavelength and propagation distance are assumed to be sufficient parameters. I have assumed these parameters are sufficient for the following reasons:

1. Mean terrain height determines the distance into shadow region.

2. Variance of the terrain height determines the number of diffraction points (knife-edges).

3. Signal wavelength is a fundamental parameter for any propagation analysis.

4. Propagation distance is also a fundamental propagation parameter.

Also the following assumptions are used to create a stochastic channel model.

- Only first order effects are considered significant. That is, the effects of each path-loss factor (mean, variance, wavelength, and distance) are independent of each other.

- Only L_{shadow} will be considered. L_{lit} is less than 6 dB over irregular terrain.

However, the communication modes (e.g. air-to-ground) and the intervening terrain heights relative to the height of the Tx and the Rx should be considered in predicting additional path-loss over rough terrain. If the terrain blocks any portion of the LOS path, then diffraction path-loss must be considered. Hence, in the next section, the fundamental definitions of communication modes and new definitions of communication links for different rough terrain conditions will be introduced.

5.3 Communication Link Conditions

Communication links are typically defined for the four different modes shown in Table 5.1. In these fundamental definitions for communication links, the terrain conditions

Communication Link	Position of the Tx	Position of the Rx
Air-to-Air	Air	Air
Air-to-Ground	Air	Ground
Ground-to-Air	Ground	Air
Ground-to-Ground	Ground	Ground

Table 5.1   Fundamental Definitions of communication modes

between the Tx and the Rx are ignored and only the positions of the Tx and the Rx are considered. Hence, additional diffraction path-loss (L_{shadow}) might only be expected in the case of Ground-to-Ground communications. For the other communication modes, one might be tempted to neglect the additional diffraction path-loss (L_{shadow}).

However, these assumptions are not true in general. As shown in Fig.5.1, it can

be assumed that some obstacles block the LOS between the Tx and the Rx in Air-to-Air communication whereas the Ground-to-Ground communication link has a clean LOS between the Tx and the RX. Thus, more inclusive communication link definitions which take into account the terrain conditions between the Tx and the Rx are required. In this thesis, the definitions depicted in Table 5.2 and Fig.5.2 for communication links will be used.. Note that any of the four link conditions in Table 5.2 could occur for any of the four modes in Table 5.1.
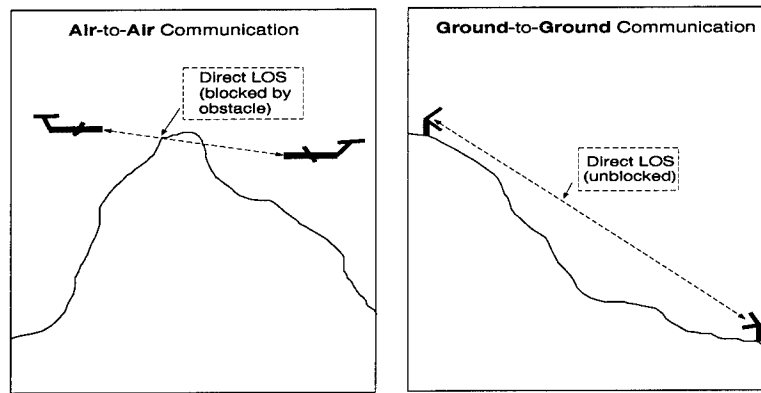
Figure 5.1   The direct LOS and Obstacle

Communication Link	LOS(line of sight) between Tx and Rx	Height of Tx	Height of Rx
LINK I		Lower than highest point of the Obstacles	Lower than highest point of the Obstacles
LINK II	Blocked by Obstacles	Higher than highest point of the Obstacles	
LINK III		Lower than highest point of the Obstacles	Higher than highest point of the Obstacles
LINK IV	Unblocked LOS between Tx and Rx	*No Consideration*	*No Consideration*

Table 5.2   Terrain Condition

These new expanded communication link definitions (Table 5.2) provide the correct perspective for analyzing the effects of rough terrain for any of the communication modes (Table 5.1). Since the additional diffraction path-loss will differ for each case, each link condition (I, II, III, IV) will result in a different stochastic propagation model. One should

Terrain Condition For **LINK I**

Highest Point

Height(m)

ht

hr

Direct
LOS
between
Tx and Rx

Tx   Rx

(a)

Terrain Condition For **LINK II**

Highest Point
of the Obstacles

ht

Height(m)

hr

Direct
LOS
between
Tx and Rx

Tx   Rx

(b)

Terrain Condition For **LINK III**

Highest Point
of the Obstacles

Height(m)

hr

Direct
LOS
between
Tx and Rx

ht

Tx   Rx

(c)

Terrain Condition For **LINK IV**

Direct
LOS
between
Tx and Rx

ht

Height(m)

hr

Tx   Rx

(d)

Figure 5.2   Terrain Condition for LINK I, II, III, and IV

note that a particular mode (e.g. air-to-ground) could pass through a variety of link conditions (I, II, III, IV) over time as the Tx and/or the Rx move relative to one another and relative to the intervening terrain.

In the next section, a stochastic propagation model is introduced. The path-loss analytic prediction method, the Real Terrain Diffraction Model (RTDMOD), introduced in chapter 4 will be used to create a stochastic propagation channel model which will be named the Universal Terrain Channel Model (UTCMOD). However, developing a stochastic model (UTCMOD) from the analytic prediction method (RTDMOD) is a little cumbersome. Hence, the modeling method will be explained first in section 5.4 and then the stochastic model for each communication link condition (I, II, III, IV) will be introduced in section 5.5.

5.4   UTCMOD Development from Monte-Carlo Simulations of RTDMOD

In chapter 4, a computer program which calculates propagation path-loss from real terrain data was introduced. One can use this diffraction based computer program to create a stochastic channel model that predicts path-loss as a simple function of terrain roughness statistics. The basic approach is to select an appropriate parametric form for the stochastic model and then estimate the coefficients and exponents by running numerous *Monte Carlo* simulations using RTDMOD. The first step is to build a Random Terrain Generator (RTG) to create the synthetic random terrain required for the *Monte Carlo* simulations.

5.4.1   Random Terrain Generator (RTG).   The RTG must be able to generate synthetic random terrain that has some specified height statistics. The random terrain data used in the simulations were generated by the random terrain generator (RTG) shown in Fig.5.3. The mean(M_{ter}) and variance(V_{ter}) of the terrain height can be estimated directly from the terrain height(H_{ter}) data:

$$M_{ter} \quad = \quad E\{H_{ter}\} \quad \text{mean of terrain height between the Tx and the Rx} \qquad (5.1)$$

$$V_{ter} \quad = \quad E\{H_{ter} - M_{ter}\}^2 \text{variance of terrain height between the Tx and the Rx} (5.2)$$
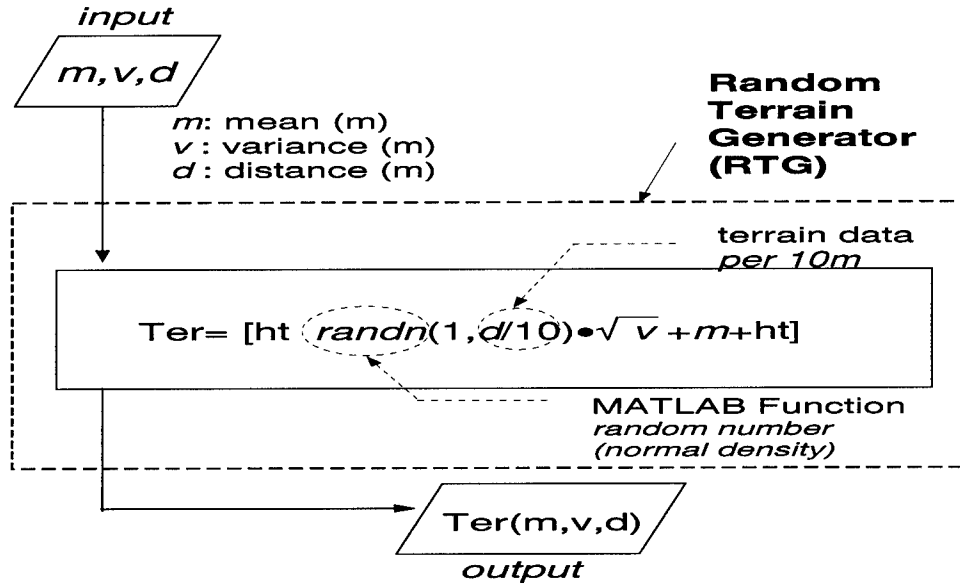
Figure 5.3   Random Terrain Generator (RTG)

where $E\{\cdot\}$ is the expectation operator. However, only the terrain height fluctuations relative to the transmitter height is important. Hence, the mean used to generate the terrain is the relative mean (M_{Tx}) (i.e. relative to the height of the Tx) and is calculated by subtracting the height of the Tx (H_{Tx}) from the expected value of the terrain height (M_{ter}).

$$M_{Tx} = M_{ter} - H_{Tx} \qquad (5.3)$$

From now on, the relative mean (M_{Tx}) and the variance (V_{ter}) will be used to characterize the terrain.

5.4.2   **Path-Loss Generators.**   The random terrain data with a specific variance (V_{ter}) and relative mean (M_{Tx}) values can be generated by RTG. As discussed in section 5.2, it will be assumed that the mean, variance, propagation distance, and wavelength (frequency) can be considered sufficient path-loss parameters. Also the effect of each path-loss parameters are assumed to be independent of each other. Hence, it is possible to devise a stochastic model using the following path-loss generators.

1. MBPLG (mean based path-loss generator): Estimate path-loss as a function of the mean terrain height.

2. MVBPLG (mean and variance based path-loss generator): Estimate path-loss as a function of the mean terrain height and the variance of terrain height.

3. MVWBPLG (mean, variance, and wavelength based path-loss generator): Estimate path-loss as a function of the mean terrain height, the variance of terrain height, and the signal wavelength.

4. MVWDBPLG (mean, variance, wavelength, distance based path-loss generator): Estimate path-loss as a function of the mean terrain height, the variance of terrain height, the signal wavelength, and the propagation distance.
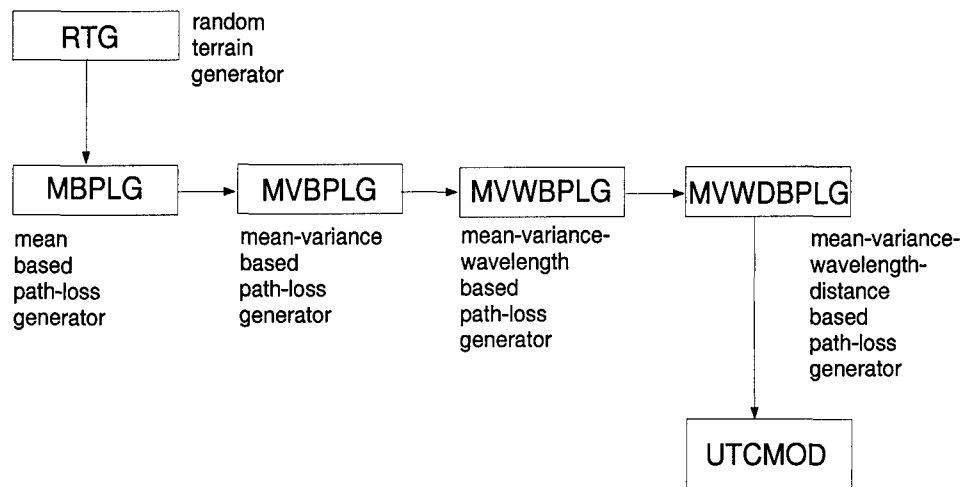
Figure 5.4   Universal Terrain Channel Model (UTCMOD) development steps

To help understand how the stochastic model was developed, an example for the LINK I case will be explained in detail.

5.4.2.1 **MBPLG.**   Fig.5.4 shows the steps for developing the stochastic model. The first step is to create the mean based path-loss equation using the MBPLG. Referring to Fig.5.5, the MBPLG works in the following way:
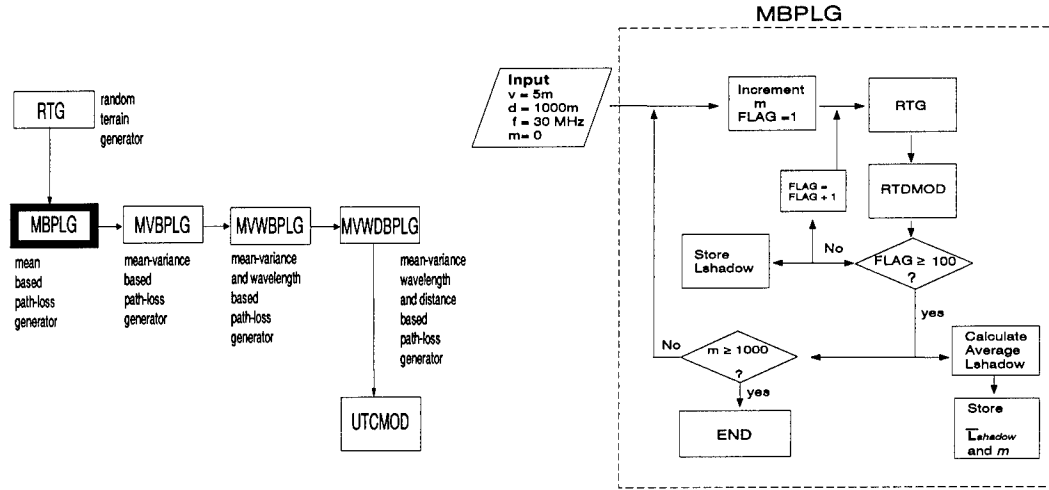
Figure 5.5   Mean Based Path-Loss Generator (MBPLG)

1. Assume the very small variance (V_{ter} = 5m) so that the variance based path-loss can be neglected.

2. Fix the propagation distance (d=1000m) and carrier frequency (f=30MHz).

3. Select one specific mean value (M_{Tx} = 10m) and generate random terrain data using the RTG.

4. Calculate L_{shadow} with the diffraction based computer program introduced in chapter 4.

5. Repeat steps 1 ∼ 4 100 times using the same mean (10m), variance (5m), distance (1000m), and carrier frequency (30MHz).

6. Calculate the average L_{shadow} for the specific mean value (M_{Tx} = 10m).

7. Change the mean value and repeat step 1 ∼ 6 for different mean values. Create a table of the mean based values for L_{shadow} as shown in Table 5.3.

8. Assume the mean based path-loss equation has the following form:

$$L_{shadow} = [M_{Tx}]^{k1} \cdot k2 \tag{5.4}$$

M_{Tx}	$\bar{L}_{shadow}$	Mean Based Model for L_{shadow}
10m	$(\bar{L}_{shadow})_{m=10}$	$(10)^{k1} \cdot k2$
50m	$(\bar{L}_{shadow})_{m=50}$	$(50)^{k1} \cdot k2$
100m	$(\bar{L}_{shadow})_{m=100}$	$(100)^{k1} \cdot k2$
$\vdots$	$\vdots$	$\vdots$
1000m	$(\bar{L}_{shadow})_{m=1000}$	$(1000)^{k1} \cdot k2$

Table 5.3   Mean based L_{shadow}

9. Determine the value of k1 and k2 which minimizes the difference between Table 5.3 and Eq.5.4. The variance of the difference between Table 5.3 and Eq.5.4 is the smallest when k1=0.5 and k2=(0.09). Even though a bias exists as shown in Fig.5.6, the bias can be assumed to be a distance (1000m) based loss[1].
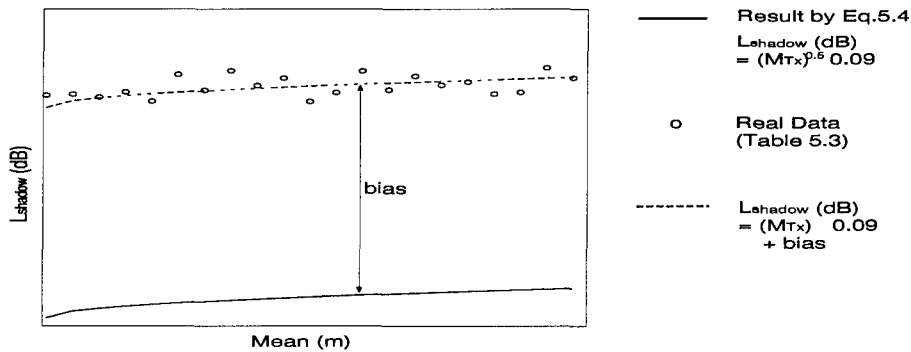
Figure 5.6   MBPLG biased results

10. Rewrite the mean based path-loss equation to account for the bias.

$$L_{shadow}(dB) = \sqrt{M_{Tx}}(0.09) + bias \tag{5.5}$$

[1]The bias value which is assumed to be a distance based loss will be explained in section 5.4.2.4.

5.4.2.2 **MVBPLG.** The next step is to develop the mean-variance based path-loss equation using the MVBPLG. Referring to Fig.5.7, the MVBPLG works in the following way:
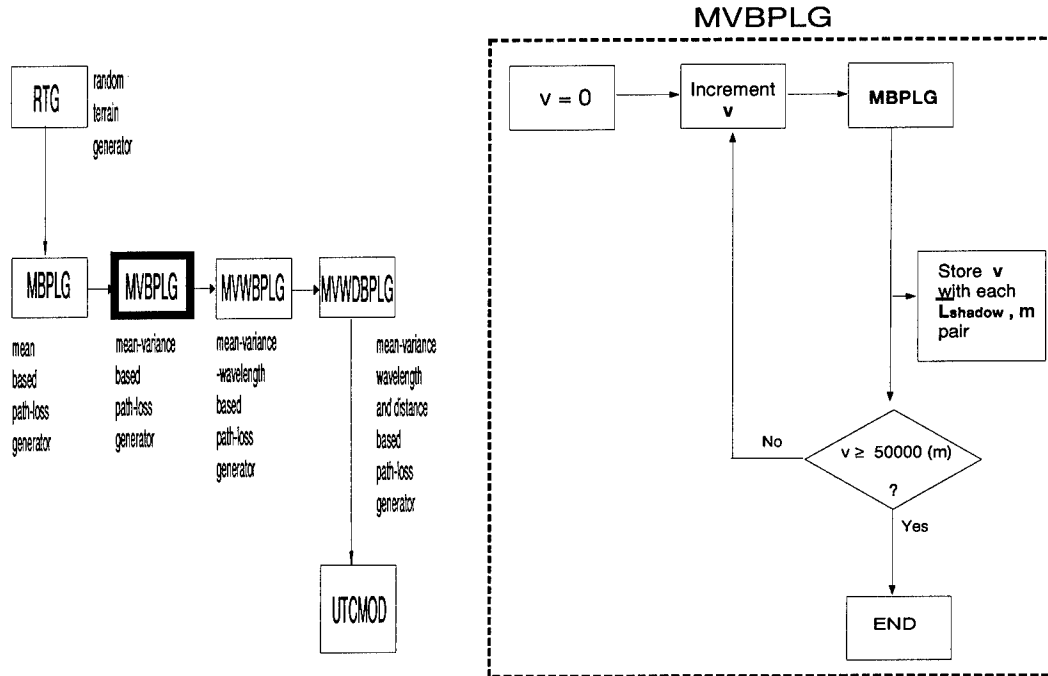
Figure 5.7 Mean-Variance Based Path-Loss Generator (MVBPLG)

1. Select one specific variance (V_{ter} = 10m).

2. Repeat step 2 ∼ 7 of MRPLG of previous section.

3. Change the variance and repeat step 1 and 2 for the new variance. Create a table of the mean-variance based values for L_{shadow}. Since the MBPLG already gave the mean based term, one can now solve for the variance based terms in Table 5.4.

V_{ter}	M_{Tx}	$\bar{L}_{shadow}$	Mean-Variance Based Model for L_{shadow}
	10m	$(\bar{L}_{shadow})_{m=10,v=10}$	$[\sqrt{10}\ (0.09) + \text{bias}] + (10)^{k3} \cdot k4$
	50m	$(\bar{L}_{shadow})_{m=50,v=10}$	$[\sqrt{50}\ (0.09) + \text{bias}] + (10)^{k3} \cdot k4$
10m	100m	$(\bar{L}_{shadow})_{m=100,v=10}$	$[\sqrt{100}\ (0.09) + \text{bias}] + (10)^{k3} \cdot k4$
	$\vdots$	$\vdots$	$\vdots$
	1000m	$(\bar{L}_{shadow})_{m=1000,v=100}$	$[\sqrt{1000}\ (0.09) + \text{bias}] + (10)^{k3} \cdot k4$
	10m	$(\bar{L}_{shadow})_{m=10,v=100}$	$[\sqrt{10}\ (0.09) + \text{bias}] + (100)^{k3} \cdot k4$
	50m	$(\bar{L}_{shadow})_{m=50,v=100}$	$[\sqrt{50}\ (0.09) + \text{bias}] + (100)^{k3} \cdot k4$
100m	100m	$(\bar{L}_{shadow})_{m=100,v=100}$	$[\sqrt{100}\ (0.09) + \text{bias}] + (100)^{k3} \cdot k4$
	$\vdots$	$\vdots$	$\vdots$
	1000m	$(\bar{L}_{shadow})_{m=1000,v=100}$	$[\sqrt{1000}\ (0.09) + \text{bias}] + (100)^{k3} \cdot k4$
$\vdots$	$\vdots$	$\vdots$	$\vdots$
	10m	$(\bar{L}_{shadow})_{m=10,v=50000}$	$[\sqrt{10}\ (0.09) + \text{bias}] + (50000)^{k3} \cdot k4$
	50m	$(\bar{L}_{shadow})_{m=50,v=50000}$	$[\sqrt{50}\ (0.09) + \text{bias}] + (50000)^{k3} \cdot k4$
50,000m	100m	$(\bar{L}_{shadow})_{m=100,v=50000}$	$[\sqrt{100}\ (0.09) + \text{bias}] + (50000)^{k3} \cdot k4$
	$\vdots$	$\vdots$	$\vdots$
	1000m	$(\bar{L}_{shadow})_{m=1000,v=50000}$	$[\sqrt{1000}\ (0.09) + \text{bias}] + (50000)^{k3} \cdot k4$

Table 5.4   Mean-Variance based L_{shadow}

4. Assume the $(\Delta dB)_v$ in Table 5.4 has the following form:

$$(\Delta dB)_v = [V_{ter}]^{k3} \cdot k4 \qquad (5.6)$$

5. Determine the value of k3 and k4 which minimizes the difference between the $(\Delta dB)_v$ values in Table 5.4 and Eq.5.6. The variance of the difference between Table 5.4 and Eq.5.6 is the smallest when k1=0.75 and k2=(0.16).

6. Rewrite the mean-variance based path-loss equation in the following way:

$$L_{shadow}(dB) = \sqrt{M_{Tx}}(0.09) + (V_{ter})^{0.75}(0.16) + bias \qquad (5.7)$$

5.4.2.3 **MVWBPLG.** The next step is to develop the mean-variance-wavelength based path-loss equation using the MVWBPLG. Referring to Fig.5.8, the MVWBPLG works in the following way:
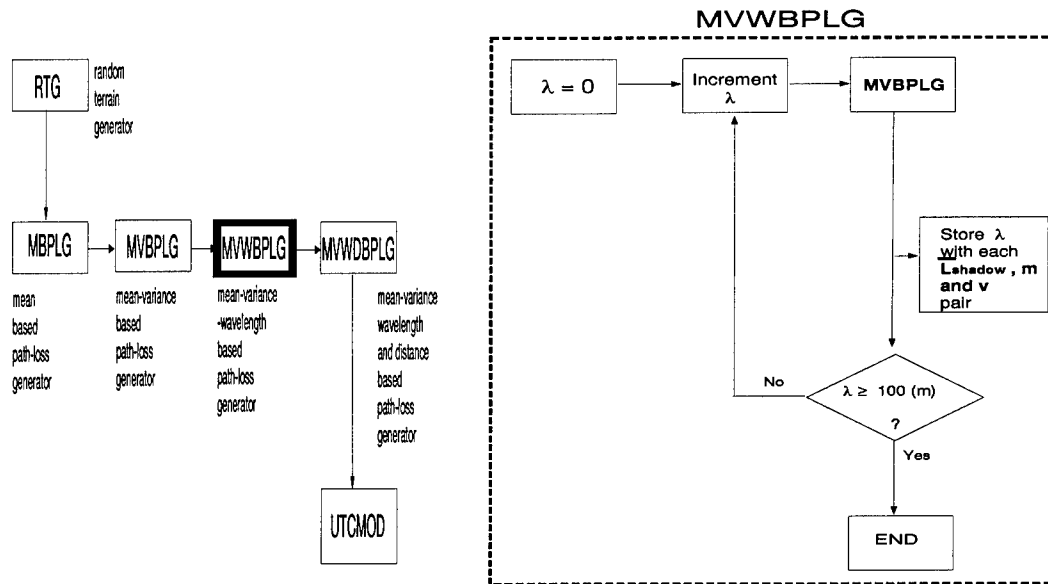
Figure 5.8 MVWBPLG (mean-variance-wavelength based path-loss generator) and Result

1. Select one specific signal wavelength ($\lambda = 5$m) .

2. Repeat step 1 $\sim$ 3 of the MVBPLG described in the previous section.

3. Change the wavelength and repeat the steps 1 and 2.

4. Find the functional relationship between L_{shadow} and the wavelength. For different wavelengths, the mean based value and the variance based value double as wavelength is reduced by one-tenth.

Frequency (MHz)	λ (m)	V_{ter} (m)	M_{Tx} (m)	$\bar{L}_{shadow}$	Mean-Variance-Wavelength Based Model for L_{shadow}
3	100	10	10	$(\bar{L}_{shadow})_{\lambda=100,m=10,v=10}$	$\sqrt{10}(0.09)(10/100)^{k5}$ $+ (10)^{0.75}(0.16)(10/100)^{k5}$ $+$ bias
			50	$(\bar{L}_{shadow})_{\lambda=100,m=50,v=10}$	$\sqrt{50}(0.09)(10/100)^{k5}$ $+ (10)^{0.75}(0.16)(10/100)^{k5}$ $+$ bias
			100	,,	,,
			$\vdots$	$\vdots$	$\vdots$
			1000	,,	,,
		100	,,	,,	,,
		$\vdots$	$\vdots$	$\vdots$	$\vdots$
		50000	,,	,,	,,
30	10	,,	,,	,,	,,
60	5	,,	,,	,,	,,
150	2	,,	,,	,,	,,
300	1	10	10	$(\bar{L}_{shadow})_{\lambda=1,m=10,v=10}$	$\sqrt{10}(0.09)(10/1)^{k5}$ $+ (10)^{0.75}(0.16)(10/1)^{k5}$ $+$ bias
			50	$(\bar{L}_{shadow})_{\lambda=1,m=50,v=10}$	$\sqrt{50}(0.09)(10/1)^{k5}$ $+ (10)^{0.75}(0.16)(10/1)^{k5}$ $+$ bias
			100	,,	,,
			$\vdots$	$\vdots$	$\vdots$
			1000	,,	,,
		100	,,	,,	,,
		$\vdots$	$\vdots$	$\vdots$	$\vdots$
		50000	,,	,,	,,

Table 5.5   Mean-Variance-Wavelength relative L_{shadow}

5. Determine the value of k5. Derive the mean-variance-wavelength relative path-loss equation. $(10/\lambda)^{0.3}$ accounts for the fact that the loss values double as the wavelength is reduced by one-tenth.

$$L_{shadow}(dB) = \sqrt{M_{Tx}}(0.09)(10/\lambda)^{0.3} + (V_{ter})^{0.75}(0.16)(10/\lambda)^{0.3} + bias \qquad (5.8)$$

5.4.2.4 **MVWDBPLG and** L_{shadow} **for LINK I case.**   The last step is to complete the mean-variance-wavelength-distance based path-loss equation using the MVWDBPLG. Referring to Fig.5.9, the MVWDBPLG works in the following way:
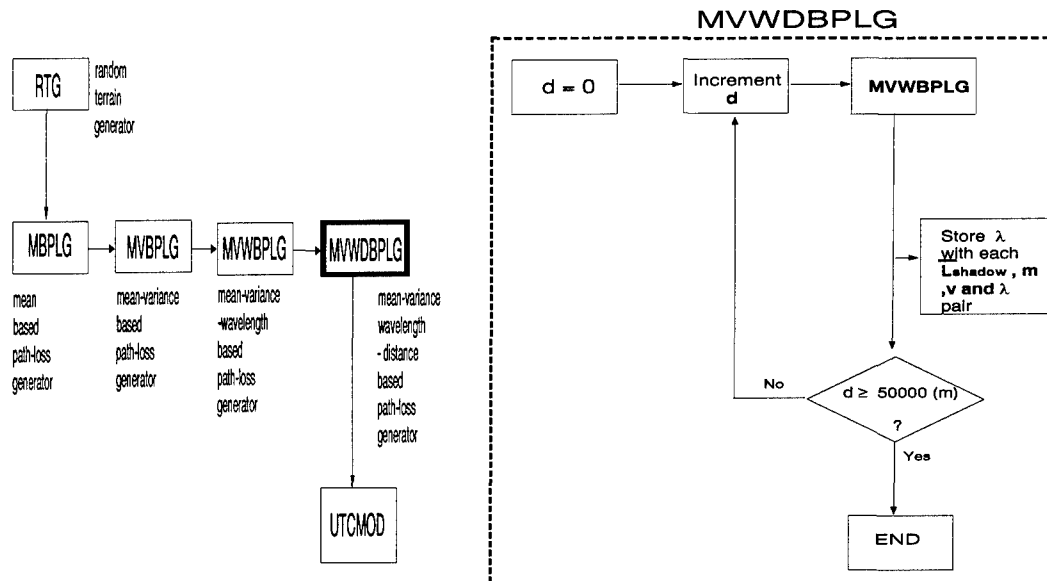
Figure 5.9   MVWDBPLG (mean-variance-wavelength-distance based path-loss generator) and Result

1. Select one specific propagation distance (d=5000m).

2. Repeat steps 1 $\sim$ 4 of the MVWBPLG described in the previous section.

3. Change the distance and repeat the steps 1 and 2. Create a list of the mean-variance-wavelength-distance based L_{shadow} as shown in Table 5.6.

Distance (m)	λ (m)	V_{ter} (m)	M_{Tx} (m)	$\bar{L}_{shadow}$	Mean-Variance-Wavelength-Distance Based Model for L_{shadow}
500	100	10	10	$(\bar{L}_{shadow})_{d=500,\lambda=100,m=10,v=10}$	$\sqrt{10}(0.09)(10/100)^{0.3}$ $+ (10)^{0.75}(0.16)(10/100)^{0.3}$ $+ \text{k6} + (\text{k7})\ log_{10}(500/1000)$
			$\vdots$	$\vdots$	$\vdots$
			1000	"	"
		100		"	"
			$\vdots$	$\vdots$	$\vdots$
		5000		"	"
	$\vdots$	$\vdots$	$\vdots$	$\vdots$	$\vdots$
	1	"	"	"	"
$\vdots$	$\vdots$	$\vdots$	$\vdots$	$\vdots$	$\vdots$
50000	"	"	"	"	"

Table 5.6   Mean-Variance-Wavelength-Distance based L_{shadow}

4. Assume the $(bias)_d$ terms in Table 5.6 have the following form:

$$(bias)_d = k6 + (k7)log_{10}(d/1000) \qquad (5.9)$$

5. Find the value of k6 and k7 which minimizes the difference between Table 5.6 and Eq.5.9. The difference between Table 5.6 and Eq.5.9 is the smallest when k6=20 and k7=13.

6. Rewrite the mean-variance-wavelength-distance based path-loss equation in the following way:

$$L_{shadow}(dB) = \sqrt{M_{Tx}}(0.09)(10/\lambda)^{0.3} + (V_{ter})^{0.75}(0.16)(10/\lambda)^{0.3} + 20 + 13log_{10}(d/1000) \qquad (5.10)$$

Finally, Eq.5.10 is the Universal Terrain Channel Model (UTCMOD) for the LINK I case. After numerous simulations and calculations, L_{shadow} for the LINK II, LINK III and LINK IV cases can be derived in a similar manner. In the next section, UTCMODs for the other communication links (LINK II, III, and IV) will be introduced.

5.4.3 L_{shadow} **for LINK II/III and LINK IV cases.** Using the same method as that used for LINK I, the path-loss equation for the LINK II case is

$$L_{shadow}(dB) = \sqrt{M_{Tx}}(0.11)(10/\lambda) + (V_{ter})^{0.75}(0.16)(10/\lambda) + 4 + 13log_{10}(d/1000). \quad (5.11)$$

As shown in Fig.5.10, LINK II is identical to LINK III except for the direction of propa-
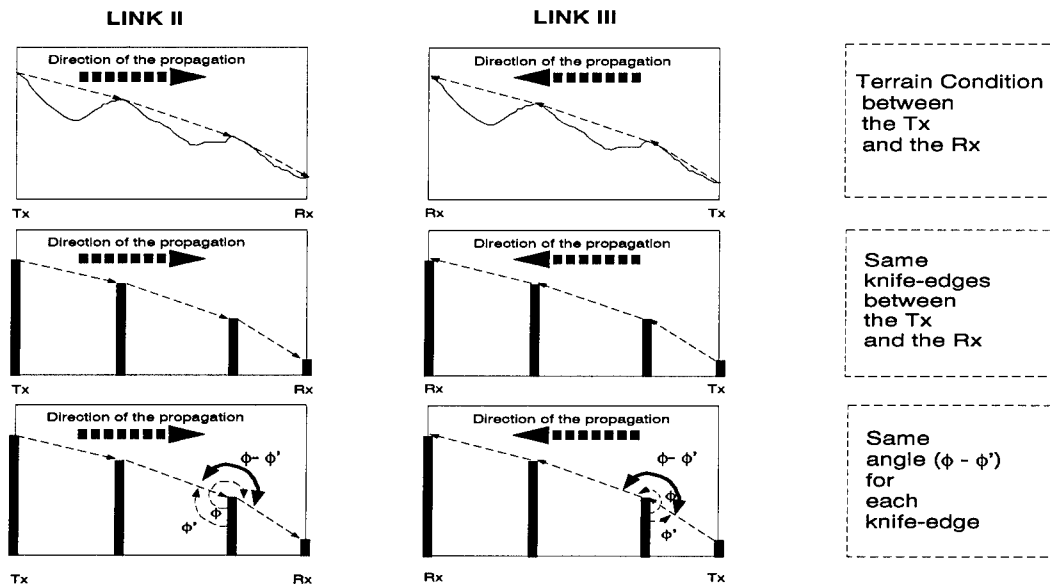
Figure 5.10   The comparison of the terrain and knife-edges for LINK II/III

gation. After making the following observations, clearly L_{shadow} for LINK III is the same as LINK II. Both have the same

1. The diffraction points for point-to-point communication are the same regardless of the propagation direction.

2. As seen in Fig.5.10, each diffraction point (knife-edge) has the same angle difference (ϕ - ϕ') for both link conditions (LINK II and LINK III).

3. As explained in chapter 3, diffraction path-loss can be predicted from the distance between the knife-edges (ρ) and the angle difference (ϕ - ϕ'). Hence, L_{shadow} for LINK III can be estimated with same equation for LINK II.

Therefore, L_{shadow} for LINK III is

$$L_{shadow}(dB) = \sqrt{M_{Tx}}(0.11)(10/\lambda) + (V_{ter})^{0.75}(0.16)(10/\lambda) + 4 + 13log_{10}(d/1000) \quad (5.12)$$

which is identical to Eq.5.11.

If the communication link between the Tx and the Rx is the LINK IV condition, then the LOS between the Tx and the Rx is unobstructed within at least 0.6 F_1 and diffraction is negligent. Hence, L_{shadow} for LINK IV is zero.

$$L_{shadow}(dB) = 0 \quad (5.13)$$

5.5   UTCMOD Summary and Sample Applications

In summary, UTCMOD for predicting the additional path-loss due to diffraction can be written in the following form.

$$L_{shadow}(dB) = M(dB) + V(dB) + R(dB) \quad (5.14)$$

where

$M(dB)$: mean based path-loss.

$V(dB)$: variance based path-loss.

$R(dB)$: distance based path-loss.

and the wavelength based path-loss is included in M (dB) and V (dB). The specific expression for M, V, and R for each link case are summarized in Table 5.7.

$$L_{shadow}(\text{dB}) = \text{M}(\text{dB}) + \text{V}(\text{dB}) + \text{R}(\text{dB})$$

Communication Link	M(dB)	V(dB)	R(dB)
LINK I	$\sqrt{|M_{Tx}|} \cdot \left(\frac{10}{\lambda}\right)^{0.3} \cdot (0.09)$	$(|V_{Ter}|)^{0.75} \cdot \left(\frac{10}{\lambda}\right)^{0.3} \cdot (0.16)$	$20 + 13 \cdot log_{10}\frac{d}{1000}$
LINK II/III	$\sqrt{|M_{Tx}|} \cdot \left(\frac{10}{\lambda}\right) \cdot (0.11)$	$(|V_{Ter}|)^{0.75} \cdot \left(\frac{10}{\lambda}\right) \cdot (0.16)$	$4 + 13 \cdot log_{10}\frac{d}{1000}$
LINK IV	0	0	0

Table 5.7   UTCMOD parameters

5.5.1 Frequency Based Form for UTCMOD.

Table 5.7 can be revised to have expressions in terms of frequency rather than wavelength by noting that

$$\lambda = \frac{3 \cdot 10^8}{f} \tag{5.15}$$

and

$$13 \cdot log_{10}\frac{d}{1000} = 13 \cdot [log_{10}d - 3] = 13 \cdot log_{10}d - 39. \tag{5.16}$$

The results of the conversion from wavelength to frequency are shown in Table 5.8.

5.5.2 Sample Application Using UTCMOD.

In the previous section, the Universal Terrain Channel Model (UTCMOD) for various communication links was introduced. In this section, a MATLAB subroutine, *JANG2.m*, that calculates additional diffraction based path-loss using the UTCMOD will be discussed. The simulation depicted in Fig.5.11 computes L_{shadow} between the Tx (origin point) and every possible receiving point. L_{shadow} was calculated using the following steps:

1. Compute the M_{Tx} and V_{ter} between the Tx and the Rx from the real terrain data. Fig.5.12 shows the input terrain data.

$$L_{shadow}(\text{dB}) = M(\text{dB}) + V(\text{dB}) + R(\text{dB})$$

Condition	M(dB)	V(dB)	R(dB)
I	$\sqrt{|M_{Tx}|} \cdot (5.14 \times 10^{-4}) \cdot f^{0.3}$	$(|V_{Ter}|)^{0.75} \cdot (9.14 \times 10^{-4}) \cdot f^{0.3}$	-19 $+13 \cdot log_{10}$d
II/III	$\sqrt{|M_{Tx}|} \cdot (3.67 \times 10^{-9}) \cdot f$	$(|V_{Ter}|)^{0.75} \cdot (5.33 \times 10^{-9}) \cdot f$	-35 $+13 \cdot log_{10}$d
IV	0	0	0

Table 5.8   UTCMOD parameterized on frequency

2. Determine the Link condition between the Tx and the RX and use the appropriate equation from Table 5.8 to calculate L_{shadow}. The Link conditions were defined in section 5.3 (Table 5.2).

3. Plot the results. Fig.5.13 shows the resulting L_{shadow} predictions for the terrain data shown in Fig.5.12.

5.6 UTCMOD Validation

The prediction of path-loss is a very important step in planning an efficient ground wireless radio system. Hence, a number of prediction methods (models) have been developed. These are exemplified by the Egli model [*Egli*, 1957], the Longley-Rice model [*Longley and Rice*, 1968], the Okumura method [*Okumura et al.*, 1968], and the Hata model [*Hata*, 1980], which are all statistical propagation models. The Hata model, which is based on the Okumura method, is a widely used propagation model [*Delisle et al.*, 1985] [*Peterson et al.*, 1995]. Hence, in this section, path-loss predictions of my stochastic model (UTCMOD) will be compared with the predictions of the Hata model as a preliminary validation of UTCMOD.

(a). Jang2.m (MATLAB Function)   (b). PL-sto.m (MATLAB Function)
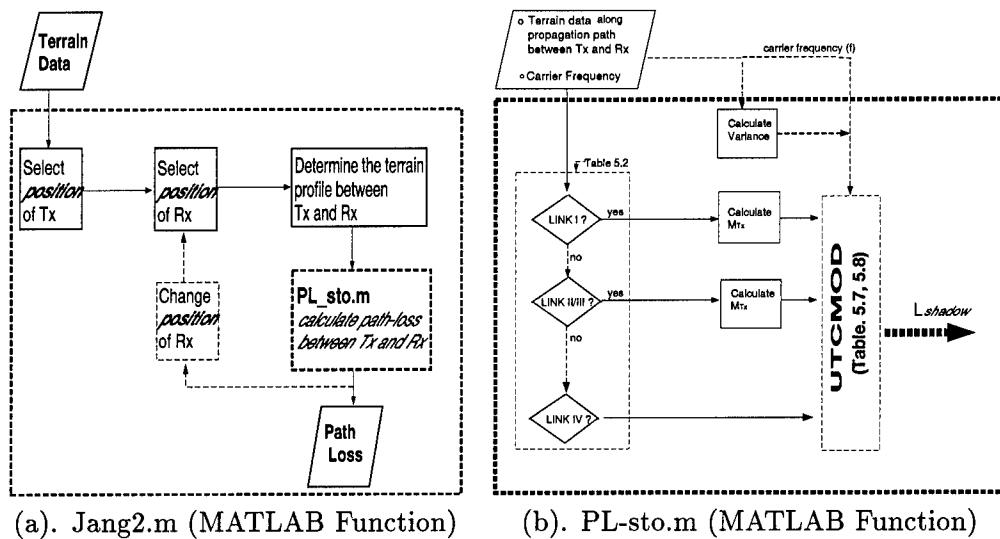
Figure 5.11   Diffraction path-loss compution using UTCMOD

(a)   (b)
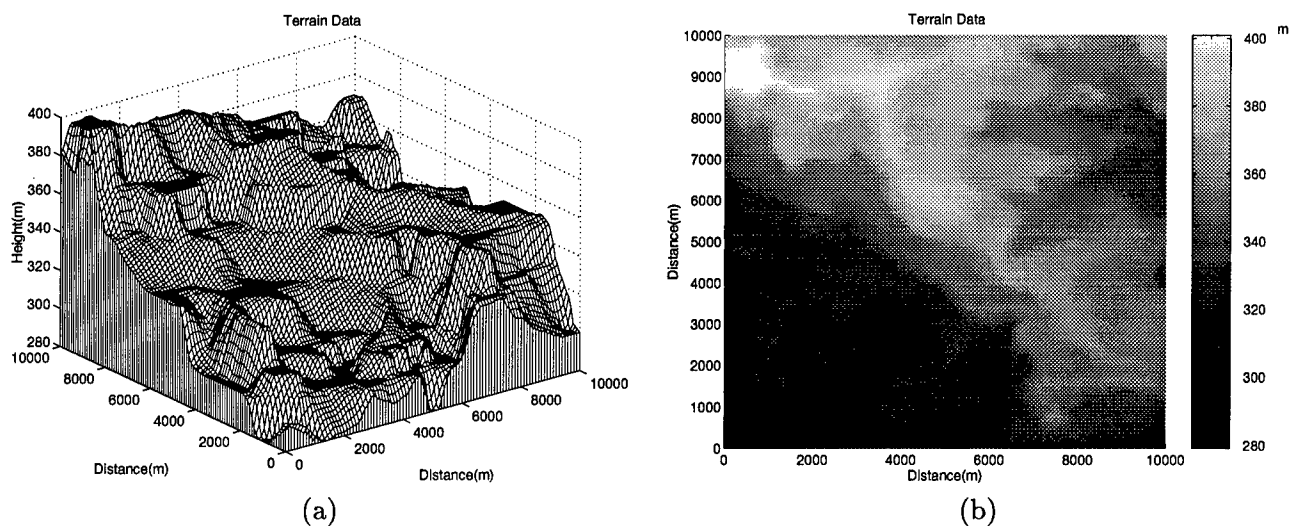
Figure 5.12   Sample input Terrain Data

(a)   (b)
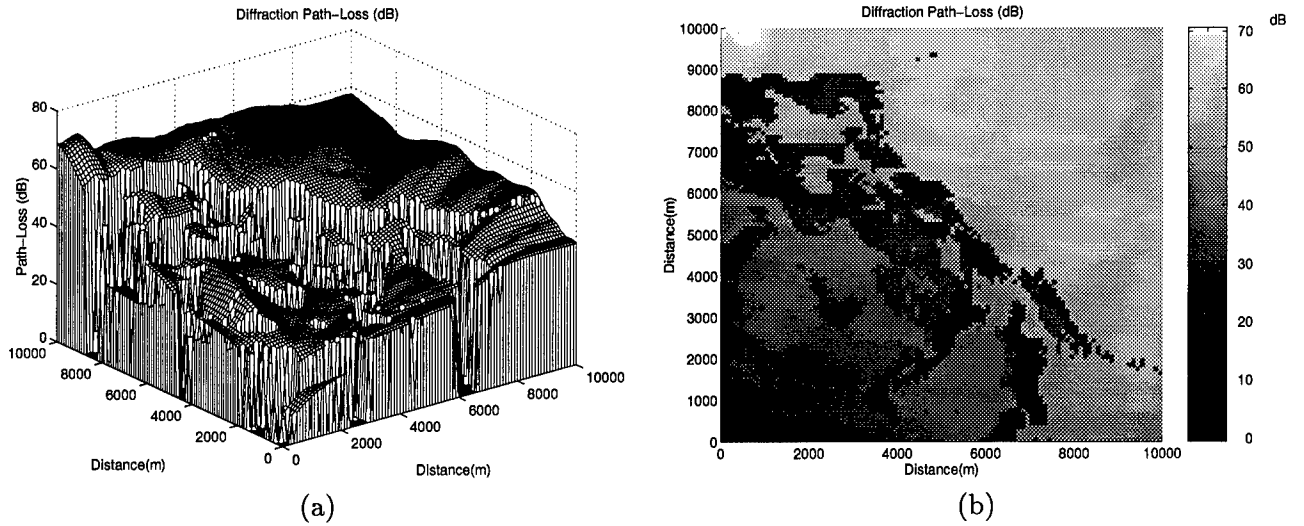
Figure 5.13 L_{shadow} for each receiving point (f = 30MHz)

5.6.1   **Hata Model.**   Hata presented the urban area propagation loss as a standard formula and supplied correction equations for other situations. The standard formula for median path-loss in large urban areas is given by

$$L(dB) = 69.55 + 26.16log(f_c) - 13.82log(h_{te}) - \alpha(h_{re}) - (44.9 - 6.55log(h_{te})) + log(d) \quad (5.17)$$

where the correction parameter, α, is used to reduce the mean error. For example,

$$\alpha(h_{re}) = 8.29[log(1.54h_{re})]^2 - 1.1(dB) \quad\quad \text{for large city,} \quad f_c < 300MHz$$

$$\alpha(h_{re}) = 3.2[log(11.75h_{re})]^2 - 4.97(dB) \quad\quad \text{for large city,} \quad f_c > 300MHz$$

In Eq.5.17, Hata model predicts total propagation path-loss ($L_{total} = L_{free} + L_{shadow}$) as a function of carrier frequency (f_c), Tx antenna height (h_{te}), Rx antenna height (h_{re}), and propagation distance (d). The Hata model is based on the basic conditions of the Okumura method which can be summarized as follows [*Delisle et al.*, 1985]:

1. Propagation losses are computed between the antennas.

2. Smooth terrain is assumed and the additional losses due to each obstacle are not taken into account.

3. A basic formulation for propagation losses is established for an urban environment and then a correction factor must be introduced to adjust for other cases.

In the Hata model, propagation path-loss is very sensitive to propagation distance but the terrain roughness is neglected. Hence, Hata model is well suited for plane urban area but is insufficient for irregular terrain.

5.6.2 **UTCMOD.** UTCMOD predicts additional path-loss based on signal diffraction. The model calculates path-loss from terrain roughness statistics (mean and variance) and fundamental parameters (distance and carrier frequency). As an example, Table 5.9 shows the path-loss parameters for LINK I, II, III, IV conditions using UTCMOD.

$$L_{total}(dB) = L_{free}(dB) + L_{shadow}(dB) \tag{5.18}$$

where

$$L_{free}(dB) = 20log_{10}[\frac{4\pi \cdot d}{\lambda}] \tag{5.19}$$

and

$$L_{shadow}(dB) = M(dB) + V(dB) + R(dB) \tag{5.20}$$

Condition	M(dB)	V(dB)	R(dB)
I	$\sqrt{|M_{Tx}|} \cdot (5.14 \times 10^{-4}) \cdot f^{0.3}$	$(|V_{Ter}|)^{0.75} \cdot (9.14 \times 10^{-4}) \cdot f^{0.3}$	$-19 + 13 \cdot log_{10}d$
II/III	$\sqrt{|M_{Tx}|} \cdot (3.67 \times 10^{-9}) \cdot f$	$(|V_{Ter}|)^{0.75} \cdot (5.33 \times 10^{-9}) \cdot f$	$-35 + 13 \cdot log_{10}d$
IV	0	0	0

Table 5.9 UTCMOD parametric terms for LINK I, II, III, IV conditions

Mainly, terrain roughness (irregularity) determines terrain statistics which in turn determine the additional path-loss. Propagation distance contributes very little to the additional path-loss because over the rough terrain, diffraction is the primary phenomena. However, distance is accounted for in the free space path-loss term. Finally, UTCMOD covers all communication link conditions and is suitable for rough mountain areas.

5.6.3 **Comparison of UTCMOD and Hata model .** The Hata model and UTCMOD are based on different terrain conditions. The Hata model applies primarily to urban areas whereas UTCMOD applies to rough mountainous terrain. Also, the models use different parameters to predict path-loss. Hence, it is of interest to evaluate how UTCMOD compares with the Hata model for a specific scenario. The details of the comparison are given below:

1. Hata Model

   - Tx Antenna height (h_{te}) is the base radio station antenna height in meters. Two different h_{te} (5m and 30m) were used.

   - Rx Antenna height (h_{re}) is the mobile antenna height in meters. An h_{re} of 1m was used.

   - Terrain is assumed to be a 10m average building height in an urban area.

2. Universal Terrain Channel Model (UTCMOD)

   - Tx relative mean (M_{Tx}) is the average height of the terrain relative to the height of Tx point.

   - Terrain Variance (V_{Ter}) is the variance of the terrain height.

3. Comparison

   - For h_{te} =5m, an average building height of 10m,and h_{re} is 1m, the points of the Tx and the Rx are lower than terrain height. This represents the LINK I condition in UTCMOD. Hence, in this case, the Hata model is comparable to the LINK I case of UTCMOD.

- For h_{te} =30m, the point of the Tx higher and the Rx is lower than the terrain height which represents the LINK II condition in UTCMOD. Hence, in this case, the Hata model is comparable to the LINK II case of UTCMOD.

The comparison parameters are summarized in Table 5.10. Path-loss difference in deci-

h_{te} (m)	Hata Model	UTCMOD
5	$h_{re} = 1\text{m}$ Average building height : 10m	M_{Tx} = (Average terrain height - h_{te}) = (10m-5m) = 5m 0m < V_{Ter} < 100m
30		M_{Tx} = (Average terrain height - h_{te}) = (10m-30m) = -20m 0m < V_{Ter} < 100m

Table 5.10 Pertinent parameters for comparing the Hata model and UTCMOD

bels as a function of frequency is shown in Fig.5.14. UTCMOD predicts a slightly higher path-loss than the Hata model because the Hata model assumed a smooth terrain and the additional losses due to each obstacle are not taken into account. The models are in good agreement (within 1dB/km) over both a broad carrier frequency range and a large terrain height variance range. With UTCMOD, we can also predict how SS, other wide bandwidth, and variable frequency communication schemes, propagate over rough terrain. In the next section, a SS propagation path-loss channel model will be introduced.

5.7 Spread Spectrum Communication Channel Model

Although SS methods are often effective in reducing multi-path interference problems, path-loss of SS in extraordinarily complex propagation paths such as those characterized by extremely rugged terrain is not well understood[*Woener et al*, 1995]. Rough terrain has many different communication obstacles which increase the complexity of the direct path. Since prediction of path-loss is an important step towards improving SS methods in ground communication, a propagation channel model for SS will now be introduced.

5.7.1 Spread Spectrum Channel Bandwidth.   As described in section 2.3, the transmitted bandwidth of a SS signal is determined by a pseudo-noise (PN) code.
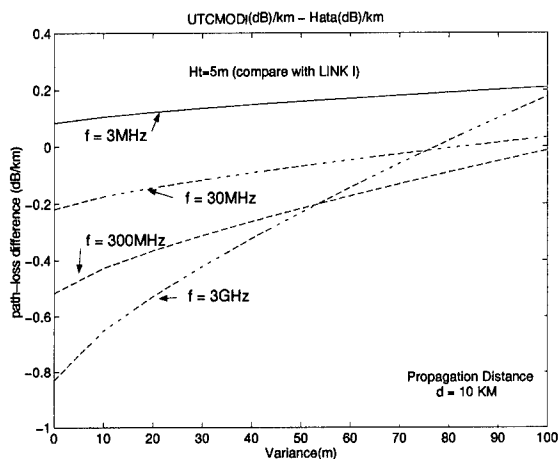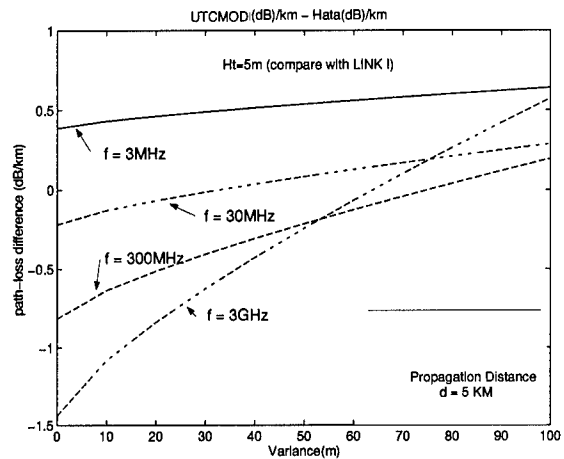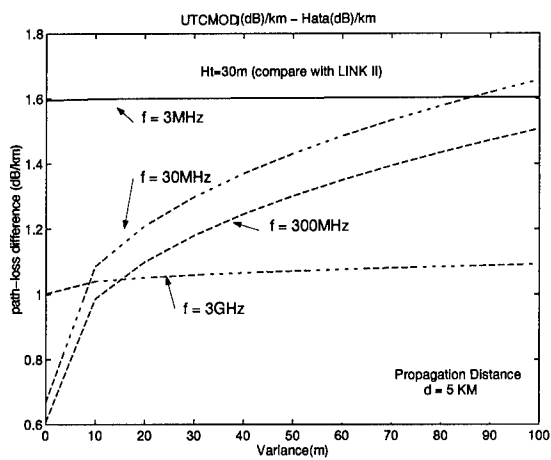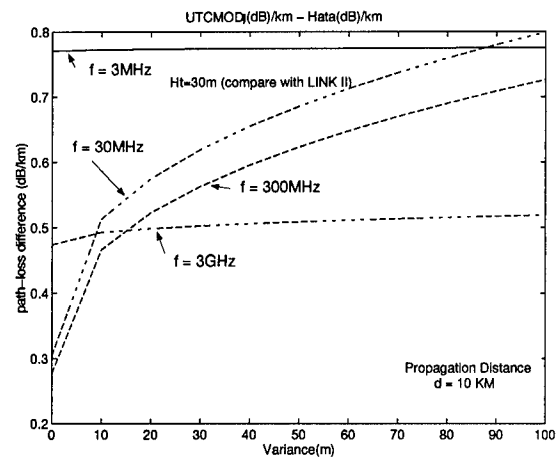
Figure 5.14   Difference between the Hata and UTC models' path-loss prediction.

In DSSS system, the bandwidth is a direct function of the chip rate. In FHSS system, bandwidth is determined by the number of discrete hopping frequencies. A SS system is a system in which the transmitted signal is spread over a frequency band that is much wider than the minimum bandwidth required to send the signal. Hence, the propagation frequency (f_p) parameter for diffraction path-loss of a SS signal is different from a non-SS signal (narrow band signal) carrier frequency parameter.

In the DSSS technique, first the PN code is modulated onto the information signal using one of several modulation techniques (eg. BPSK, QPSK, etc). Then, a doubly balanced mixer is used to multiply the RF carrier and PN modulated information signal. This process causes the RF signal to be replaced with a very wide bandwidth. That means there is a broad band of propagating frequencies in addition to the RF carrier frequency and the range is(*See the section 2.3*).

$$f_l(Hz) \quad < \quad f_p(Hz) < f_h(Hz) \tag{5.21}$$

$$f_l(Hz) \quad = \quad f_c(Hz) - R_c(Hz) \tag{5.22}$$

$$f_h(Hz) \quad = \quad f_c(Hz) + R_c(Hz) \tag{5.23}$$

where f_c is carrier frequency, R_c is the chip rate, f_l is the lowest frequency, f_h is the highest frequency.

However, in FHSS, the incoming digital stream is shifted in frequency by an amount determined by a code that spreads the signal power over a wide bandwidth. The FHSS transmitter is a pseudo-noise PN code controlled frequency synthesizer. The instantaneous frequency output of the transmitter jumps from one value to another based on the pseudo-random input from the code generator. Varying the instantaneous frequency results in an output spectrum that is effectively spread over the range of frequencies generated. In FHSS, a number of discrete frequencies will be used to the propagated signal. Hence, the range of the propagation frequency (f_p) is

$$f_l(Hz) < f_p(Hz) < f_h(Hz) \tag{5.24}$$

where

$$f_l(Hz) = f_c(Hz) \qquad (5.25)$$

and

$$f_h(Hz) = [f_0 + k \cdot \Delta f](Hz) \qquad (5.26)$$

where k is the number of discrete frequencies that is determined by the SS code and Δf is the hop frequency spacing.

The propagation frequency (f_p) of a SS signal is different from that of the narrow band signal and has the range $(f_l < f_p < f_h)$. Therefore, UTCMOD (Table 5.8) should be extended to be a function of f_l and f_h to predict the path-loss of a SS signal. In the next section, a channel model which estimates additional diffraction path-loss of a SS signal will now be presented.

5.7.2 A Modified UTCMOD for Spread Spectrum Signals.

Additional propagation path-loss (L_{shadow}) can be estimated with the relative path-loss parameters (α, M, V, and R) which were given in Table 5.8. As a example, L_{shadow} for the case of LINK I is;

$$L_{shadow} = \sqrt{|M_{Tx}|} \cdot (5.14 \times 10^{-4}) \cdot f^{0.3} + (|V_{Ter}|)^{0.75} \cdot (9.14 \times 10^{-4}) \cdot f^{0.3} + 13 \cdot log_{10}d - 19 \quad (5.27)$$

If we assume, in SS communication, the probability of occurance for each frequency between f_l and f_h is the same, then the additional path-loss for SS (LSS_{shadow}) in decibels can be approximated by the mean value of L_{shadow} in decibel over the bandwidth of the SS signal.

$$
\begin{aligned}
LSS&_{shadow}(dB) \\
&= \frac{\int_{f_l}^{f_h} [L_{shadow}(dB)]df}{[f_h - f_l]} \\
&= \sqrt{|M_{Tx}|} \cdot (5.14 \times 10^{-4}) \cdot \frac{\int_{f_l}^{f_h} [f^{0.3}]}{[f_h - f_l]} + (|V_{Ter}|)^{0.75} \cdot (9.14 \times 10^{-4}) \cdot \frac{\int_{f_l}^{f_h} [f^{0.3}]}{[f_h - f_l]} + 13 \cdot log_{10}d - 19 \\
&= \sqrt{|M_{Tx}|} \cdot (5.14 \times 10^{-4}) \cdot \frac{[f_h^{1.3} - f_l^{1.3}]}{(1.3)[f_h - f_l]} + (|V_{Ter}|)^{0.75} \cdot (9.14 \times 10^{-4}) \cdot \frac{[f_h^{1.3} - f_l^{1.3}]}{(1.3)[f_h - f_l]} + 13 \cdot log_{10}d - 19
\end{aligned}
$$

Therefore LSS_{shadow} for the case of LINK I:

$$LSS_{shadow} = \sqrt{|M_{Tx}|} \cdot (3.95 \times 10^{-4}) \cdot \frac{[f_h^{1.3} - f_l^{1.3}]}{[f_h - f_l]} + (|V_{Ter}|)^{0.75} \cdot (7.03 \times 10^{-4}) \cdot \frac{[f_h^{1.3} - f_l^{1.3}]}{[f_h - f_l]} + 13 \cdot log_{10} d - 19$$

$$(5.28)$$

Using the same method, additional propagation path-loss for different communication links can be derived. The results are given in Table 5.11.

Clearly, UTCMOD for SS signals is different from that for narrowband signals because

$$LSS_{shadow} = \text{M (dB)} + \text{V (dB)} + \text{R (dB)}$$

Link condition	M(dB)	V(dB)	R(dB)
LINK I	$\sqrt{|M_{Tx}|} \cdot \frac{3.95 \times 10^{-4}}{f_h - f_l} \cdot [f_h^{1.3} - f_l^{1.3}]$	$(|V_{Ter}|)^{0.75} \cdot \frac{7.03 \times 10^{-4}}{f_h - f_l} \cdot [f_h^{1.3} - f_l^{1.3}]$	$-19 + 13 log_{10}$ d
LINK II / III	$\sqrt{|M_{Tx}|} \cdot \frac{1.835 \times 10^{-9}}{f_h - f_l} \cdot [f_h^2 - f_l^2]$	$(|V_{Ter}|)^{0.75} \cdot \frac{2.665 \times 10^{-9}}{f_h - f_l} \cdot [f_h^2 - f_l^2]$	$-35 + 13 log_{10}$ d
IV	0	0	0

Table 5.11   Shadow Diffraction Path-Loss for SS

SS signals have a range of propagating frequencies. Also the frequency range of DSSS is different from FHSS. However, the diffraction path-loss effected by the terrain does not vary much over typical SS bandwidths. Fig.5.15 shows the additional path-loss results for different propagating frequencies over the same terrain (*See Fig.5.12 for the input terrain data and Table 5.12 for the BW of each of the three cases*). The results for all three cases

Figure	Propagation Frequency	Bandwidth
Fig.5.15. (a)	$f_p = 30$MHz	Narrow Band Signal
Fig.5.15. (b)	28MHz $< f_p < 32$MHz	BW=4MHz
Fig.5.15. (c)	30MHZ $< f_p < 80$MHz	BW=50MHz

Table 5.12   Propagation Frequency and Results

are very similar with only a change in the path-loss magnitude scale. The purpose of this

comparison is show the effect of the terrain on SS signals and show that knowledge of the terrain is important toward understanding SS propagation over rough terrain. Even though SS methods are effective in reducing multi-path interference problems, SS methods are susceptible to signal diffraction path-loss. However, the diffraction path-loss can be predicted by UTCMOD for SS (Table 5.11) and prediction of such path-losses will be an important step towards improving SS methods in ground communication.

(a)   (b)   (c)
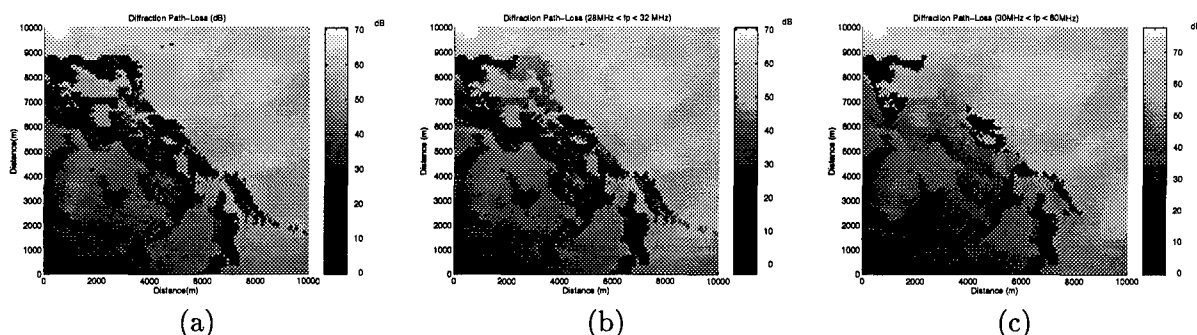
Figure 5.15 L_{shadow} for each receiving point.

5.8 Summary

Universal Terrain Channel Model (UTCMOD), a reasonable propagation model for estimating the mean path-loss of signal propagation over rough mountainous terrain, was derived from analyzing the terrain effects on signal propagation and is valid over various frequency ranges. UTCMOD is applicable to many different kinds of terrain conditions whereas the Hata model is most relevant for terrain conditions characteristic of large cities or medium-small cities. By considering communication link conditions, UTCMOD provides the correct perspective for analyzing propagation effects. In section 5.6, UTCMOD is compared with the Hata model. The models are in good agreement (within 1 dB/km) over both a broad carrier frequency range and a large terrain height variance range. In section 5.7, UTCMOD for SS signals was derived because prediction of path-losses an important step towards improving SS methods in ground communication.

In the next chapter, an application of the Universal Terrain Channel Model (UTC-MOD) to the analysis of tactical communication will be introduced.

VI. An Application of UTCMOD to the Analysis of Tactical Communication

6.1 Overview

A systems engineer is interested in knowing the area coverage associated with a specific system in a particular environment. In military tactical communication, an additional objective is to reduce, as much as possible, the range at which the signal can be intercepted by unfriendly receivers while at the same time maintaining, or even improving, the communication range of the intended receiver. This is referred to as Low Probability of Interception (LPI) communications.

Existing LPI theory ignores terrain conditions while other performance metrics of communication systems are emphasized to satisfy the objective of LPI communication. However, as discussed in the previous chapter, terrain conditions are an important parameter which determines the received power, P_r, in a wireless communication system. Hence, terrain conditions should be considered in the analysis of LPI communication systems.

In this chapter, the terrain quality factor (Q_{TER}) which can be computed with UTCMOD and sample applications will be introduced. First, basic LPI theory and the current LPI quality factor, Q_{LPI}, will be explained in section 6.2 and section 6.3. Then the terrain quality factor (Q_{TER}) which accounts for terrain effects will be introduced in section 6.4. Finally, the tactical quality factor (Q_{TAC}) which can be used to estimate the probability of interception and other tactical applications of this new quality factor will be introduced in section 6.5.

6.2 Basic LPI Theory

Basic LPI communication theory was developed to analyze typical military wireless communication scenarios and communication links to assess their vulnerability to interception. An overview of this relatively new theory is now presented to provide the necessary background for understanding the changes suggested in subsequent sections.

6.2.1 **Typical Military Wireless Communication Scenario .** Fig.6.1 shows
a typical military wireless communication scenario. While the communication Rx[1] is the
intended receiver, the interception Rx[2] is the unintended receiver which attempt to detect
and exploit the transmitted signal to intercept the transmitted information.

The objective of any LPI communication system is to relay information from the
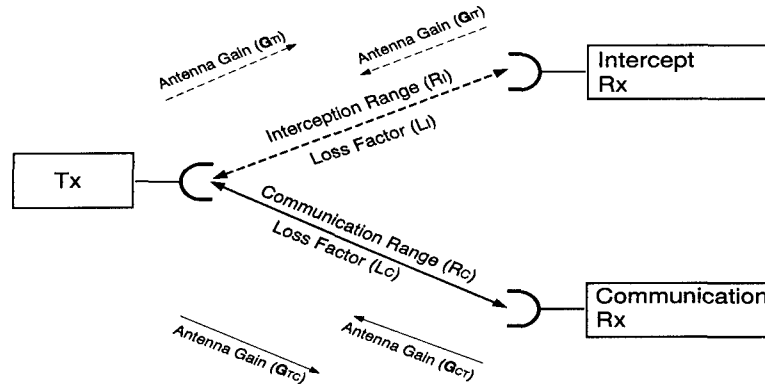
Figure 6.1   The typical military wireless communication scenario

Tx to the Rx while minimizing the ability of an unauthorized listener to intercept, classify,
or otherwise exploit the transmitted signal. Communication systems can use a variety of
techniques for reducing the probability of interception such as steerable high gain antennas,
adaptive transmitter power control, and waveforms with large time-bandwidth products
and noise-like spectra to name a few. Likewise, the interceptor has similar technologies,
such as directional, low sidelobe antennas and adaptive filtering [*Mills*, 1994].

6.2.2 **Communication Link Analysis.**   If terrain conditions are ignored, then
the received signal power (P_r) is

$$P_r = \frac{P_t G_t G_r \lambda^2}{(4\pi d)^2 L} \qquad (6.1)$$

where L is the sum of the all other losses except L_{shadow}.

In LPI communication, this simple link equation can be used to compare the received

---

[1]Communication Rx means intended (or friendly) Rx.
[2]Interception Rx means unintended (or unfriendly) Rx.

power at the intended Rx (S_C) to the received power at the interception Rx (S_I). Thus, referring to Fig.6.1, the received power at the intended Rx (S_C)

$$S_C = \frac{P_t G_{TC} G_{CT} \lambda^2}{(4\pi R_C)^2 L_C} \tag{6.2}$$

where

- S_C is the received signal power at the intended Rx

- G_{TC} is the Tx antenna gain in the direction of the intended Rx

- G_{CT} is the intended Rx antenna gain in the direction of the Tx

- R_C is the distance between the Tx and the intended Rx

- L_C is the atmospheric loss factor.

Consequently the received signal power to noise PSD can be expressed in the terms of the link parameters:

$$\frac{S_C}{N_{SC}} = \frac{P_t G_{TC} G_{CT}}{L_C N_{SC}} (\frac{\lambda}{4\pi R_C})^2 \tag{6.3}$$

Solving Eq.6.3 for the maximum communication range (R_C) yields

$$R_C = \sqrt{\frac{P_t G_{TC} G_{CT}}{L_C N_{SC}} (\frac{\lambda}{4\pi})^2 \frac{1}{S_C/N_{SC}}}. \tag{6.4}$$

The maximum interception range (R_I) can be estimated by the same type link parameters. Thus referring to Fig.6.1, the received power at the interception Rx (S_I) is

$$S_I = \frac{P_t G_{TI} G_{IT} \lambda^2}{(4\pi R_I)^2 L_I} \tag{6.5}$$

where

- G_{TI} is the Tx antenna gain in the direction of the unintended Rx

- G_{IT} is the unintended Rx antenna gain in the direction of the Tx

- R_I is the distance between the Tx and the intercept Rx

- L_I is the atmospheric loss factor between the Tx and the intercept Rx.

Analogous to Eq.6.3, the received signal power to noise PSD ratio can be expressed in the terms of the link parameters:

$$\frac{S_I}{N_{SI}} = \frac{P_t G_{TI} G_{IT}}{L_I N_{SI}} (\frac{\lambda}{4\pi R_I})^2 \tag{6.6}$$

Solving Eq.6.6 for the maximum interception range (R_I) yields

$$R_I = \sqrt{\frac{P_t G_{TI} G_{IT}}{L_I N_{SI}} (\frac{\lambda}{4\pi})^2 \frac{1}{S_I/N_{SI}}}. \tag{6.7}$$

6.2.3 **Possible Communication and Interception Areas.** In the previous section, expressions for the maximum communication range (R_C) and the maximum interception range (R_I) were derived. R_C and R_I indicate a geometric range from the Tx and thus determine the possible communication area (A_C) and the possible interception area (A_I) as shown in Fig.6.2. Usually, the interception Rx requires a lower signal-to-noise

(a) (b)
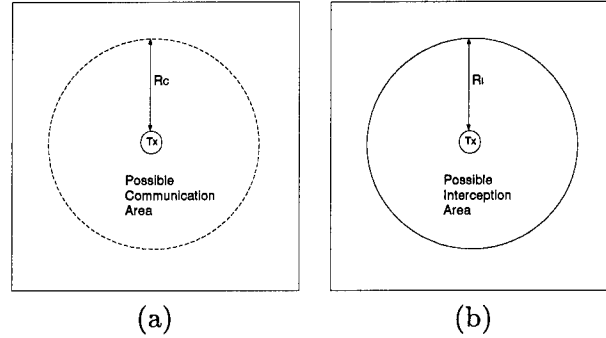
Figure 6.2   The relationship between the geometrical range and the possible geometrical area. (a). R_C and the possible communication area. (b). R_I and the the possible interception area.

ratio (SNR) to detect the presence of a signal. Hence, without employing LPI techniques, R_I is usually longer than R_C and hence A_I is larger than A_C. That means the interception Rx can detect the signal outside of A_C. However, when LPI techniques are employed, the interception Rx needs to move closer to detect the signal. Some of these techniques are high gain directional antennas, adaptive interference suppression filters, and custom wave design. The main objective of these techniques and LPI communication is to reduce

R_I while simultaneously maintaining, or even improving (i.e. lengthening), R_C. In other words, the objective of the LPI communication is increase the ratio of R_C to R_I (R_C / R_I).

In the initial LPI formulation [*Gutman and Prescott*, 1989], this ratio was the primary metric for assessing LPI performance. Thus $20log(\frac{R_C}{R_I})$ became known as the LPI quality factor or Q_{LPI}. First, the existing Q_{LPI} which excludes terrain conditions will be introduced in section 6.3, and then a new terrain quality factor, Q_{TER}, which represents terrain effects will be introduced in section 6.4.

6.3 LPI Quality Factors

Using the expressions for the communication and interception ranges given previously, one can derive an expression for the LPI quality factor, Q_{LPI}, as follows:

$$R_C^2 = \frac{P_t G_{TC} G_{CT}}{L_C N_{SC}} (\frac{\lambda}{4\pi})^2 \frac{1}{S_C/N_{SC}} \tag{6.8}$$

$$R_I^2 = \frac{P_t G_{TI} G_{IT}}{L_I N_{SI}} (\frac{\lambda}{4\pi})^2 \frac{1}{S_I/N_{SI}} \tag{6.9}$$

$$(\frac{R_C}{R_I})^2 = (\frac{G_{CT} G_{TC}}{G_{IT} G_{TI}})(\frac{N_{SI}}{N_{SC}})(\frac{S_I/N_{SI}}{S_C/N_{SC}})(\frac{L_I}{L_C}). \tag{6.10}$$

The LPI quality factor is defined in decibels as

$$Q_{LPI} = 10log[(\frac{R_C}{R_I})^2] = 20log(\frac{R_C}{R_I}). \tag{6.11}$$

Also the LPI quality factor can be written as the sum of individual subsystem level quality factors.

$$20log(\frac{R_C}{R_I}) = Q_{ANT} + Q_{IS} + Q_{MOD} + Q_{ATM} \tag{6.12}$$

where

$$Q_{ANT} = 10log(\frac{G_{CT} G_{TC}}{G_{IT} G_{TI}}) \qquad \text{antenna quality factor} \tag{6.13}$$

$$Q_{IS} = 10log(\frac{N_{SI}}{N_{SC}}) \qquad \text{interference suppression quality factor} \tag{6.14}$$

6-5

$$Q_{MOD} = 10log(\frac{S_I/N_{SI}}{S_C/N_{SC}}) \qquad \text{modulation quality factor} \qquad (6.15)$$

$$Q_{ATM} = 10log(\frac{L_I}{L_C}) \qquad \text{atmospheric quality factor.} \qquad (6.16)$$

6.3.1 Antennas Quality Factor (Q_{ANT}) . The Q_{ANT} was defined as

$$Q_{ANT} = 10log(\frac{G_{CT}G_{TC}}{G_{IT}G_{TI}}) \qquad (6.17)$$

This quality factor highlights the effect of the antenna gains on Q_{LPI}. If the Tx uses a directional antenna with high gain in the desired direction and small side lobes or nulls in interceptor direction, then a large G_{TC} and a small G_{TI} will increase Q_{ANT} and reduce the probability of interception. This forces the interception Rx is move closer to the Tx in order to maintain the original probability of interception.

6.3.2 Interference Suppression Quality Factor (Q_{IS}). The Q_{IS} was defined as

$$Q_{IS} = 10log(\frac{N_{SI}}{N_{SC}}) \qquad (6.18)$$

This quality factor is basically a design comparison of how well the intended Rx suppresses interference compared to the interception Rx. If N_{SC}, the total interference at the intended Rx input, is lower than N_{SI}, the total interference at the interception Rx input, then the probability of interception will be reduced or the interception Rx is forced to move closer to maintain the same probability of interception.

6.3.3 Modulation Quality Factor (Q_{MOD}) . The Q_{MOD} was defined as

$$Q_{MOD} = 10log(\frac{S_I/N_{SI}}{S_C/N_{SC}}) \qquad (6.19)$$

This is the most important factor since it is the essence of system performance. In the Q_{MOD}, S_C / N_{SC} is the SNR required for a specific probability of bit error, P_b, in the

intended Rx, whereas S_I / N_{SI} is the SNR required for the same P_b in the interception Rx. Usually, the interception Rx requires a lower SNR for a given P_b. However, we can increased the SNR required by the interception Rx and decreased the SNR required by the intended Rx by using special techniques such as transmitting waveforms with large time-bandwidth products and noise-like spectra.

6.3.4 Atmospheric Quality Factor (Q_{ATM}).

The atmospheric quality factor, Q_{ATM}, accounts for the relative atmospheric effects in the communication and intercept links. It is defined as

$$Q_{ATM} = \xi_I R_I - \xi_C R_C \tag{6.20}$$

where ξ_I and ξ_C are loss factors, expressed in dB/km or dB/mile. Sometimes, the path losses in the intended links and the interception links can be assumed to be equal (excluding the free space loss) if the interception and the intended receiver are close together and operate in essentially the same atmospheric conditions. In these cases, Q_{ATM} can be neglected. In those cases where Q_{ATM} can not be neglected, the reader is referred to Ghordlo's work [*Ghordlo*, 1996] for a detailed treatment of Q_{ATM}.

6.3.5 Sample LPI Application and Limitations of Q_{LPI}.

Solving Eq.6.12 for R_I yields

$$20 log(R_I) = 20 log(R_C) - [Q_{ANT} + Q_{IS} + Q_{MOD} + Q_{ATM}] \tag{6.21}$$

or

$$R_I = 10^{log(R_C) - [Q_{ANT} + Q_{IS} + Q_{MOD} + Q_{ATM}]/20} \tag{6.22}$$

$$= 10^{log(R_C)}/10^{[Q_{ANT} + Q_{IS} + Q_{MOD} + Q_{ATM}]/20} \tag{6.23}$$

$$= \frac{R_C}{10^{(0.05)[Q_{ANT} + Q_{IS} + Q_{MOD} + Q_{ATM}]}}. \tag{6.24}$$

If we ignore terrain effects, R_I can be estimated by Eq.6.24. In this case A_I is a circle centered on the Tx. Hence, the signal can be intercepted when the interception Rx is inside the circle A_I. Fig.6.3 shows the possible interception area for a specific transmitter location and three different values of Q_{ANT}. To exemplify the analysis, the following conditions were

1. R_C is the maximum possible communication range and is fixed at 5km.

2. To compare the results, three different Q_{ANT} (0, positive, negative) are used.

3. The other quality factors are assumed to be 0 (dB).

Fig.6.3 demonstrates how one can reduce R_I (A_I) while maintaining the original R_C (A_C) by taking advantage of the relative antenna gains in the pertinent directions.

| Figure	Q_{ANT}	R_I	Note
Fig.6.3.b	0 (dB)	5(km)	
Fig.6.3.c	10(dB)	1.6(km)	Assume Q_{IS}=Q_{ATM}=Q_{MOD} = 0(dB)
Fig.6.3.d	-5(dB)	8.9(km)	

Table 6.1   The Q_{LPI} application results.

However, this form of Q_{LPI} which ignores terrain effects is not sufficient to accurately characterize the ground communication because terrain effects can be significant. For the current Q_{LPI} definition, changing the position of the intended Rx along an arc of radius R_C does not alter R_I or A_I . This is demonstrated in Fig.6.4. Note that the results are identical to those shown in Fig.6.3.

However, if terrain effects were considered, the results could be have been much different. As explained in chapter 5, additional path-loss (L_{shadow}) will be caused by the terrain and L_{shadow} is very sensitive to the position of the Tx and the Rx. Hence, to improve the analysis of LPI communication over rough terrain, the terrain effects (L_{shadow}) should be considered. In the next section, a new formulation of Q_{LPI} which considers terrain effects will be introduced.
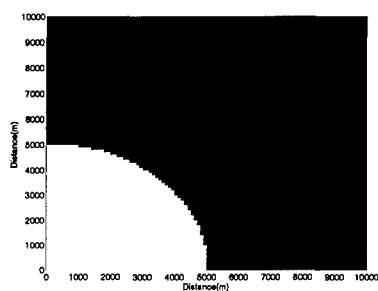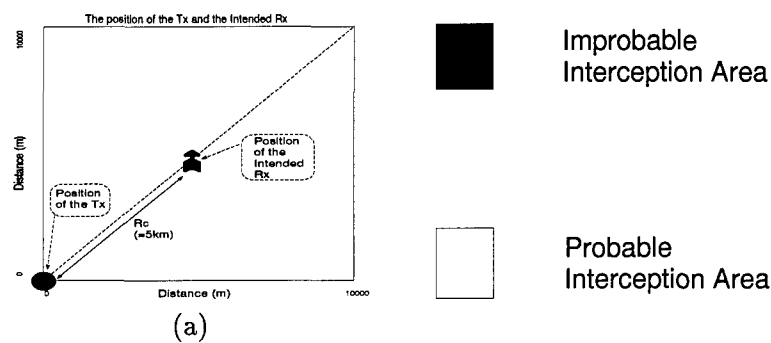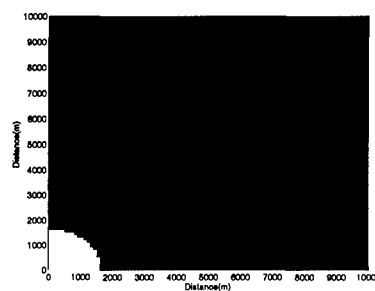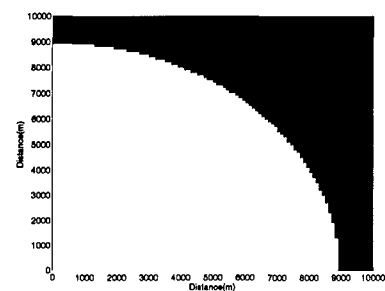
Figure 6.3   The position of the Tx and the intended Rx, and the possible interception area (see the Table 6.1).

Figure 6.4   The different position of the intended Rx and the possible interception area.

6.4 The Terrain Effect and Q_{LPI}

In the chapter 5, UTCMOD for estimating L_{shadow} as a function of terrain parameters (M_{rel}, V_{rel}, frequency, etc.) was introduced. In the past, terrain effects were ignored in LPI analysis and L_{shadow} was assumed to be 0 dB in all directions. As shown earlier, the LPI quality factor, Q_{LPI}, is then computed as follow:

$$Q_{LPI} = 20log(\frac{R_C}{R_I}) = Q_{ANT} + Q_{IS} + Q_{MOD} + Q_{ATM} \qquad (6.25)$$

However, in the real wireless communication scenarios, L_{shadow} is caused by signal diffracted from the terrain and is an important parameter for determining communication range. Thus Q_{LPI} must be revised to include a terrain quality factor, Q_{TER}, which accounts for the effects of terrain on signal propagation loss.

$$L_{shadow}(dB) = M(dB) + V(dB) + R(dB)$$

Link Condition	M(dB)	V(dB)	R(dB)
I	$\sqrt{|M_{Tx}|} \cdot (5.14 \times 10^{-4}) \cdot f^{0.3}$	$(|V_{Ter}|)^{0.75} \cdot (9.14 \times 10^{-4}) \cdot f^{0.3}$	$-19 + 13 \cdot log_{10}d$
II/III	$\sqrt{|M_{Tx}|} \cdot (3.67 \times 10^{-9}) \cdot f$	$(|V_{Ter}|)^{0.75} \cdot (5.33 \times 10^{-9}) \cdot f$	$-35 + 13 \cdot log_{10}d$
IV	0	0	0

Table 6.2   UTCMOD diffraction path-loss parameters.

6.4.1 LPI Quality Factor (Q_{LPI}).
Including terrain effects, the received power at the intended Rx (S_C) is estimated as follows:

$$S_C = \frac{P_t G_{TC} G_{CT} \lambda^2}{(4\pi R_C)^2 L_C [L_{shadow}]_{TC}} \qquad (6.26)$$

where

- L_C is the atmospheric loss factor (*See Fig.6.1*).

- $[L_{shadow}]_{TC}$ is the diffraction path-loss between the Tx and the intended Rx.

Also the received signal power to noise PSD is

$$\frac{S_C}{N_{SC}} = \frac{P_t G_{TC} G_{CT}}{L_C N_{SC} [L_{shadow}]_{TC}} (\frac{\lambda}{4\pi R_C})^2 \qquad (6.27)$$

From Eq.6.27, solving for the maximum communication range (R_C) yields

$$R_C = \sqrt{\frac{P_t G_{TC} G_{CT}}{L_C N_{SC}} \frac{\lambda^2}{(4\pi)^2} \frac{1}{S_C/N_{SC}} \frac{1}{[L_{shadow}]_{TC}}}. \qquad (6.28)$$

R_I can be estimated with similar steps. The received power at the interception Rx is

$$S_I = \frac{P_t G_{TI} G_{IT} \lambda^2}{(4\pi R_I)^2 L_I [L_{shadow}]_{TI}} \qquad (6.29)$$

where

- L_I is the atmospheric loss factor between the Tx and the intercept Rx (*See Fig.6.1*).

- $[L_{shadow}]_{TI}$ is the diffraction path-loss between the Tx and the interception Rx.

The received signal power to noise PSD can be expressed in the terms of the link parameters:

$$\frac{S_I}{N_{SI}} = \frac{P_t G_{TI} G_{IT}}{L_I N_{SI} [L_{shadow}]_{TI}} (\frac{\lambda}{4\pi R_I})^2 \qquad (6.30)$$

From Eq.6.30, solving for the maximum interception range (R_I) yields

$$R_I = \sqrt{\frac{P_t G_{TI} G_{IT}}{L_I N_{SI}} \frac{\lambda^2}{(4\pi)^2} \frac{1}{S_I/N_{SI}} [L_{shadow}]_{TI}} \qquad (6.31)$$

Dividing Eq.6.28 by Eq.6.31 and squaring the results yields

$$(\frac{R_C}{R_I})^2 = (\frac{G_{CT} G_{TC}}{G_{IT} G_{TI}})(\frac{N_{SI}}{N_{SC}})(\frac{S_I/N_{SI}}{S_C/N_{SC}})(\frac{L_I}{L_C})(\frac{[L_{shadow}]_{TI}}{[L_{shadow}]_{TC}}) \qquad (6.32)$$

Finally, the LPI quality factor which includes the terrain effects is defined as follows:

$$Q_{LPI} = Q_{ANT} + Q_{IS} + Q_{MOD} + Q_{ATM} + Q_{TER} \tag{6.33}$$

where

$$Q_{TER} = 10log(\frac{[L_{shadow}]_{TI}}{[L_{shadow}]_{TC}}) \tag{6.34}$$

6.4.2 **Terrain Quality Factor** (Q_{TER}). In rough terrain, the terrain statistics are sensitive to the position of the Tx and the Rx. Hence, the terrain statistics between the Tx and the intended Rx are different from the terrain statistics between the Tx and the interception Rx. Also, the specific link condition between the Tx and the Rx influences
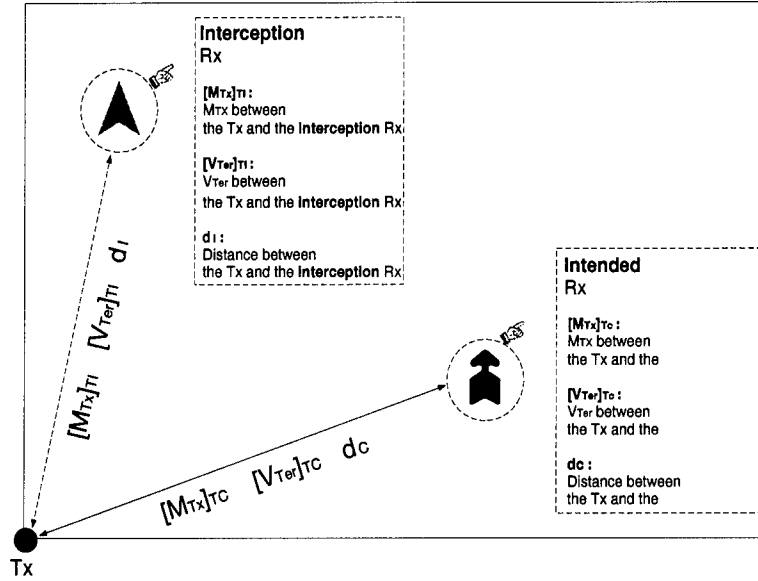

Figure 6.5 The terrain parameters between the Tx and the Rx

L_{shadow} (see Table 6.2). Thus, Q_{TER} can be estimated by the following steps:

1. Determine the positions of the Tx, the intended Rx, and the interception Rx.

2. Estimate $[L_{shadow}]_{TC}$.

   - Determine the terrain statistics between the Tx and the intended Rx (Fig.6.5).

   - Check the link condition between the Tx and the intended Rx.

- Estimate the $[L_{shadow}]_{TC}$ with Table 6.2.

3. Estimate $[L_{shadow}]_{TI}$.

   - Determine the terrain statistics between the Tx and the interception Rx (Fig.6.5).

   - Check the link condition between the Tx and the interception Rx.

   - Estimate the $[L_{shadow}]_{TI}$ with Table 6.2.

4. Estimate the Q_{TER}.

$$Q_{TER} = 10log(\frac{[L_{shadow}]_{TI}}{[L_{shadow}]_{TC}}) \tag{6.35}$$

The terrain quality factor (Q_{TER}) is sensitive to the positions of the Tx, the intended Rx, and the interception Rx. The Fig.6.6.a shows the position of the Tx and the intended Rx. Fig.6.6.b shows the height variation of the terrain. For fixed Tx and intended Rx locations, Q_{TER} was computed as a function of the position of the interception Rx. Fig.6.7 shows Q_{TER} for each specific point assuming the interception Rx is on that point. Since

$$20log(\frac{R_C}{R_I}) = Q_{ANT} + Q_{IS} + Q_{MOD} + Q_{ATM} + Q_{TER}. \tag{6.36}$$

Then, one can calculate R_I for a fixed Tx position and each fixed intended Rx position. Then A_I can be computed from R_I. However, A_I is no longer a valid interception metric because the Q_{TER} (or $[L_{shadow}]_{TC}$ and $[L_{shadow}]_{TI}$) are very sensitive to the position of the Tx, the intended Rx, and the interception Rx. Therefore, the probability of interception is estimated not by the range (or the area) but by the relative positions of the Tx, the intended Rx, and the interception Rx. In the next section, a new interception metric will be introduced.

6.5 Tactical Quality Factor (Q_{TAC})

LPI communication theory has been developed to characterize the military communication objective of maximizing R_C with respect to R_I. Using the existing Q_{LPI} which ignores terrain conditions (roughness), R_I can be computed with Eq.6.21 through Eq.6.24.
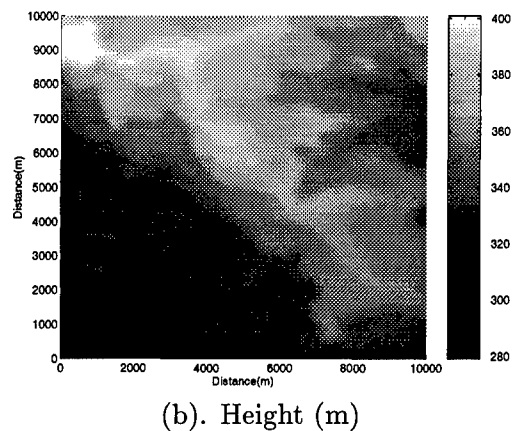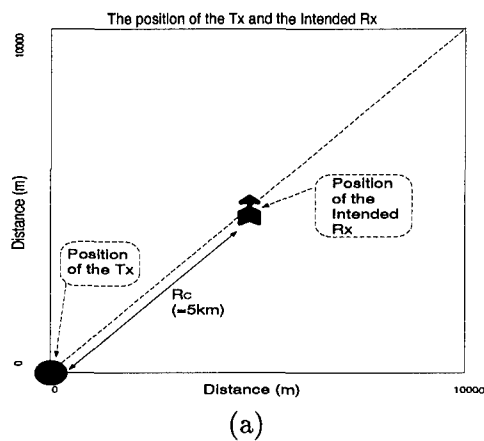
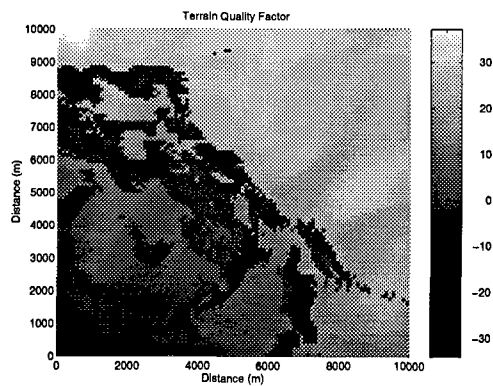Figure 6.6   (a).The position of the Tx and the intended Rx. (b).The terrain condition (height, m).

Figure 6.7   The Q_{TER} for each possible interception point (dB).

Specifically

$$R_I = \frac{R_C}{10^{(0.05)[Q_{ANT}+Q_{IS}+Q_{MOD}+Q_{ATM}]}}$$ (6.37)

The interception Rx has a high probability of detecting the signal when the range between the Tx and the interception Rx is less than R_I.

However, in the real communication, this is not an accurate characterization because L_{shadow} and hence Q_{TER} are very sensitive to the relative transmitter and receiver location. Hence, a new measure which estimates the probability of the interception is desired. In this thesis, the tactical quality factor (Q_{TAC}) is suggested for this new measure.

6.5.1 **Basic Theory of** Q_{TAC}. Eq.6.27 represents the required signal-to-noise ratio for a given probability of detection at the intended Rx. From Eq.6.27, the required transmit power, P_t, can be estimated.

$$(P_t)_{SC} = \frac{S_C}{N_{SC}} \frac{L_C[L_{shadow}]_{TC}N_{SC}}{G_{TC}G_{CT}} (\frac{4\pi R_C}{\lambda})^2$$ (6.38)

where $(P_t)_{SC}$ is the required transmit power from the Tx to the intended Rx.

Similarly, the P_t required by the interception Rx is

$$(P_t)_{SI} = \frac{S_I}{N_{SI}} \frac{L_I[L_{shadow}]_{TI}N_{SI}}{G_{TI}G_{IT}} (\frac{4\pi R_I}{\lambda})^2.$$ (6.39)

where $(P_t)_{SI}$ is the required transmit power from the Tx to the interception Rx.

Then the ratio $(P_t)_{SI}$ to $(P_t)_{SC}$ can be written as follows:

$$\frac{(P_t)_{SI}}{(P_t)_{SC}} = \frac{\frac{S_I}{N_{SI}} \frac{L_I[L_{shadow}]_{TI}N_{SI}}{G_{TI}G_{IT}} (\frac{4\pi R_I}{\lambda})^2}{\frac{S_C}{N_{SC}} \frac{L_C[L_{shadow}]_{TC}N_{SC}}{G_{TC}G_{CT}} (\frac{4\pi R_C}{\lambda})^2}$$ (6.40)

$$= (\frac{G_{CT}G_{TC}}{G_{IT}G_{TI}})(\frac{N_{SI}}{N_{SC}})(\frac{S_I/N_{SI}}{S_C/N_{SC}})(\frac{L_I}{L_C})(\frac{[L_{shadow}]_{TI}}{[L_{shadow}]_{TC}})(\frac{R_I}{R_C})^2$$ (6.41)

In Eq.6.41, the ratio $(P_t)_{SI}$ to $(P_t)_{SC}$ is a function of the quality factors and the distances. Recall that L_{shadow} is also a function of distance. R_I is the distance between the Tx and the interception Rx whereas R_C is the distance between the Tx and the intended Rx. Since, $(\frac{R_I}{R_C})^2$ is a result of the spherical wave spreading out or what is commonly called free space

loss, I will call this the free space distance quality factor (Q_{DIS}). Q_{DIS} in dB given by:

$$Q_{DIS} = 20log(\frac{R_I}{R_C}).\qquad(6.42)$$

Finally, the tactical quality factor is defined as

$$Q_{TAC} = 10log(\frac{(P_t)_{SI}}{(P_t)_{SC}}) = Q_{SYS} + Q_{ENV}\qquad(6.43)$$

where

$$Q_{SYS} = Q_{ANT} + Q_{IS} + Q_{MOD}\qquad(6.44)$$

and

$$Q_{ENV} = Q_{ATM} + Q_{TER} + Q_{DIS}\qquad(6.45)$$

Note that Q_{SYS} is exactly the old Q_{LPI} and only contains system design parameters. Q_{ENV}, on the other hand, contains all of the parameters that depend on the particular operating environment of the system. Q_{TAC} represents the analytical relationship between $(P_t)_{SC}$ and $(P_t)_{SI}$. If the Q_{TAC} is 10 dB, then the interception Rx cannot intercept the signal on that point unless the Tx increases the transmitted power 10dB. On the other hand, if Q_{TAC} is -10 dB, then the interception Rx can intercept the signal at that point until Tx decreases the transmitted power 10dB. However, after decreasing the transmitted power 10dB, the intended Rx also cannot detect the signal. Thus, friendly communications must change their tactics (e.g. move closer together) to obtain a positive Q_{TAC} and deny the enemy an opportunity to intercept the friendly signal. Hence, Q_{TAC} is an new approach for analyzing tactical communication (COMM) and electronic warfare (EW) scenarios that accounts for the effects of terrain and possibly allows one to exploit terrain to create a COMM/EW advantage. In the next section, examples of Q_{TAC} applications will be introduced.

6.5.2 Sample Q_{TAC} Applications for Analyzing the LPI Performance of a Tactical Communication System.

Q_{TAC} represents the analytical relationship between the required $(P_t)_{SC}$ and $(P_t)_{SI}$ based on terrain effects and all of the other qual-

ity factors. Since Q_{TAC} is sensitive to the positions of the Tx and the Rx, it has wide applicability for analyzing tactical communication (COMM) and electronic warfare (EW) scenarios for the wireless communication. In this thesis, an example of how to estimate potential interception positions (areas) and how to optimize the Tx position will demonstrate the power of this approach for analyzing LPI communication systems and tactical implementations.

6.5.2.1 **Possible Interception Regions.** In the section 6.3.5, the potential interception area was estimated with the previous Q_{LPI} definition which ignores terrain effects. In this section, the potential interception area will be estimated with Q_{TAC} and compared to the results in the section 6.3.5 (Fig.6.3).

For fixed Tx and intended Rx positions (Fig.6.8.a), Q_{TAC} for each point can be readily calculated and displayed (Fig.6.8.b). At points where Q_{TAC} is greater than 20 dB, the interception Rx cannot detect the signal unless the Tx power increases by at least 20 dB. Hence, the interception Rx must do something (e.g. increase antenna gain) to increase the performance of the intercept link or move to more favorable location (i.e. $Q_{TAC} < 0$) to detect and intercept the signal. However, at the point where Q_{TAC} is -30 dB, the interception Rx detects the signal until the Tx power decreases by at least 30 dB. Of course, this loss in transmit power, P_t, must be compensated for by a comparable gain in some other quality factor to ensure successful communication on the intended link. Therefore, at any points where Q_{TAC} is less than 0 dB the interception Rx detects the signal and these points comprise the potential interception region. Fig.6.8.c shows the most likely interception regions predicted by Q_{TAC}. Fig.6.8.d shows the estimated potential interception area predicted by Q_{LPI}. For simplicity in this example, only Q_{TER} and Q_{DIS} are considered while the other quality factors are assumed to be 0 dB. Clearly, the terrain effects are apparent in Fig.6.8.c whereas they are absent in Fig.6.8.d. This strikingly demonstrates the superiority of using the tactical quality factor, Q_{TAC}, as an LPI performance assessment tool compared to the previously accepted LPI quality factor, Q_{LPI}, approach.
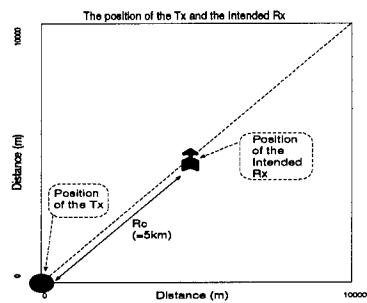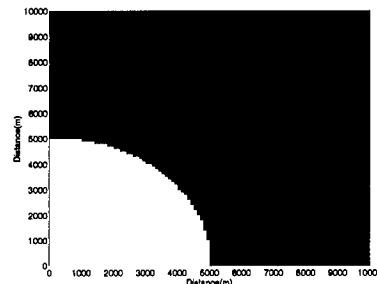
(a). Equipment locations
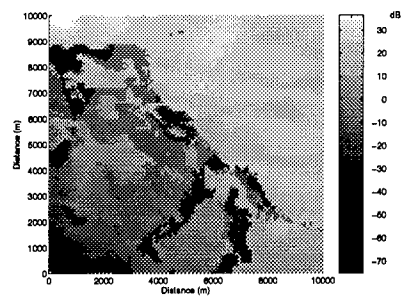
(b). Q_{TAC} values in a rough terrain
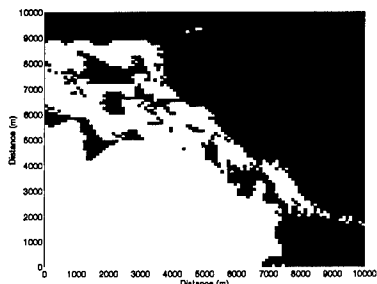
(c). Most likely interception region
predicted by Q_{TAC}

(d). Potential interception area
predicted by Q_{LPI}

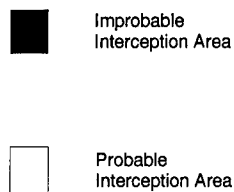Improbable
Interception Area

Probable
Interception Area

Figure 6.8 A comparison of Q_{TAC} and Q_{LPI} predictions of region vulnerable to interception.

6.5.2.2 Using Q_{TAC} to Locate Optimum LPI Transmitter Positions.

In a tactical communication scenario, finding the Tx position that affords an advantage to the intended Rx and a disadvantage to the interception Rx would be very useful to strategists, tacticians, and communication system planners. If we know the interception Rx position, then advantageous transmitter locations can be determined using the Q_{TAC} LPI metric. Fig.6.9 shows Q_{TAC} and the suggested Tx positions for the anticipated interception and intended Rx positions. For simplicity in this example, only Q_{TER} and Q_{DIS} were considered and while other quality factors were assumed to be 0 dB. Again, the power of the Q_{TAC} metric is readily apparent as the results depicted in Fig.6.9.c could be a valuable addition to a commander's assessment of the battle field.
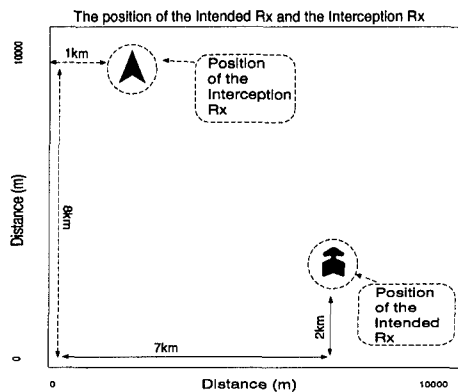
(a).The Rx positions
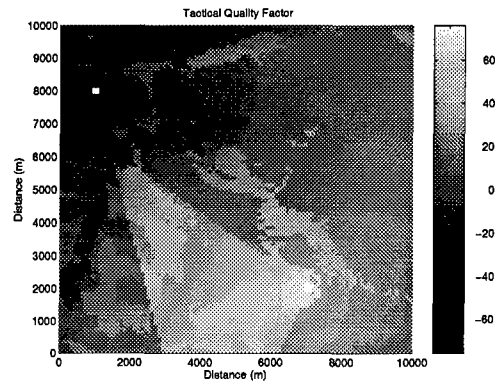
(b).Q_{TAC} for every possible Tx location
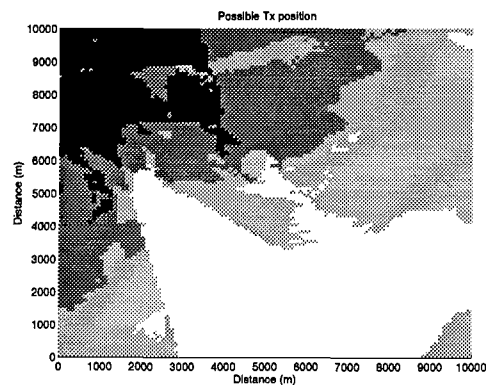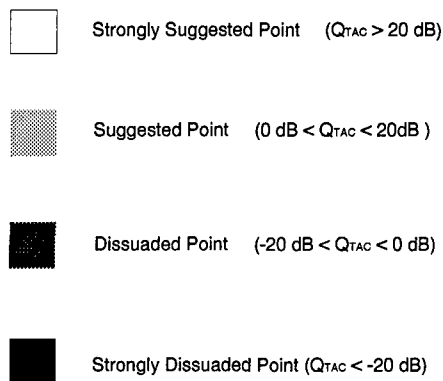
(c) Final Tx position recommendation.

Figure 6.9   Tx location recommendations using Q_{TAC}.

6.6 Summary

In military wireless communication scenarios, terrain can be used to create a communication advantage for friendly forces. By using a newly developed stochastic model (UTCMOD) which estimates the terrain effects (L_{shadow}) on radiowave propagation, many tactical communication (COMM) and electronic warfare (EW) scenarios can be readily analyzed and optimized for LPI performance. Specifically, by maximizing Q_{TER}, we can use terrain to achieve a tactical communication advantage.

Previous Q_{LPI} definitions are overly simplistic, too sensitive to range, and ignore terrain effects. Q_{TAC} on the other hand, overcomes the Q_{LPI} shortcomings. Two Q_{TAC} applications were demonstrated to exhibit the tactical utility of this metric. Using Q_{TER} and Q_{TAC} to assess LPI performance allows one to exploit terrain to achieve a tactical communication advantage by creating sub-optimum conditions for the enemy and ensuring the best possible conditions for friendly forces.

VII. Conclusions and Recommendations

This research originated with the intent to analyze terrain effects on signal propagation and to improve the analysis of tactical communication scenarios over rough terrain. Thus the objectives of this research were the following:

1. Apply a reasonable propagation model for analyzing the mean path-loss of signal propagation over rough mountainous terrain that is valid over various frequency ranges.

2. Provide a valuable tool and insight for analyzing LPI characteristics of ground communication systems.

These objectives were achieved and the results of this research exceeded expectations. This chapter summarizes the results and conclusions and recommends future research motivated by what was discovered during this effort.

7.1 Summary

Universal Terrain Channel Model (UTCMOD), a broad banded propagation model for estimating the mean path-loss of signal propagation over rough mountainous terrain, was developed by simulating terrain effects on signal propagation.

Using UTCMOD, many tactical communication (TAC COMM) and electronic warfare (EW) scenarios can be analyzed. Furthermore, two new quality factors, Q_{TER} and Q_{TAC}, resolved numerous shortcomings of a previously defined LPI quality factor or Q_{LPI} This new method of LPI analysis allows one to exploit terrain to create a communication advantage for friendly forces.

7.1.1 UTCMOD Summary.
The prediction of path-loss is a very important step in planning an effective ground wireless radio system. Hence, several propagation models which are based on experimental results have been developed for point-to-point mobile communication. Of these models, the Hata model, a widely used model, was in-

troduced in Chapter II. However, the Hata model is not sufficient for predicting path-loss in rough terrain. The model is most relevant for terrain conditions characteristic of large cities or medium-small cities. Thus it is inadequate for many different kinds of terrain conditions that may be encountered. Hence, a channel model that estimates mean path-loss over many different kinds of terrain conditions is desired.

To derive a reasonable propagation model, E_{total} at the receiving point based on McNamara's signal diffraction theory was discussed in Chapter III. After comparing computations using Balanis' wedge equation with computations using McNamara's knife-edge equation, it was shown that the McNamara knife-edge equation is reasonable for a variety of wedge-like obstacles. Using McNamara diffraction calculations, Real Terrain Diffraction Model (RTDMOD) was developed. RTDMOD can predict path-loss from real terrain data and is not limited by the number of obstruction. However, RTDMOD is computationally intensive. Hence, a computationally efficient stochastic propagation channel model was created that is easy to apply to any terrain conditions.

UTCMOD, developed using RTDMOD, is a reasonable propagation model for estimating the mean path-loss between the Tx and the Rx and it's validity was tentatively verified by comparing the results with the Hata model. To estimate the terrain effects on signal propagation, UTCMOD has the following desirable qualities:

1. UTCMOD is applicable to many different kinds of terrain conditions. The model estimates the additional path-loss from the mean and the variance of the terrain height, the propagation distance, and the carrier frequency (Table 5.8). Since the terrain statistics (mean and variance) determine the path-loss, UTCMOD is applicable to many different kinds of terrain conditions whereas the Hata model is most relevant for terrain conditions characteristic of large cities or medium-small cities.

2. UTCMOD considers the communication link condition. In addition to the fundamental definitions of communication modes (Table 5.1), the communication link conditions are important for estimating the path-loss. New expanded communication link definitions described in chapter 5 (Table 5.2) provide the correct perspective for analyzing the propagation effects.

3. UTCMOD is valid over various frequency ranges and estimates the mean path-loss of spread spectrum (SS) signal propagation. SS signals have a frequency range ($f_l < f_p < f_h$). If we assume the probability of occurance for each frequency between f_l and f_h is the same, then the path-loss can be approximated by UTCMOD (Table 5.11).

7.1.2 **Tactical Communication (TAC COMM) and Electronic Warfare (EW) Scenarios.** In military tactical communication (TAC COMM) and electronic warfare (EW) scenarios, Low Probability of Interception (LPI) is an important issue. Thus, LPI communication theory has been developed throughout the past decade. However, the existing LPI theory is not sufficient for real wireless communication because

1. The previous analysis methods using Q_{LPI} ignore the terrain effects on signal propagation. Thus, if the position of the intended Rx is changed but R_C and the other quality factors are held constant, then the predicted interception area will be the same. However, in real wireless communication that is not true because variable terrain effects will change the potential interception regions.

2. Q_{LPI}, as previously defined, is incompatible with other quality factors which are a function of distance. The current Q_{LPI} assesses LPI performance using the ($\frac{R_C^2}{R_I^2}$) metric. Thus, if any quality factor is a function of distance, the existing Q_{LPI} metric does not work. As a example, if $Q_{ATM} = 4log(R_I)$ - $3log(R_C)$, then

$$20log(R_C) - 20log(R_I) = Q_{ANT} + Q_{IS} + Q_{MOD} + 4log(R_I) - 3log(R_C) \quad (7.1)$$

$$23log(R_C) - 24log(R_I) = Q_{ANT} + Q_{IS} + Q_{MOD}. \quad (7.2)$$

Now, it is very difficult to estimate the LPI performance from the Eq.7.2. Furthermore, if a new quality factor is introduced that is explicitly a function of distance, then it is very difficult to estimate the LPI performance by adding the new quality factor to the existing Q_{LPI}.

Fortunately, these problems can be resolved by using Q_{TER} and Q_{TAC}. Q_{TER} represents the path-loss relationship between $[L_{shadow}]_{TC}$, the additional diffraction path-losses be-

tween the Tx and the intended Rx, and $[L_{shadow}]_{TI}$, the additional diffraction path-loss between the Tx and the interception Rx. Q_{TAC} represents the analytical relationship between $(P_t)_{SC}$, the required transmitted power for the communication link, and $(P_t)_{SI}$, the required transmitted power for the interception link. Q_{TAC} was based on the existing LPI performance metric, Q_{LPI}, and Q_{TER}. Hence, the first problem associated with Q_{LPI} can be solved with Q_{TER} and the second problem with Q_{LPI} can be solved with Q_{TAC}. Finally, Q_{TER} and Q_{TAC} can be used to analyze tactical communication (TAC COMM) and electronic warfare (EW) scenarios in order to exploit terrain to create a communication advantage for friendly forces.

Again it is worth emphasizing that although this work caste in a military perspective, all of the models, quality factors, and concepts are directly applicable in currently expanding commercial applications involving signal propagation in mountainous rural areas.

7.2 Recommendations

This thesis provided a stochastic propagation channel model (UTCMOD) and highlighted it's usefulness in tactical situations. Throughout this thesis, only the two dimensional (2-D) signal diffraction (forward diffraction) was considered for estimating the effects of terrain. In 2-D diffraction theory, only the elevation angles between the Tx, obstacle, and the Rx are considered when calculating the total field at the receiving point (E_{total}). However, the signals are omni-directionally diffracted at the diffraction point (obstacle) and the Rx can detect the sideward diffracted signals that was diffracted by an obstacle at an azimuth angle that is different from the azimuth angle of the Tx. If we consider very rough ground conditions, sometimes the path-loss of the sideward diffracted signals can be lower than the path-loss of the forward diffracted signal. Hence, expanding the analysis to include three dimensional (3-D) diffraction theory is recommended to improve the performance assessment of ground wireless communications.

In 3-D diffraction theory, both of the elevation and the azimuth angle are considered to calculate the total field at the receiving point (E_{total}). Also the 3-D diffraction channel model should focus on finding the elevation and the azimuth angle of the diffraction point

which causes the lowest propagation path-loss. If we can determine these critical angles, then the performance of the radio system can be greatly improved by adjusting the gain of the antenna in that direction.

Appendix A. Abbreviations and Symbols

A.1 Abbreviations

CDMA: Code Division Multiple Access

DG Method: Daygout Method

DSSS: Direct Sequence Spread Spectrum

EC: Electronic Combat

EP Method: Epstein-Peterson Method

EW: Electronic Warfare

FHSS: Frequency Hopping Spread Spectrum

FSK: Frequency Shift Keying

GTD: Geometric Theory of Diffraction

LOS: Line of Sight

LPI: Low Probability of Interception

MBPLG: Mean based path-loss generator

MVBPLG: Mean-variance based path-loss generator

MVWBPLG: Mean-variance-wavelength based path-loss generator

MVWDBPLG: Mean-variance-wavelength-distance based path-loss generator

PEC: Perfect Electrically Conducting

PN: Pseudo-Noise

RTDMOD: Real Terrain Diffraction Model

RTG: Random Terrain Generator

SS: Spread Spectrum

TAC COMM: Tactical Communication

THSS: Time Hopping Spread Spectrum

UTCMOD: Universal Terrain Channel Model

A.2 Symbols

$\alpha(h_{re}, f_c)$: Correction factor in Hata model

$\mathcal{A}$: Spatial attenuation

A_r: Effective area of the receiver antenna

β: Wave number $(= 2\,\pi\,/\,\lambda)$

$C(x)$: Fresnel cosine integral

$\mathcal{D}$: Diffraction coefficient.

d: Propagation distance between transmitter and receiver

Δf: Hop frequency spacing

$E_{diffraction}$: Diffraction field

$E_{incidence}$: Incidence field

E_{total}: Total field at receiving point

$(E_{total})_A$: Total field at the receiving point in actual communication

$(E_{total})_F$: Total field at the receiving point in free space

F_1: First Fresnel zone radius

f_c: Carrier frequency

f_h: Highest frequency of the propagation bandwidth

f_l: Lowest frequency of the propagation bandwidth

G_r: Receiver antenna gain

G_t: Transmitter antenna gain

h_c: Path clearance

h_{re}: Receiver antenna height

h_{te}: Transmitter antenna height

H_{Tx}: Terrain height of the transmitter

λ: Signal wavelength$(=\frac{3 \times 10^8}{frequency})$

$L_{atmosphere}$: Atmospheric path-loss

L_{free}: Free space path-loss

L_{lit}: Lit diffraction path-loss

L_{shadow}: Shadow diffraction path-loss

$[L_{shadow}]_{TC}$: Shadow diffraction path-loss between the transmitter and the intended receiver

$[L_{shadow}]_{TI}$: Shadow diffraction path-loss between the transmitter and the interception receiver

LSS_{shadow}: Shadow diffraction path-loss for Spread Spectrum

M_{ter}: Mean of terrain height

M_{Tx}: Relative mean of terrain height

ϕ: Observation angle. Angle between obstacle and the receiver

ϕ': Incidence angle. Angle between the transmitter and obstacle

P_{av}: Average received signal power density

P_B: Probability of bit error

P_r: Received signal power

P_t: Transmitted signal power

Q_{ANT}: Antenna quality factor

Q_{ATM}: Atmospheric quality factor

Q_{DIS}: Free space distance quality factor

Q_{ENV}: Environmental quality factor

Q_{IS}: Interference suppression quality factor

Q_{LPI}: LPI quality factor

Q_{MOD}: Modulation quality factor

Q_{SYS}: System quality factor

Q_{TAC}: Tactical LPI quality factor

Q_{TER}: Terrain LPI quality factor

R_c: Chip rate

R_C: Communication range

R_I: Interception range

Rx: Receiver

S(x): Fresnel sine integral

Tx: Transmitter

v: Diffraction parameter

v_p: Velocity of propagation

V_{ter}: Variance of terrain height

W_d: Signal bandwidth before spreading

W_{ss}: Signal bandwidth after spreading

Appendix B. **KRAUS Diffraction Method**

Huygens' principle of physical optics can be used to explain the apparent bending of radio waves around obstacles,i.e., the diffraction of waves. A diffracted ray is one that follows a path that cannot be interpreted as either reflection or refraction [*Kraus*, 1992].

As an example, consider a uniform plane wave incident on a conducting half-plane,
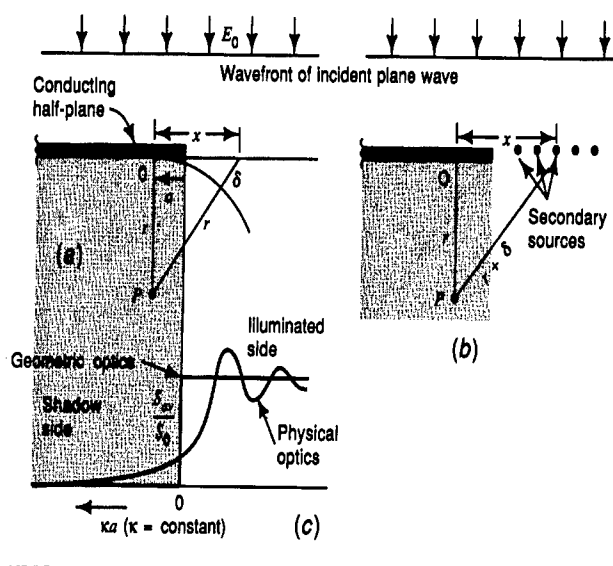

Figure B.1   Plane wave incident from above onto a conducting half-plain with resultant power-density variation below the plane as obtained by physical optics.

as in Fig.B.1. We want to calculate the electric field at point P by using Huygens' principle;

$$E = \int_{\text{over x axis}} dE \qquad \text{(B.1)}$$

where dE is the electric field at P due to a point source at a distance x from O, as in Fig.B.1.b;

$$dE = \frac{E_0}{r} e^{-j\beta(r+\delta)} dx \qquad \text{(B.2)}$$

$$E = \frac{E_0}{r} e^{-j\beta r} \int_a^\infty e^{-j\beta\delta} dx \qquad \text{(B.3)}$$

where r is the distance from obstacle (m) and a is the distance into shadow region (m). If $\delta \ll$ r, follows that

$$\delta = \frac{x^2}{2r} \qquad (B.4)$$

When we let $k^2 = 2/r\lambda$ and u = kx, Eq.B.3 becomes

$$E = \frac{E_0}{kr}e^{-j\beta r}\int_{ka}^{\infty}e^{-j\pi u^2/2}du \qquad (B.5)$$

which can be rewritten as

$$E = \frac{E_0}{kr}e^{-j\beta r}\left(\int_0^{\infty}e^{-j\pi u^2/2}du - \int_0^{ka}e^{-j\pi u^2/2}du\right) \qquad (B.6)$$

The Integrals in Eq.B.6 have the form of Fresnel integrals[*Abramowitz and Stegun*, 1964].

$$C(x) = \int_0^x cos\frac{\pi u^2}{2}du \qquad \text{Fresnel cosine integral} \qquad (B.7)$$

$$S(x) = \int_0^x sin\frac{\pi u^2}{2}du \qquad \text{Fresnel sine integral} \qquad (B.8)$$

Also, from the Fig.B.2, $C(\infty) \approx S(\infty) \approx \frac{1}{2}$. So that Eq.B.6 can be written

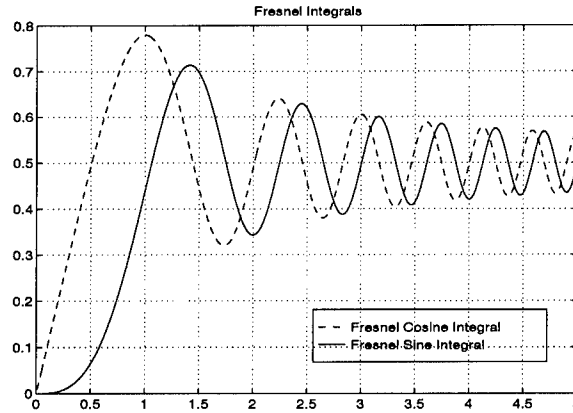Figure B.2   Fresnel Integrals.

$$E = \frac{E_0}{kr}e^{-j\beta r}\left(\frac{1}{2} + j\frac{1}{2} - [C(ka) + jS(ka)]\right) \qquad (B.9)$$

where

$$k = \sqrt{2/r\lambda} \qquad\qquad (B.10)$$

Appendix C. Balanis' Wedge Diffraction Equation

In his reference [*Balanis*, 1989], Balanis represents total field at the receiving point in the following form:

$$E_{total} = E_0 \cdot \mathcal{D} \cdot \mathcal{A} \cdot e^{-j\beta s} \qquad (C.1)$$

where

$$
\begin{aligned}
E_0 &= \text{Free space field strength} \\
\mathcal{D} &= \text{Diffraction coefficient} \\
\mathcal{A} &= \text{Spatial attenuation} \\
\beta &= 2\pi/\lambda \\
s &= \text{Propagation distance}, m
\end{aligned}
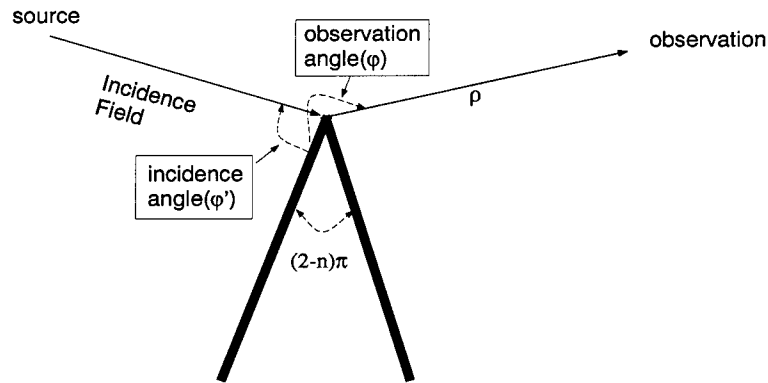$$

C.1   Diffraction Coefficient ($\mathcal{D}$)

Figure C.1   Incidence angle(ϕ') and Observation angle(ϕ).

Fig.C.1 shows the incidence angle(ϕ') and the observation angle(ϕ). The diffraction coefficient($\mathcal{D}$) can be calculated with the incidence angle(ϕ') and the observation angle(ϕ).

$$\mathcal{D}(\rho, \phi, \phi', n) = \mathcal{D}^i(\rho, \phi - \phi', n) - \mathcal{D}^r(\rho, \phi + \phi', n) \tag{C.2}$$

where angle of wedge is (2-n)π and n can be any real number. Also

$$\mathcal{D}^i(\rho, \phi - \phi', n) = -\frac{e^{-j\pi/4}}{2n\sqrt{2\pi\beta}} \cdot cot[\frac{\pi + (\phi - \phi')}{2n}] \cdot \mathcal{F}[\beta\rho\mathcal{G}(\phi - \phi')] \tag{C.3}$$

$$-\frac{e^{-j\pi/4}}{2n\sqrt{2\pi\beta}} \cdot cot[\frac{\pi - (\phi - \phi')}{2n}] \cdot \mathcal{F}[\beta\rho\mathcal{G}(\phi - \phi')] \tag{C.4}$$

$$\mathcal{D}^r(\rho, \phi + \phi', n) = \frac{e^{-j\pi/4}}{2n\sqrt{2\pi\beta}} \cdot cot[\frac{\pi + (\phi + \phi')}{2n}] \cdot \mathcal{F}[\beta\rho\mathcal{G}(\phi + \phi')] \tag{C.5}$$

$$+\frac{e^{-j\pi/4}}{2n\sqrt{2\pi\beta}} \cdot cot[\frac{\pi - (\phi + \phi')}{2n}] \cdot \mathcal{F}[\beta\rho\mathcal{G}(\phi + \phi')] \tag{C.6}$$

where

$$\mathcal{G}(\phi \pm \phi') = 1 + cos[(\phi \pm \phi')] \tag{C.7}$$

$$\mathcal{F}[\beta\rho\mathcal{G}(\phi \pm \phi')] = 2j\sqrt{\beta\rho\mathcal{G}(\phi \pm \phi')}e^{j\beta\rho\mathcal{G}(\phi\pm\phi')} \int_{\sqrt{\beta\rho\mathcal{G}(\phi\pm\phi')}}^{\infty} e^{-ju^2} du \tag{C.8}$$

Using the computer program, the diffraction coefficient($\mathcal{D}$) can be calculated. However, the diffraction coefficient($\mathcal{D}$) is a function of $cot[\pi \pm (\phi \pm \phi')]$. Thus, if $\phi \pm \phi' = m\pi$ for any integer m, then $cot[\pi \pm (\phi \pm \phi')]$ is infinite and the computation is invalid.

C.2 Spatial Attenuation ($\mathcal{A}$)

Cylindrical wave incidence is considered for calculating spatial attenuation($\mathcal{A}$). Thus

$$\mathcal{A} = \frac{1}{\sqrt{\rho \cdot sin(\beta_0)}}. \tag{C.9}$$

where ρ is the distance between the diffraction point and the observation point and β_0 is the angle as shown in Fig.C.2.
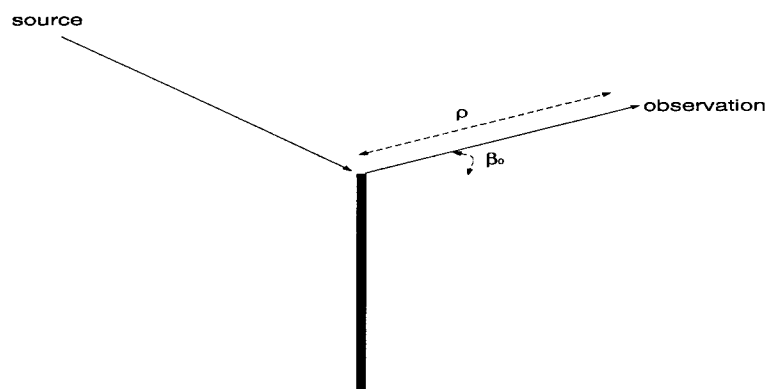
Figure C.2   Distance and angle for calculating the spatial attenuation

Appendix D. **Lit Diffraction (L_{lit}) for Multiple Subpath Edges**

D.1 **Basic Theory for Computing L_{lit}**

Eq.3.2 represents the total electric field at the receiving point. In the lit region, the total field is composed of an incidence field and a diffraction field. The diffraction field due to one subpath obstacle can be estimated by subtracting the incidence field from the total field.

$$E_{diffraction} = E_{total} - E_{incidence} \tag{D.1}$$

The total field in the lit region due to multiple subpath obstacles is

$$E_{total} = \sum_{i=1}^{N} E_i + E_{incidence} \tag{D.2}$$

where N is the number of lit edges (subpath obstacles) and E_i is the diffraction field, $E_{diffraction}$, due to the i-th lit edge (subpath obstacle). In Fig.D.1, the total field at the Rx is composed of an incidence field and three different diffraction fields.

However, Eq.D.2 is not practical for calculating L_{lit} over rough terrain because of the

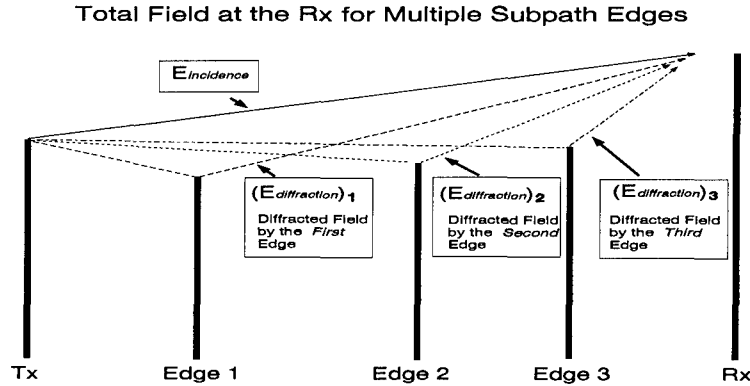**Total Field at the Rx for Multiple Subpath Edges**

Figure D.1 E_{total} at the Rx for multiple subpath edges

many possible paths one could consider. Hence, a new method that derives lit diffraction path-loss over multiple subpath obstacles using path clearance(h_c) and the first Fresnel zone radius(F_1) is simple to use.

D.2 A Sample Approximation for L_{lit}

The field intensity beyond a subpath obstacle depends on the form of the obstacle. The loss due to a knife-edge obstacle is 6 dB, but the corresponding value for a smooth earth is about 20 dB [*Bullington*, 1977]. Fig.D.2.a shows the lit diffraction path-loss for different diffraction parameter, v, where

$$v = \sqrt{2}\frac{h_c}{F_1} \tag{D.3}$$

and

$$h_c \quad : \quad \text{Path clearance (Fig4.2)}$$

$$F_1 \quad : \quad \text{Radius of First Fresnel zone.}$$

Fig.D.2.b shows the path-loss as a function of $\frac{h_c}{F_1}$. Note that the lit diffraction path-loss linearly decreases as $\frac{h_c}{F_1}$ increases until $\frac{h_c}{F_1}$ equals 0.6. To avoid path-loss a clearance of about $(0.6)F_1$ or more is required. Thus if a clearance of about $(0.6)F_1$ or more exists, then the diffraction effect of the subpath obstacle can be ignored.

Based on these ideas, I suggest the following equation for estimating lit diffraction
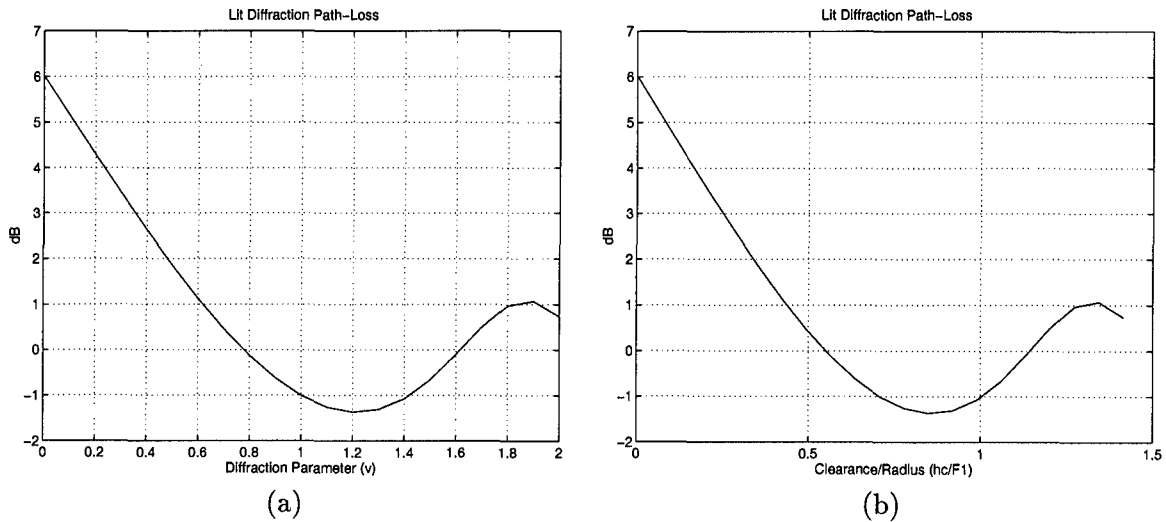

Figure D.2   Lit diffraction path-loss for different diffraction parameter

path-loss due to obstacles with path clearance(h_c) and first Fresnel zone radius(F_1):

$$L_{lit}(dB) \quad = \quad 6 - (\frac{h_c}{F_1})10 \qquad \text{for } 0 < h_c < (0.6)F_1 \qquad (D.4)$$

$$L_{lit}(dB) \quad = \quad 0 \qquad \text{for } h_c \geq (0.6)F_1 \qquad (D.5)$$

In multiple subpath obstacle situations, only the obstacle that is closest to the LOS(line of sight) projection between the Tx and the Rx will be considered. All of the other obstacles will be ignored. Hence,

$$F_1 \quad = \quad \sqrt{\frac{\lambda \cdot dt \cdot dr}{dt + dr}} \qquad (D.6)$$

$$L_{lit}(dB) \quad = \quad 6 - (\frac{h_c}{F_1})10 \qquad \text{for } 0 < h_c < (0.6)F_1 \qquad (D.7)$$

where

- h_c: Height difference between LOS(line of sight) and terrain height for the obstacle that is closest to the LOS.

- d_t: Distance between Tx and the obstacle that closest to the LOS.

- d_r: Distance between obstacle and Rx.

Fig.D.3 shows the construction for h_c, d_t, and d_r for Eq.D.6 when there are multiple subpath obstacles.

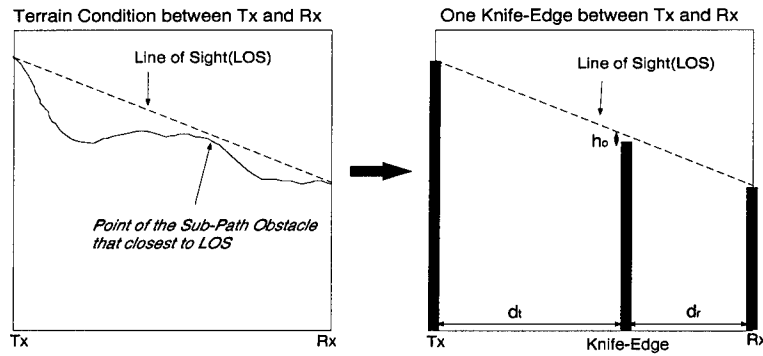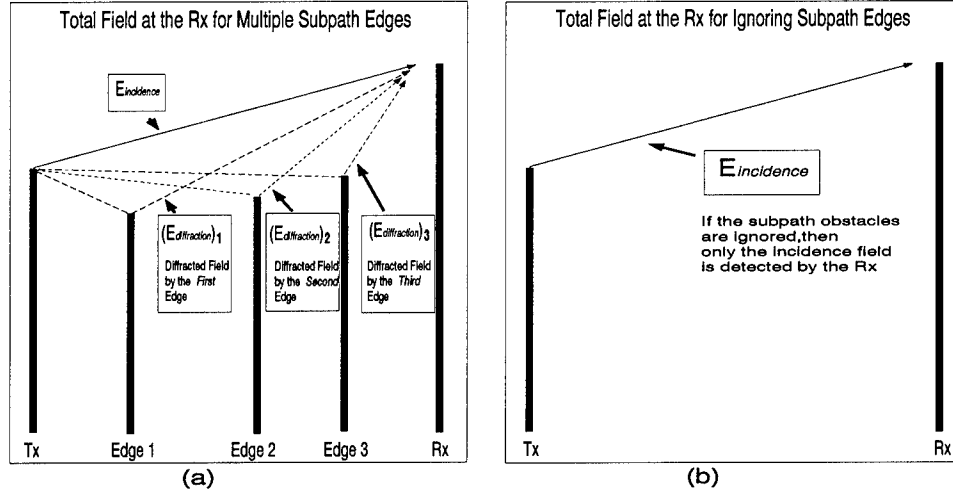Figure D.3 Find lit diffraction knife-edge from real terrain

D.3 Difference

Figure D.4 E_{total} at the Rx by the different consideration. (a). Consider multiple subpath obstacles (b). Ignore the obstacles (*Free space*)

In Fig.D.4, if there are muliple subpath edges between the Tx and the Rx (Fig.D.4.a), then E_{total} at the Rx is

$$(E_{total})_A = E_{incidence} + (E_{diffraction})_1 + (E_{diffraction})_2 + (E_{diffraction})_3 \qquad (D.8)$$

where

$(E_{total})_A$:   Total field at the Rx in actual communication

$(E_{diffraction})_n$:   Diffracted field by the n-th subpath obstacle

However, if the effects of muliple subpath edges are ignored (Fig.D.4.b), then E_{total} at the Rx is

$$(E_{total})_F = E_{incidence} \qquad (D.9)$$

where

$(E_{total})_F$:   Total field at the Rx through free space

Finally, using Eq.D.8 and Eq.D.9 ,the L_{lit} is estimated.

$$L_{lit} = \frac{\frac{(E_{total})_F (E_{total}^*)_F}{2Z}}{\frac{(E_{total})_A (E_{total}^*)_A}{2Z}} \qquad (D.10)$$

$$= |\frac{(E_{total})_F}{(E_{total})_A}|^2 \qquad (D.11)$$

The Eq.D.11 represents the basic equation which estimates L_{lit} over multiple subpath obstacles. Fig.D.5 shows L_{lit} difference in decibel between with basic theory and with suggested equation. The difference between two method is very small over $0 < h_c/F_1 <$ (0.6). Hence, through research suggested equation (Eq.D.7) will be used for estimating L_{lit} over multiple subpath obstacles.
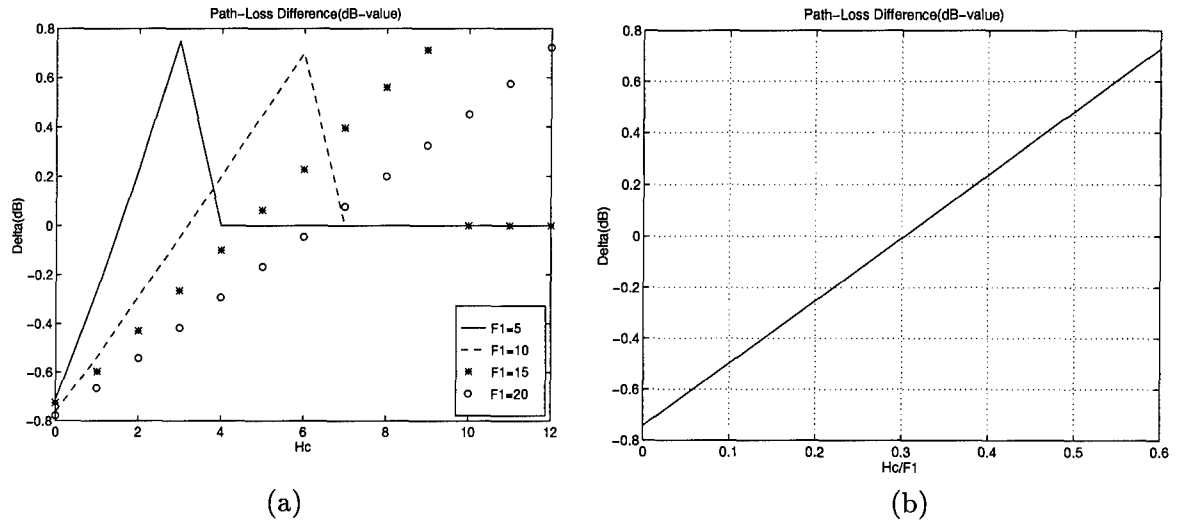

(a)   (b)

Figure D.5 L_{lit} difference in decibel between basic theory and suggested equation

Appendix E. **MATLAB Codes**

The MATLAB codes used in this thesis can be found on the world wide web at *www.afit.af.mil/Schools/EN/ENG/LABS/C3EMRT/jyc.htm.*

1. RTDMOD

   - Estimates propagation path-loss from real terrain datas

   - PL-total.m : For *n by 1* input data

   - jang1.m : For *n by m* input data

2. UTCMOD

   - Estimates propagation path-loss by using the terrain statistics

   - PL-sto.m : For *n by 1* input data

   - jang2.m : For *n by m* input data

3. UTCMOD for SS

   - Estimates propagation path-loss of spread spectrum communication

   - PL-SS.m : For *n by 1* input data

   - jangss.m : For *n by m* input data

Appendix F. **Bibliography**

Abramowitz, M. and Stegun, I. A., *Handbook of Mathematical Functions with Formulas, Graphs, and Mathematical Tables*, U.S. Government Printing Office, Washington, D. C., 1964.

Balanis, C. A., *Advanced Engineering Electromagnetics*, John Wiley and Sons, Inc., New York, 1989.

Bullington, K., "Radio Propagation at Frequencies above 30 Mc," *Proc. IRE*, Vol. 35, No. 10, pp. 1122-1136, 1947.

Burnside, W. D., Yu, C. L., and Marhefka, R. J., "A Technique to Combine the Geometrical Theory of Diffraction and Moment Method," *IEEE Trans.*, AP-23, pp. 551 - 558, 1975.

Delisle, G. Y., Lefevre, J., Lecours, M., and Chouinard, J., "Propagation Loss Prediction: A Comparative Study with Application to the Mobile Radio Channel," *IEEE Transaction on Vehicular Technology*. Vol. VT-34, No. 2, May, 1985

Egli, J. J., "Radio Propagation above 40 Mc over Irregular Terrain," *Proc. IRE*. Vol.45, No. 10, pp. 1383-1391, Oct 1957.

Feher, Kalilo, *Wireless Digital Communication Modulation And Spread Spectrum Applications*, Prentice-Hall: NJ, 1995.

Flock, W. L., *Propagation Effects on Satellite Systems at Frequencies Below 10 GHz*, NASA Reference Publication 1108, 1987

Ghordlo, A., *Analysis of Multimode Low-Probability-of-Intercept (LPI) Communications With Atmospheric Effects*, MS thesis, AFIT/GE/ENG/96D-03, School of Engineering, Air Force Institute of Technology(AU), Wright-Patterson AFB OH, December 1996.

Gutman, L. L. and Prescott, G. E., " System Quality Factors for LPI Communications," *IEEE Aerospace and Electronics Systems Magazine,* pp. 25-28, December 1989.

Hata, Masaharu, "Emprical Formula for Propagation Loss in Land Mobile Radio Services," *IEEE Transactions on Vehicular Technology*, Vol. VT-29, No. 3, pp. 317-325, August 1980.

Ishimaru, A., *Electromagnetic Wave Propagation, Radiation, and Scattering*, Plenum Press, New York, 1991.

Jeruchim, M. C., Balaban, Philip, and Shanmugan, K. S., *Simulation of Communication System*, Plenum Press, New York, 1992.

Keller, J. B., "Geometric Theory of Diffraction," *J. Opt. Soc. Am.*, 52, pp. 116-130, 1962.

Kraus, J.D., *Electromagnetics*, McGraw-Hill, Inc., 1992.

Lascody, James A., *Narrowband Interference Suppression in Spread Spectrum Communication Systems*. MS thesis, AFIT/GE/ENG/95D-13, School of Engineering, Air Force Institute of Technology(AU), Wright-Patterson AFB OH, December 1995.

Liebe, H. J. "MPM-An Atmospheric Millimeter-Wave Propagation Model," *International Journal of Infrared and Millimeter Waves*, Vol. 20, No. 5, pp.1069-1089, September-October 1985.

Longley, A G., and Rice, P. L., "Prediction of Tropospheric radio Transmission Loss Over Irregular Terrain; A Computer Method,' *ESSA Technical Report*, ERL 79-ITS 67, 1968.

MATLAB User's Guide (High-Performance Numeric Computation and Visualization Software), The Math Work Inc., 1992.

McNamara, D. A., Pistorius, C. W. I., Malherbe, J. A. G., *Introduction to the Uniform Geometrical Theory of Diffraction*, U.S. Artech House, MA, 1990.

Mills, R. F. *Detectable models and Waveform Design for Multiple Access Low-Probability-of-Interception Networks*. PhD dissertation. University of Kansa, Kansas KA, 1994.

O'Brien, W. J., Seibert, J., Vogel, B., and Young, P. *On Achieving Network LPI for Spread Spectrum Communication*, chap.3, E-System, Inc., Virginia, Oct. 1985.

Okumura, T., Ohmori, E., and Fukuda, K., "Field Strength and Its Variability in VHF and UHF Land Mobile Service," *Review Electrical Communication Laboratory*, Vol. 16, No. 9 - 10, pp. 825-873, September-October 1968.

Parsons, J. D., "Wideband characterization of fading mobile radio channels," *Proc. IEE, Pt. F*, vol.129, 1982.

Parsons, J. D., *The Mobile Radio Propagation Channel*, Prentice-Hall, New Jersey, 1992.

Pathak, V. P., and Kouyoumjian, R. G., " An analysis of the radiation from apertures in curved surface by the geometrical theory of diffraction", *Proc. IEEE*, 62, pp. 1438 - 1447, 1974.

Peterson, R. L., Ziemer, R. E., and Borth, D. E., *Introduction to Spread Spectrum Communications*, Prentice-Hall, Inc.,New Jersey, 1995.

Pogorzelski, R. J., *A Note on Some Common Diffraction Link Loss Models*, Radio Science, Vol 17, pp 1536-1540. 1982.

Rappaport, T. S., "Wireless personal communications," *IEEE Antennas Propagat. Mag.*, vol 33, 1991.

Rappaport, T. S., *Wireless Communications Principles and practice*, Prentice-Hall, New Jersey, 1996.

Sass, P. F., "Why is the Army Interested in Spread Spectrum?" *IEEE Communication Mag.*, Vol 21, pp. 23-25, July 1983.

Sklar, Bernard, *Digital communications*, chap.4, Prentice-Hall, Inc., New Jersey, 1988.

Vogler, L. E.*An Attenuation Function for Multiple Knife-Edge Diffraction*, Radio Science, Vol 17, pp 1541-1546. 1982.

Woerner, B. D., Rappaport, T. S., and Reed, J. H., *Wireless Personal Communications Research Development*, Kluwer Academic Publishers, Massachusetts, 1995.

B

Balanis' equation, 3-6

> Diffraction coefficient ($\mathcal{D}$), 3-6, C-2

> Spatial attenuation ($\mathcal{A}$), 3-6, C-2

Bullington's idea, 4-14

C

Channel model

> Deygout(DG) method, 4-14

> Egli model, 1-1, 2-2, 2-11

> Epstein-Peterson(EP) method, 4-14

> Free space model, 1-1, 2-2

> Hata model, 1-1, 2-2, 2-11, 5-21

>> Correction parameter, 1-2, 2-11

> Longley-Rice model, 1-1, 2-2, 2-11

> Okumura method, 1-1, 2-2, 2-11

> Real Terrain Diffraction Model (RTDMOD), 4-14, 4-18, 5-1

> Universal Terrain Channel Model (UTCMOD), 5-1, 5-17, 5-19

>> Path-loss generator, 5-7

>> MBPLG, 5-8

>> MVBPLG, 5-10

>> MVWBPLG, 5-12

>> MVWDBPLG, 5-14

Lit diffraction, 3-1, 3-4

Low probability of interception

    LPI, 1-2

    LPI quality factors (Q_{LPI}), 1-2

Low Probability of Interception (LPI)

    Antenna quality factor (Q_{ANT}), 6-6

    Atmospheric quality factor (Q_{ATM}), 6-7

    Interference suppression quality factor (Q_{IS}), 6-6

    LPI quality factor (Q_{LPI}), 6-5

    Modulation quality factor (Q_{MOD}), 6-6

    Possible interception area (A_I, 6-4

    Tactical quality factor (Q_{TAC}), 6-1, 6-16

    Terrain quality factor (Q_{TER}), 6-1, 6-11

M

MATLAB code

    JANG1.m, 4-13

    JANG2.m, 5-12

    PL-total.m, 4-13

    PL-sto.m, 5-12

Multi-path interference, 1-2, 2-2, 2-6, 4-1

    Rejection capability, 2-4

N

Null-to-null bandwidth, 2-6

P

Path clearance (F_1), 4-5

Vita

Capt. You-Cheol Jang ████████████████████████████████████
███████████████. In March 1987 he entered the Korea Military Academy (KMA).
In March 1991, he graduated from the KMA with a Bachelor of Science degree in Electrical
Engineering, and was commissioned in the Republic of Korea Army. After the Officer's
Basic Course in the Army Communication School, he was assigned to 31st ROK Army
Infantry Division as a Battalion signal officer. In July 1992, he was assigned to Special
Forces as a Battalion signal officer. In July 1993, he took the Officer's English Course for
six months, and was assigned to 26th ROK Army Infantry Division as a Regiment signal
officer. In March 1995, he entered AFIT enrolled in the School of Engineering, Department
of Electrical and Computer Engineering. After graduation, Capt. Jang will be serving in
the Republic of Korea Army.

VITA-1

REPORT DOCUMENTATION PAGE

Form Approved
OMB No. 0704-0188

1. AGENCY USE ONLY (Leave blank)	2. REPORT DATE	3. REPORT TYPE AND DATES COVERED
	June 1997	Master's Thesis

4. TITLE AND SUBTITLE

Diffraction Analysis and Tactical Applications of Signal Propagation Over Rough Terrain

5. FUNDING NUMBERS

6. AUTHOR(S)

You-Cheol Jang

7. PERFORMING ORGANIZATION NAME(S) AND ADDRESS(ES)

Air Force Institute of Technology, WPAFB OH 45433-6583

8. PERFORMING ORGANIZATION REPORT NUMBER

AFIT/GE/ENG/97J-01

9. SPONSORING/MONITORING AGENCY NAME(S) AND ADDRESS(ES)

Kris Kim
31 Grenier Street
Hanscom AFB MA 01731

10. SPONSORING/MONITORING AGENCY REPORT NUMBER

11. SUPPLEMENTARY NOTES

12a. DISTRIBUTION/AVAILABILITY STATEMENT

Approved for Public release; Distribution Unlimited

12b. DISTRIBUTION CODE

13. ABSTRACT (Maximum 200 words)

The free space propagation model and many existing propagation channel models do not adequately predict path-loss in ground communication over rough terrain. Hence, two new propagation channel models, Real Terrain Diffraction Model (RTDMOD) and Universal Terrain Channel Model (UTCMOD), were developed. RTDMOD can account for an almost unlimited number of obstacles and has the advantage of predicting the significant diffraction point locations as well as the total path-loss for a given set of real terrain data. A computationally efficient stochastic channel model, UTCMOD, was also developed from numerous *Monte Carlo* simulations using RTDMOD. UTCMOD is applicable to many different kinds of terrain conditions and provides the correct perspective for analyzing the propagation effects. Also UTCMOD can be used to optimize many tactical communication (TAC COMM) and electronic warfare (EW) scenarios for Low Probability of Interception (LPI) performance. Since, Low Probability of Interception (LPI) is important in both military and commercial applications, methods of analyzing LPI communication have been developed throughout the past decade. However, the existing LPI formulation is not sufficient because the previous LPI quality factor definitions are overly simplistic, too sensitive to range, and ignore atmosphere and terrain effects. Fortunately, these problems can be resolved by using a new terrain quality factor, Q_{TER}, and a tactical quality factor, Q_{TAC}. Finally, Q_{TER} and Q_{TAC} can be used to analyze TAC COMM and EW scenarios in order to exploit terrain to create a communication advantage for friendly forces.

14. SUBJECT TERMS

Ground Communication, Signal propagation, Channel model, Low-Probability-of-Interception (LPI), LPI communication, LPI quality factor, Tactical communication, Electronic warfare

15. NUMBER OF PAGES

141

16. PRICE CODE

17. SECURITY CLASSIFICATION OF REPORT	18. SECURITY CLASSIFICATION OF THIS PAGE	19. SECURITY CLASSIFICATION OF ABSTRACT	20. LIMITATION OF ABSTRACT
UNCLASSIFIED	UNCLASSIFIED	UNCLASSIFIED	UL

GENERAL INSTRUCTIONS FOR COMPLETING SF 298

The Report Documentation Page (RDP) is used in announcing and cataloging reports. It is important that this information be consistent with the rest of the report, particularly the cover and title page. Instructions for filling in each block of the form follow. It is important to *stay within the lines* to meet *optical scanning requirements*.

Block 1. Agency Use Only *(Leave blank)*.

Block 2. Report Date. Full publication date including day, month, and year, if available (e.g. 1 Jan 88). Must cite at least the year.

Block 3. Type of Report and Dates Covered. State whether report is interim, final, etc. If applicable, enter inclusive report dates (e.g. 10 Jun 87 - 30 Jun 88).

Block 4. Title and Subtitle. A title is taken from the part of the report that provides the most meaningful and complete information. When a report is prepared in more than one volume, repeat the primary title, add volume number, and include subtitle for the specific volume. On classified documents enter the title classification in parentheses.

Block 5. Funding Numbers. To include contract and grant numbers; may include program element number(s), project number(s), task number(s), and work unit number(s). Use the following labels:

C	-	Contract	PR	- Project
G	-	Grant	TA	- Task
PE	-	Program Element	WU	- Work Unit Accession No.

Block 6. Author(s). Name(s) of person(s) responsible for writing the report, performing the research, or credited with the content of the report. If editor or compiler, this should follow the name(s).

Block 7. Performing Organization Name(s) and Address(es). Self-explanatory.

Block 8. Performing Organization Report Number. Enter the unique alphanumeric report number(s) assigned by the organization performing the report.

Block 9. Sponsoring/Monitoring Agency Name(s) and Address(es). Self-explanatory.

Block 10. Sponsoring/Monitoring Agency Report Number. *(If known)*

Block 11. Supplementary Notes. Enter information not included elsewhere such as: Prepared in cooperation with...; Trans. of...; To be published in.... When a report is revised, include a statement whether the new report supersedes or supplements the older report.

Block 12a. Distribution/Availability Statement. Denotes public availability or limitations. Cite any availability to the public. Enter additional limitations or special markings in all capitals (e.g. NOFORN, REL, ITAR).

DOD - See DoDD 5230.24, "Distribution Statements on Technical Documents."
DOE - See authorities.
NASA - See Handbook NHB 2200.2.
NTIS - Leave blank.

Block 12b. Distribution Code.

DOD - Leave blank.
DOE - Enter DOE distribution categories from the Standard Distribution for Unclassified Scientific and Technical Reports.
NASA - Leave blank.
NTIS - Leave blank.

Block 13. Abstract. Include a brief *(Maximum 200 words)* factual summary of the most significant information contained in the report.

Block 14. Subject Terms. Keywords or phrases identifying major subjects in the report.

Block 15. Number of Pages. Enter the total number of pages.

Block 16. Price Code. Enter appropriate price code *(NTIS only)*.

Blocks 17. - 19. Security Classifications. Self-explanatory. Enter U.S. Security Classification in accordance with U.S. Security Regulations (i.e., UNCLASSIFIED). If form contains classified information, stamp classification on the top and bottom of the page.

Block 20. Limitation of Abstract. This block must be completed to assign a limitation to the abstract. Enter either UL (unlimited) or SAR (same as report). An entry in this block is necessary if the abstract is to be limited. If blank, the abstract is assumed to be unlimited.